THE UNIVERSITY OF CHICAGO

# OPTOGENETIC ANALYSIS OF RHOA-MEDIATED FURROW FORMATION DURING CYTOKINESIS

A DISSERTATION SUBMITTED TO

THE FACULTY OF THE DIVISION OF THE BIOLOGICAL SCIENCES

AND THE PRITZKER SCHOOL OF MEDICINE

IN CANDIDACY FOR THE DEGREE OF

DOCTOR OF PHILOSOPHY

DEPARTMENT OF MOLECULAR GENETICS AND CELL BIOLOGY

BY

ELIZABETH WAGNER

CHICAGO, ILLINOIS

AUGUST 2016

Table of contents

**List of Figures**

## Chapter 1: Introduction


### Abstract

Cytokinesis is the final stage of cell division in which an actomyosin-based contractile ring physically divides the cell into two genetically equivalent daughter cells. The cytokinetic cleavage furrow is controlled by the position of the anaphase spindle and this positioning is critical to ensure that cells divide properly to generate two genetically equivalent daughter cells. The anaphase spindle performs this function, in part by controlling the activity of the small GTPase RhoA, which is required for actomyosin-based contractile ring assembly and furrow ingression during cytokinesis. However, it remains unclear whether the spindle makes additional contributions to furrow assembly or whether a local zone of RhoA activity is sufficient to give rise to furrow formation. Likewise it is not known whether the entire cortex equally responsive to RhoA and whether the spindle modulates the response to active RhoA? Furthermore is contractile ring assembly subject to cell cycle regulation? Here, we have addressed these and other questions by using optogenetics to gain tight spatial and temporal control of RhoA activity in mammalian cells. Light-mediated recruitment of a RhoGEF domain to the plasma membrane leads to rapid induction of RhoA activity, as indicated by accumulation of a RhoA biosensor, myosin II, and F-actin. Light-mediated induction of RhoA activity, leads to assembly of cytokinetic furrows that partially ingress. Furthermore, furrow formation in response to RhoA activation is not temporally or spatially restricted. These results indicate RhoA activation is sufficient to induce assembly of functional contractile rings and furrow formation.

## 1.1 RhoGTPase signaling and regulation

RhoA belongs to the Rho family of small GTPases, which are a class of signaling molecules involved in a wide variety of cellular processes. Since their discovery, a wealth of information about the biochemical function and regulation of GTPase signaling have been uncovered and will be briefly reviewed in Chapter 1.1. Numerous biological processes are associated with and require the local activation of Rho family GTPases. However, the detailed molecular mechanisms of how local GTPase activities are spatial and temporally regulated to generate specific cellular functions are less well understood. To better understand these mechanisms, precise spatial and temporal control of GTPase signaling is imperative.

### 1.1.1 Small GTPases behave as molecular switches

The Rho family of small GTPases are a major group of the Ras superfamily of small GTPases that are present in all eukaryotes(Rojas et al., 2012). Rho GTPases function as molecular switches that control a wide variety of signal transduction pathways by cycling between an active GTP-bound and inactive GDP-bound state (Vetter and Wittinghofer, 2001). Rho GTPases undergo an ordered series of post-translational modifications that generate a lipid tail on a C-terminal CAAX motif. These modifications mediate subcellular localization to the plasma membrane and/or endomembranes which is required for biological activity (Roberts et al., 2008). In the active GTP-bound conformation, membrane localized GTPases interact with various downstream effectors to elicit diverse cellular responses.

GTPase cycling is regulated by three classes of proteins: guanine nucleotide exchange factors (GEFs), guanine nucleotide activating proteins (GAPs) and guanine nucleotide exchange

inhibitors (GDIs). GEF's activate GTPases by promoting the exchange of GTP for GDP(Schmidt and Hall, 2002a). GAPs inactivate GTPases by increasing their intrinsic hydrolysis rate of GTP to GDP. GDI's bind to the C-terminus of Rho GTPases extracting them from the membrane and sequestering them in the cytosol in their GDP bound state (Vetter and Wittinghofer, 2001) (Figure 1).

### 1.1.2 Regulation of GEFs

Many cellular processes are dependent on tightly controlled GTPase activities, therefore their activators, GEFs, are themselves also highly regulated. In human cells there are over 70 RhoGEFs identified which all share the conserved Dbl homology (DH) domain (Rossman et al., 2005), which is the minimal catalytic domain necessary for GTPase activation (Hart et al., 1994). Of those GEFs characterized by either in vitro nucleotide exchange assays or by overexpression in vivo, several have been shown to be specific for a single GTPase, while others are capable of activating multiple GTPases. The exact mechanisms of activation for each GEF vary quite a bit, however some general regulatory mechanisms have emerged including: autoinhibition and subcellular localization.

Although GEF's are quite structurally diverse, their N-termini can commonly form intramolecular interactions with the DH containing C-termini inducing autoinhibition of the GEF activity. For many GEFs including, Vav, Tiam1, Net1, and Ect2, the latter of which will be discussed in detail in this thesis, removal of the N-terminal region leads to constitutive activation when expressed in vivo (Chan et al., 1996; Katzav et al., 1991; Miki et al., 1993; van Leeuwen et

al., 1995). Relief of autoinhibition can occur through various mechanisms, including post-translational modifications and/or protein-protein interactions.

GTPase activation mostly occurs at the plasma membrane or other endomembranes, therefore subcellular localization of GEFs to these structures is another mode of their regulation. In the majority of GEFs the DH domain is found in tandem with a Pleckstrin homology (PH) domain. PH domains are best-characterized for their ability to bind to phosphoinositides and are proposed to mediate membrane localization of GEFs (Lemmon and Ferguson, 2000; Rebecchi and Scarlata, 1998). Deletion of the PH domain of RhoA-specific GEF LARG, which will be discussed in more detail later in this thesis, inhibits membrane localization and GEF activity in vivo. Addition of an exogenous membrane binding domain is sufficient to rescue localization and GEF activity of LARG (Aittaleb et al., 2009). For some GEFs, their PH domains make additional protein-protein interactions that can contribute to GEF activity. For example the PH domains of the GEFs Dbs and LARG, also bind directly to Rho GTPases and this interaction enhanced catalytic GEF activity of DH domains (Rossman et al., 2002) (Kristelly et al., 2004). Additional allosteric protein-protein interactions may also contribute to membrane localization of GEFs. For example various GEFs localize in response to activated transmembrane receptors. Vav is recruited to activated T and B-cell receptors via an interaction with adaptor proteins(Bustelo, 2000). p115RhoGEF and LARG are recruited in response to GPCR activation by binding directly to Gα13 through a RGS domain(Bhattacharyya and Wedegaertner, 2000).

Another mode of regulating GEF localization and activity is by sequestration. Both Net1 and Ect2 contain NLS sequences which localize them to the nucleus. Ect2 is released upon nuclear

envelope breakdown and plays an important role in regulating cytokinesis (Prokopenko et al., 1999; Tatsumoto et al., 1999) and will be discussed in further detail in Chapter 1.4. Net1 contains a nuclear export signal which can regulate its nuclear exit and ability to activate Rho GTPase signaling (Schmidt and Hall, 2002b).

RhoGEFs can also behave as signaling nodes. Several GEFs, such as Pix and ITSN, bind directly to downstream effectors effectively tethering them to GTPases to increase the efficiency of signal transduction (Hussain et al., 2001; Li et al., 2003). This scaffolding behavior can help to induce positive feedback or tune the response by biasing GTPase interaction with specific downstream effectors (Coyle and Lim, 2016). RhoGEFs can also act to coordinate different signaling pathways such as heterotrimeric G-protiens with GTPase signaling. The RhoGEFs, p155RhoGEF, PDZ, and LARG, contain regulatory of G-protein signaling (RGS) domains which have GAP activity towards Gα proteins. In response to GPCR activation, these GEFs bind to and inactive Gα protein signaling while this interaction simultaneously localizes and activates the RhoGTPase GEF activity presumably through relief of autoinhibition (Bhattacharyya and Wedegaertner, 2000).

A critical goal of my thesis was to gain optical control of the activity of the small GTPase RhoA. Our plan to accomplish this was to engineer light-mediated control of a RhoA-specific GEF. In order to do so our strategy was to control the subcellular localization of a GEF derivative that is relatively inactive in the cytosol but active when recruited to the membrane.

### 1.1.4 Rho GTPase Effectors

The Rho GTPase family including Rac1, Cdc42, and RhoA are best-known for their roles in regulating the actin cytoskeleton network(Hall, 1998). In many cell types, Rac1 induces actin polymerization at the cell edge to promote lamellipodia formation and membrane ruffling, RhoA generates contractile actomyosin filaments known as stress fibers, and Cdc42 promotes actin polymerization at the cell periphery to form filopodia (Hall, 1998). Although each GTPases is associated with the formation of distinct cellular structures, there is some overlap of the downstream effectors activated by each GTPase. Both Rac1 and Cdc42 induce Arp2/3-mediated assembly of branched actin filaments. Rac1 indirectly interacts with the Arp 2/3 activator WAVE complex (Eden et al., 2002) and Cdc42 directly binds to the Arp 2/3 activator N-WASP(Rohatgi et al., 1999). Rac1 and Cdc42 can also activate p-21 activated kinases (PAK) which have various functions including indirectly effect actomyosin contractility phosphorylation and inhibition the myosin II activator, MLC kinase (Sanders et al., 1999). RhoA promotes assembly of filamentous actin through its direct interaction with the formin, mDia (Watanabe et al., 1999). RhoA also interacts with ROCK (Rho-associated kinase) which both directly and indirectly promotes myosin II activation(Kimura et al., 1996; Watanabe et al., 1999).

In addition to regulating the actin cytoskeleton, Rho GTPases also effect various signal transduction pathways. For example, Rac1 interacts with p67phox, which is a key regulator of the phagocytic NADPH oxidase enzyme complex (Abo et al., 1991). Cdc42 interacts with the adaptor protein Par6, which required for establishing anterior-posterior polarity in *C. Elegans* embryos as well as apical-basal polarity in various epithelial cells (Watts et al., 1996; Welchman

et al., 2007). Rho GTPases can also regulate gene transcription. Although it occurs indirectly through its effects on the actin network, RhoA activation induces activation of the serum-response (SRF) transcription factor (Miralles et al., 2003). In context-dependent manner, Rac1 and Cdc42 can activate the c-Jun N-terminal kinase (JNK) and p38 mitogen-activated protein kinase (MAPK) pathways (Coso et al., 1995; Minden et al., 1995). Rho GTPases are also associated with regulating lipid metabolism through various phospholipid kinase effectors.

Additionally, there is evidence for crosstalk between Rho GTPases that can occur directly or indirectly though downstream effectors. One of the best-characterized examples is the mutually antagonist relationship between Rac1 and RhoA. Active Rac1 can directly and indirectly activate the RhoA GAP, p190RhoGAP (Kuo et al., 2011; Vicente-Manzanares et al., 2011). The Rac1 effector PAK1 is also found to phosphorylate and inactivate a number of RhoA specific GEFs (Aghajanian et al., 2009; Nimnual et al., 2003; Rosenfeldt et al., 2006). Conversely, RhoA negatively regulates Rac1 activity through it's downstream effector, ROCK, which phosphorylates and activates the Rac1 GAPs, ARH22RhoGAP and FilGAP (Ohta et al., 2006; Tsuji et al., 2002).

### 1.1.5 Diverse cellular processes regulated by Rho GTPases

The Rho family of GTPases have roles in diverse and dynamic cellular processes including morphogenesis, polarity, movement, and cell division. Often these cellular processes are dependent on precise spatial and temporal coordination of multiple Rho GTPases. Cell migration is a great example where the timing and spatial localization of Rac1, Cdc42, and RhoA activation each play a critical role in regulating cell motility. In mammalian fibroblast cells

migrating on glass surface, activation of Rac1 and Cdc42 are localized to the leading edge and promote protrusion while RhoA activation in the cell body and rear drive retraction of the trailing edge (Ridley et al., 2003). Interestingly this spatial and temporal pattern of GTPase signaling can vary depending on the cell type, migrational cue, and environment. As we learn more about the roles of GTPases signaling during various cellular processes, is has become increasing evident that the precise spatial temporal context directly influences the specific cellular responses. In order to completely understand how GTPase signaling can direct a wide variety of cellular behaviors, we need to be able to directly manipulate their activity with precise spatiotemporal precision. In particular, the goal of my thesis was to use optogenetic tools to obtain light-directed control of the small GTPase RhoA to elucidate spatial and temporal regulation of RhoA-mediated cleavage furrow formation during cytokinesis, which will be discussed in further detail in Chapter 1.2-1.5.

**1.2 The small GTPase RhoA is a master regulator of cytokinesis**

Cytokinesis is the final stage of the cell cycle where the cell is physically divided into two genetically equivalent daughter cells. Successful cytokinesis is essential for proliferation and the development and maintenance of multicellular organisms. In animal cells, cytokinesis is initiated following segregation of the duplicated chromosomes during early anaphase. A contractile ring is assembled at the cell midzone consisting of filamentous actin and non-muscle myosin II. The myosin II motor function drives constriction of the actin ring, causing the cell membrane to ingress and form a cleavage furrow. This furrow will continue to ingress until it reaches and forms the midbody structure, which are highly compressed antiparallel bundled microtubules. The midbody structure assembles factors required for abscission, which is the physical cutting of

the cell into two (Figure 2). This process requires exquisite spatial and temporal regulation and improper or incomplete division generates aneuploid cells which can lead to cell death, developmental defects, and tumorgenesis (Barr and Gruneberg, 2007).

The small GTPase RhoA is required for cleavage formation (Drechsel et al., 1997; Kishi et al., 1993; Mabuchi et al., 1993). During anaphase, local activation of RhoA marks the presumptive site of and remains high and tightly focused as the cleavage furrow ingresses (Bement et al., 2005; Yüce et al., 2005). RhoA mediates cleavage furrow formation by interacting and with various downstream effectors including, the formin mDia2, Rho-dependent kinase (ROCK), Anillin, and citron kinase to induce contractile ring assembly and furrow formation. Briefly, the formin mDia2 promotes the polymerization of filamentous actin necessary for formation of the contractile ring (Watanabe et al., 2008). ROCK regulates myosin II activation, which is a crucial component of the contractile ring that generates the force necessary for contractile ring ingression (Amano et al., 1996). The putative scaffold, Anillin, is also found to be highly concentrated in the cleavage furrow and although its function is not completely understood, it promotes myosin organization and appears to be important for maintaining the stability of the furrow position (Zhao and Fang, 2005). Through these downstream effectors, local activation of RhoA directs cleavage furrow formation during cytokinesis.

### 1.3 Models of Cleavage furrow formation

One of the major questions concerning cytokinesis that has interested biologists for decades, is what directs RhoA-mediated cleavage furrow formation so that division occurs at precisely the right time and position to generate to genetically equivalent daughter cells. Some of the earliest

evidence came from a series of micromanipulation experiments done in large invertebrate embryos by Ray Rappaport (Rappaport, 1961; 1985). In one set of experiments, sand dollar embryos were squeezed into silicone tubes and wherever the mitotic spindle was relocalized so too was the cleavage furrow. Rappaport also observed that during a specific time interval following anaphase onset if the mitotic spindle was repositioned, the initial furrow would regress and a new furrow would form at the site where the mitotic spindle was moved (Rappaport, 1985)(Figure 3A). These and other micromanipulation experiments clearly demonstrated that the mitotic spindle was responsible for directing the site of RhoA activation and cleavage furrow formation. Indeed if the mitotic spindle is removed or dissolved using microtubule depolymerizing agents at a certain time before anaphase onset, cells will fail to form a furrow (Hiramoto, 1956; Rappaport, 1985). At this time actin and myosin were localized and functionally implicated for furrow formation, however little to no other molecular detail of the proteins involved in regulating cytokinesis were known. Rather much of the work was aimed at trying to decipher which part or substructure of the mitotic spindle was responsible for orchestrating cleavage furrow formation. During anaphase, the mitotic spindle consists of two distinct pools microtubules. Radial arrays of dynamic, so-called astral, microtubules emanate from each centrosome or spindle pole. A relatively stable pool of non-kinetechore-associated, anti-parallel, bundled microtubules known as the central spindle formed between the spindle poles. In this section, I will briefly review some of the key experiments investigating how the mitotic spindle may be directing cleavage furrow formation and some of the early models that emerged to support the various findings.

In another set of Rappaport's micromanipulation experiments he demonstrated that specifically the astral MT's may play an important role in directing furrow formation. In these experiments sand dollar embryos were compressed and perforated with a glass rod resulting in a donut or "torus" shaped cell (Figure 3B). During the first division, a single furrow formed and divided the cell between the aster MT's resulting in a binucleate U-shaped cell. During the second division, furrows formed between the mitotic spindles on each arm of the U-shaped cell, as well as between the asters of the independent mitotic spindles, indicating that furrow induction can occur independent of chromosomes and the central spindle. However, these furrows were dependent on the distance between the non-spindle associated asters as this effect was not observed if the asters were further apart. In similar micromanipulation experiments in *C. elegans* embryos, juxtaposition asters were sufficient to induce furrow formation independent of chromosome and the central spindle (Baruni et al., 2008). In fused binucleate vertebrate somatic cells, Rieder also observed furrow formation between asters of independent mitotic spindles even when these mitotic spindles were up to 60uM apart (Rieder et al., 1997). These results generated a model known as the astral stimulation, where a positive furrowing inducing signal is associated with the aster MTs (Figure 4A). In regions where astral MT's may overlap, such as between the spindle poles of single or two independent mitotic spindles, this positive signal is proposed to be at it's highest resulting in furrow induction.

However in a number of experiments where the aster MT's were either repositioned or disrupted they appear to be playing a negative role in regulating cortical contractility rather then a positive role. In *C. elegans* embryos, genetic and chemical perturbations that altered the location or length of the asters, showed in regions were asters were lost increased cortical localization of

myosin II was observed(Pintard et al., 2003) (Werner et al., 2007). Increases in cortical actin were also observed in regions were astral MT's were lost by either mechanical repositioning of mitotic spindles in silkworm spermatocytes (Chen et al., 2008) or depolymerization of astral MT's in mammalian epithelial cells (Murthy and Wadsworth, 2008). Based on these results a different model for how the aster MT's may direct furrow formation was proposed. In the polar relaxation model a negative regulatory signal is associated with the aster MT's that inhibits cortical contractility. In this model, aster MT's are proposed to be in more contact with polar regions versus the equatorial region and therefore limit contractility in the poles leading to contraction at the midzone (Figure 4B). However, the polar relaxation model seems insufficient to be the only signal directing furrow formation.

For example, during Rappaport's torus experiments if polar relaxation was sufficient to generate furrows, the non-spindle furrows should also be present during the first division.
Unlike the results in larger invertebrate embryos, in smaller vertebrate cells furrow specification seems to be directed by the central spindle structure rather then the aster microtubules (Figure 4C). Wang perforated normal rat kidney (NRK) cells and found that furrows would only form on the side which the central spindle was localized and although the asters in these cells still reached the other side of the perforation they were insufficient to direct furrow initiation(Cao and Wang, 1996). Additionally in multipolar NRK cells, furrow formation correlated with the localization of the central spindle structures rather then the spindle poles (Wheatley and Wang, 1996).

As more of the molecular details of cytokinesis have been uncovered (discussed in Chapter 1.4), individually each of these initial models are not sufficient to reconcile all of the data.

Furthermore astral stimulation and polar relaxation models are based on opposite assumptions of astral MT distribution and density at the equatorial zone. There could also be some variation in the exact regulation or molecular requirements for cleavage furrow formation between different species and even throughout development. There is also strong molecular evidence that multiple independent mechanisms can generate contractile furrowing. While exceptions certainly exist, during cytokinesis in the vast majority of cell types the central spindle plays a critical role in directing furrow formation. A number of key molecular components required for furrow formation concentrate on this structure including centralspindlin and Ect2 (discussed further in Chapter 1.4). In the following section I will discuss in further detail what we now know about the central spindle-directed pathway and it's function in regulating RhoA-mediated cleavage furrow formation. In combination with the positive role of the central spindle, the ability of astral MT's to negatively regulate cortical contractility may be important to limit or focus the region of contractility to the equatorial zone to promote furrow formation (Figure 4D). However, the exact molecular mechanisms of how astral MT's negatively regulate cortical contractility remain unknown. Is their function to limit or occlude localization of upstream regulators of RhoA-mediated contractility or directly down regulate active RhoA or downstream effectors? Are there parallel pathways directed by the mitotic spindle, such as vesicle trafficking and membrane insertion that play a role in cleavage furrow formation (Drechsel et al., 1997)?

**1.4 Upstream Regulation of RhoA activation pathway during cytokinesis**

Over the past several decades, many proteins and protein complexes required for of cytokinesis have been identified. Although the exact molecular mechanisms of how each of these components are spatially and temporally coordinated is not understood, the upstream regulatory

pathway required for local activation of RhoA is relatively well understood. In this section, I will review this pathway and what is known about how RhoA activation is spatially and temporally regulated during cytokinesis.

### 1.4.1 RhoA activation is dependent upon the RhoGEF Ect2

The highly conserved RhoGEF Ect2 is a critical regulator of cytokinesis in animal cells. Although in vitro Ect2 displays GEF activity towards RhoA, Rac1, and Cdc42 (Tatsumoto et al., 1999) in vivo, Ect2's primary function appears to be locally activating RhoA at the equatorial cortex driving cleavage furrow formation. Depletion and/or loss of function studies demonstrated that human Ect2 (Kim et al., 2005) and its orthologs, Pebble (*Drosophila melanogastor*) (Prokopenko et al., 1999) and LET-21(*Caenorhabditis elegans*) (Dechant and Glotzer, 2003) are required for cytokinesis.

### 1.4.2 Regulation of Ect2 activity

Ect2's activity is regulated through various mechanisms including autoinhibition, intracellular localization, and protein-protein interactions. Autoinhibition of Ect2 is mediated by an intramolecular interaction between its N-terminal tandem BRCT domains and the C-terminal DHPH domains and overexpression of Ect2's N-terminus is sufficient to block cytokinesis in mammalian cells (Kim et al., 2005) . During interphase, Ect2 is sequestered to the nucleus by two nuclear localization sequences (NLS) at its N-terminus. Following nuclear envelope breakdown, Ect2 is initially diffusely cytoplasmic and then a portion becomes localized to the central spindle at anaphase onset (Tatsumoto et al., 1999). Central spindle localization of Ect2 is dependent on it's interaction with the RhoGAP MgcRacGAP, or also commonly known as

Cyk4(CYK-4 in *C. elegans)* (Yüce et al., 2005) (discussed in section 1.4.3). Specifically, Ect2's tandem BRCT domains bind to the N-terminal portion of Cyk4 in a phospho-dependent manner (Wolfe et al., 2009). Binding to Cyk4 is required for Ect2's localization and may also activate Ect2's catalytic activity by relieving autoinhibition. Depletion or expression of phospho-deficient Cyk4 mutants, disrupt Ect2's localization to the central spindle and RhoA-mediated cleavage furrow formation in mammalian cells (Wolfe et al., 2009; Yüce et al., 2005) (Figure 5). More recently, a second interaction between the catalytic C-termini of *C. elegans* Cyk4 and Ect2 was identified in vitro. However, the functional role of this interaction is not well understood, but genetic evidence suggests it enhances Ect2's GEF activity towards RhoA (Zhang and Glotzer, 2015).

### 1.4.3 Centralspindlin complex and central spindle assembly

In addition to binding Ect2, Cyk4 is a critical component of the protein complex known as centralspindlin. Centralspindlin is heterotetramer of a dimeric kinesin-6 motor protein, MKLP1(Zen4 in *C.elegans*), and a dimeric RhoGAP, MgcRacGAP (Cyk4) (Mishima et al., 2002). This protein complex plays numerous roles during cytokinesis including the requirement for assembly of the central spindle. Oligomerization of the centralspindlin complex is mediated by oligomerization domain of MKLP1 and is required for proper central spindle assembly (Hutterer et al., 2009). Likely oligomerization promotes the avidity of centralspindlin complex for microtubules increasing the stability and bundling of antiparallel microtubules in the midzone of the cell (Hutterer et al., 2009). Oligomerization is negatively regulated by a 14-3-3 (PAR-5 in *C.elegans*) protein that binds to phosphorylated MKLP1. The kinase Aurora B, which is a component of the CPC (chromosomal passenger complex) which also accumulates on the central

spindle, phosphorylates MKLP1 at a second site that disrupts 14-3-3 binding, and promotes oligomerization (Douglas et al., 2010). Additional microtubule bundling proteins, including PRC1 and KIF4 also localize to and are required for central spindle assembly (Mollinari et al., 2002). The central spindle structure plays a critical role in directing cleavage furrow formation by acting as a platform to which numerous upstream regulators of RhoA activation and several key mitotic kinases are concentrated.

### 1.4.4 PLK1 activity is required for RhoA-mediated cleavage formation

PLK1 is a highly conserved eukaryotic serine/threonine kinase that is essential for mitosis. PLK1 contains a C-terminal polo box domain (PBD) that acts as a phosphopeptide binding motif that targets the kinase to subcellular locations by phosphorylated substrates (Barr et al., 2004; van de Weerdt and Medema, 2006). Plk1 activity is required at several mitotic steps including, centrosome maturation, formation of bipolar spindles, and microtubule/kinetochore interactions (Barr et al., 2004);Lénárt et al., 2007; McInnes et al., 2006; Peters et al., 2006). During anaphase, Plk1 is localized to the central spindle primarily through it's interactions with PRC1,Cyk4, MKLP1 and MKLP2 (Liu et al., 2004; Lowery et al., 2007; Neef et al., 2003). At the central spindle, PLK1 phosphorylates Cyk4 at least four serine residues which are required for it's binding interaction with the tandem BRCT domains of Ect2 (Wolfe et al., 2009)(Figure 5). Inhibition of PLK1 activity using the small molecule inhibitor BI2536 or mutation of the four serine residues to alanine, block Ect2 localization to the central spindle, local activation of RhoA, and cleavage furrow formation (Petronczki et al., 2007; Wolfe et al., 2009) (Figure 5). Expression of phosphomimetic mutant of Cyk4 is sufficient to rescue Ect2 localization to the central spindle in the presence of BI 2536, however these cells fail locally activate RhoA and

form cleavage furrows (Wolfe et al., 2009). These results suggest that Plk1 may serve additional roles in promoting Rho-mediated furrow formation. For example, Ect2 has also been reported to be phosphorylated by PLK1, however the role of the phosphorylation is not understood (Niiya et al., 2006). PLK1 may also play a role in regulating RhoA-mediated contractility as several downstream effectors are implicated as Plk1 substrates including, ROCK and anillin (Liu et al., 2004; Lowery et al., 2007; Neef et al., 2003). Further work is required to define the full spectrum of Plk1 substrates required for complete activation of RhoA and contractile ring assembly during cytokinesis.

### 1.4.5 Membrane localization of Centralspindlin:Ect2 complex

Local activation of RhoA at the equatorial cortex requires cortical localization of upstream activators. Indeed, small amounts of centralspindlin:Ect2 complex can be detected on the equatorial cortex (Basant et al., 2015; Su et al., 2011)(Figure 6), but precisely how membrane association is regulated remains unclear. Several possible mechanisms, which may contribute to membrane localization of upstream regulatory pathway, are discussed in the following sections.

#### 1.4.5.1 Membrane binding centralspindlin complex

Another important role of centralspindlin oligomerization is to help promote membrane localization of the centralspindlin:Ect2 complex where it can direct the local activation of RhoA (Basant et al., 2015; Lekomtsev et al., 2012). Cyk4 contains a C1 domain, which has a relatively weak affinity for the plasma membrane (Lekomtsev et al., 2012). However upon oligomerization of centralspindlin, multimerized C1 domains would be predicted to have increased avidity for the membrane. In *C. elegans*, depletion of the negative regulator of centralspindlin oligomerization,

PAR-5, induced hyperaccumulation of membrane localized centralspindlin and hypercontractility. Conversely, Cyk4 mutants lacking the C1 domain fail to localize to the membrane and these embryos do not form a cleavage furrow (Basant et al., 2015). In mammalian cells, expression of a single C1 domain was largely cytoplasmic while tandem repeats of C1 localized well to the membrane (Lekomtsev et al., 2012). Although Cyk4 mutants lacking the C1 domain failed cytokinesis, these cells were able to initiate furrows, however, the membrane did not tightly associate with the midbody and cells failed to undergo abscission (Lekomtsev et al., 2012). One possible explanation for the differential requirements for membrane binding of centralspindlin in *C. elegan*s embryos versus mammalian cells may be related to differences in the central spindle structure. The central spindle in C. elegans embryos is quite compact and far (5-10 um's) from the cortex while in mammalian cells the structure is much broader and closer to cortex therefore furrow initiation may be less dependent on ability of centralspindlin to bind the membrane.

In addition to the Cyk4's C1 domain, the GAP domain of Cyk4 may also helps to promote RhoA activation. In *C. elegans* embryos, the ability of various Cyk4 GAP mutants to bind RhoA-GTP directly influenced the level of membrane localization, and subsequently the extent furrow formation (Zhang and Glotzer, 2015). This work also identified a second interaction between the catalytic C-termini of Ect2 and Cyk4 in vitro, however the effect of this interaction is unclear. One potential model is that full activation of Ect2 requires interaction with the Cyk4 GAP domain bound to RhoA. The ability of Cyk4 GAP domain to bind to RhoA may also promote membrane association of centralspindlin:Ect2 complex. Both mechanisms are possible and could promote positive feedback of RhoA activation.

#### 1.4.5.2 Membrane binding of Ect2 C-terminus

The RhoGEF Ect2, has also been shown to be able to associate with the membrane. In mammalian cells, membrane association of Ect2 is mediated by its PH domain and a polybasic cluster (PBC) motif in the C-terminal tail. The C-terminus containing the DHPH and PBC tail localize globally to the cell cortex. Full length Ect2 constructs either lacking the PH or PBC domains still localized to the central spindle, but were undetectable on the equatorial cortex and disruption of Ect2 membrane localization caused cells to fail to furrow (Su et al., 2011).

### 1.4.7 Cell cycle regulation of RhoA activation pathway

To ensure cleavage furrow formation occurs only after chromosome segregation, many of the upstream activators of RhoA are regulated in cell cycle dependent manner in particular through Cdk1-dependent phosphorylation. The cyclin-B dependent kinase, Cdk1, is a master regulator of mitosis and phosphorylates numerous substrates when it's activity is highest during prometaphase and metaphase. During the metaphase-anaphase transition, the anaphase-promoting complex (APC) induces the degradation Cdk1 and dephosphorylation of various substrates occurs via phosphatases (Nigg, 2001). Cdk1 phosphorylation of the kinesin MKLP1(Mishima et al., 2004) and PRC1 (Jiang et al., 1998; Mishima et al., 2002; 2004) prevent central spindle assembly by blocking microtubule binding activity. Cdk1 phosphorylation of Ect2 inhibits interaction between Ect2:Cyk4 (Yüce et al., 2005). Due to the Cdk1-dependent inhibition of the upstream activators of RhoA, it remains unclear whether this also cell cycle regulation of active RhoA or downstream effectors prior to anaphase onset.

Despite the level of molecular details known about the upstream RhoA activation pathway, it is still not well understood how local activation of RhoA is spatially and temporally regulated during cytokinesis. Additionally, is the local activation of RhoA all that is required for furrow formation or are there other spindle-directed factors that may contribute to furrow ingression? Is the spatiotemporal regulation occurring at the level of upstream activators, active RhoA-GTP, or downstream effectors? To address these types of questions we needed to be able to manipulate furrow formation at molecular level, specifically gaining spatiotemporal control of RhoA activity. Optogenetics tools provide a means to regulate protein activity with high spatial and temporal precision and will be discussed in Chapter 1.5.

**1.5 Optogenetics**

In addition to cytokinesis, nearly all cellular processes depend on precise spatial and temporal coordination of molecular events. However, the most common techniques used to dissect these molecular mechanisms often lack spatial and/or temporal resolution. Genetic techniques are useful for identifying proteins involved and/or required for specific cellular functions. The effects these types of perturbations, for example siRNA or overexpression of DN or CA mutants, occur at the cellular level and at relatively long timescales. Chemical inhibitors/stimulators are useful to gain insight to effects of dynamic behavior of their protein targets, but again lack spatial regulation. The use of fluorescent-tags have been instrumental for tracking when and where a protein of interest localizes and may have functional roles. However, these experiments only demonstrate a certain cell behavior correlates with the localization of a functionally relevant protein at specific times. Although these techniques are invaluable and have provided a wealth

of information, they are unable to directly determine what proteins are sufficient for driving specific cellular functions and how the spatiotemporal context shapes the cellular response.

Optogenetic tools have proven to be a powerful means to control protein activity with high spatial and temporal precision. These techniques utilize naturally occurring photoswitchable proteins or domains to render normally insensitive proteins responsive to light. Several families of photosensitive proteins have been used in various optogenetic systems, including rhodopsins, phytochromes, crytochromes, and LOV-domain containing proteins. Generally, these photosensitive proteins are stimulated to a photoexcited or "lit" state when a chromophore bound to the protein absorbs a photon. Photon absorption causes a change in chromophore structure that induces a conformational change in the bound protein. This effect is reversible in the absence of continuous photon stimuli and the chromophore/protein relax back to their original "dark" state conformation. The rate of conversion to the lit state and reversion to the dark state are widely variable and dependent on protein. In their naturally occurring state, these light-induced conformational changes have been harnessed to alter biological signaling of protein (Toettcher et al., 2011).

In one of the first optogenetic applications, light-controlled ion-channels were generated by direct fusion to the photosensing rhodopsin protein (Fenno et al., 2011). Rhodopsin-based systems allowed for the use of light to both trigger and silence activity in a defined subset of neurons with millisecond precision. These tools enabled fundamental experiments that probed the causal role of specific neurons in controlling circuit activity and their behavioral outcomes.

The use of optogenetic tools have given unprecedented power and precision and have been transformative for the field of neurobiology.

In addition to controlling various membrane channels, more recent optogenetic systems have been developed and used to modulate a wide variety of cytoplasmic signaling cascades in response to light with varying degrees of spatial and temporal control. Two general approaches these systems employ to control protein activity is via either allosteric regulation or dimerization. In allosteric regulation, the photosensitive protein is genetically fused directly to protein of interest and through light-induced conformational changes can allosterically control the protein's function (Figure 7A). One of the first and most dramatic examples of this was the use of a light sensitive domain to control the activity of the Rac1 GTPases which revealed the active protein can induce migration of a mammalian fibroblast (Wu et al., 2009). In dimerization-based systems, the light-mediated binding partners are genetically fused to separate proteins of interest to generate light-induced protein localization or protein-protein interactions (Figure 7 B,C). In the following section I will briefly describe the general design of a few of the more widely used optogenetic systems, how they have been used to control various signaling pathways, and each of their strengths and limitations.

PhyB/PIF

The light induced interaction of the photosensitive protein phytochromeB (PhyB) to the transcription factor Phytochrome Interacting Factor (PIF) was one of the first optogenetic systems. In response to red (650nm) light, PhyB binds to PIF within seconds (Shimizu-Sato et al., 2002) and this interaction will remain stable in dark for hours or can be reversed within

seconds using far red light (750nm) (Levskaya et al., 2009). In yeast, fusion of PhyB and PIF to separated activation domains of the transcription promoter Gal4 generated light-induced transcriptional activation. In the dark, the domains remained separate and transcription was off, however in response to red light, dimerization of PhyB-PIF3 induced complementation of Gal4 activation domains and GAL4-induced transcriptional activation (Shimizu-Sato et al., 2002). These domains have also been used in vitro to induce actin polymerization, by controlling dimerization of Cdc42 and its downstream effector WASP which is an activator of the Arp2/3 complex that polymerizes branched actin networks (Leung et al., 2008). Although these experiments demonstrate dynamic control of protein activities, these examples do not take advantage of the additional spatial control optogenetic tools can provide. Temporal and spatial regulation of various membrane signaling pathways, including small GTPases (Levskaya et al., 2009; Toettcher et al., 2013) and P13K (Toettcher et al., 2011) using the PhyB/PIF system was demonstrated in mammalian cells. In these experiments, membrane localized PhyB domain was used to recruit proteins of interest to the membrane by genetically fusing them to the PIF tag. Subcellular membrane recruitment of the catalytic DHPH domains of the GEF Tiam1 revealed that Rac-1 activation was sufficient to locally induce lamellipodium extension (Levskaya et al., 2009).

Although, the PhyB/PIF system has been used to successfully control subcellular signaling cascades with rather high temporal precision, there are several critical limitations, which have limited its use. First, PhyB is a large protein (908 amino acids) making this a rather bulky tag to genetically fuse to a wide variety of proteins. The interaction between PhyB and PIF also requires the chromophore phytocyanobilin (PCB), which is only made in plants and is not present in yeast or higher eukaryotes. PCB must be supplied exogenously to the media and this

has worked well in yeast and mammalian tissue culture, but it is unclear how well this system would work in more complex multicellular model systems. Recently the system has been shown to be functional and can control subcellular localization in zebrafish embryos (Buckley et al., 2016). For precise subcellular control and rapid inactivation of the PhyB/PIF system one requires a microscope constructed for simultaneous, two-wavelength illumination (Levskaya et al., 2009).

Cry2-CIB1

A cryptochrome-based system was designed using the photosensitive protein cytrochrome 2 (Cry2) taken from *Arabidopsis thaliana*. In response to blue light (405-488nm), Cry2 (498 amino acids) binds to the protein CIB1 (170 amino acids) within 10 seconds and will dissociate in 10 minutes (Kennedy et al., 2010). Similar to the PhyB/PIF system, dimerization of Cry2-CIB1 has been used to dynamically control transcription by bringing together split fragments reconstituting the activity of transcriptional activators in yeast and zebrafish (Hughes et al., 2012; Liu et al., 2012; Shimizu-Sato et al., 2002). This system has also been used to induce subcellular activation of a variety of membrane signaling pathways. Light-mediated membrane recruitment of Raf1, induced Raf/ERK/MEK signaling and was sufficient to induce neurite outgrowth in PC12 cells (Zhang et al., 2014). Membrane recruitment of inositol 5-phosphatase, locally decrease PIP2 and PIP3 levels inducing a suppression of membrane protrusions and ruffles (Idevall-Hagren et al., 2012). For these and other studies using Cry2/CIB to control membrane recruitment, direct fusion of photosensitive Cry2 domain to the plasma membrane have not been successful. Therefore membrane localization is typically induced by locally illuminating cytosolic Cry2-protein X which binds to membrane localized CIB1 protein. Although, local recruitment can be obtained, the diffusive nature and extended lit state

conformation of Cry2 makes controlling precise subcellular localization more difficult. Photoactivation also induces homodimerization of Cry2 which in some cases has been used to activate or inhibit protein activity depending on the construct through oligomerization, but also makes it difficult to finely titrate activation levels with light.

LOV-domain

The photoswitchable LOV domains from several organisms have been adopted for optogenetic tools. In response to blue light (405-488nm), LOV domains undergo a well-characterized conformational change causing the C-terminal Jα helix to undock from the LOV core and unfold (Crosson and Moffat, 2001; Harper et al., 2004). In the absence of continuous stimuli, the photoactivated state of the LOV-domain will spontaneously revert to its dark state conformation. The kinetics of photoactivation and reversion are dependent on the LOV variant. For most optogenetic systems, the LOV domain from *Avenia sativia* (AsLOV2) has been utilized and shown to respond to blue light within seconds and revert to its dark state conformation on a timescale of tens of seconds. Direct fusion of the LOV domain to the GTPase Rac1 generated photoactivatable Rac1 that was used to demonstrate light-mediated cell migration (Wu et al., 2009). The ability to control Rac1 activity by direct fusion to the LOV domain was fortuitous and it appears likely that significant amount of optimizing and engineering would be required for each new target protein. An attractive quality of LOV2 domain is its relatively small photoswitchable domain. It has also been shown there are many mutations which can be made to tune the physical properties, including affinity of the Jα helix for the LOV core or the photocycle duration either shortening or extending the period of time the LOV domain persists in the lit state conformation.

Although there are several optogenetic systems that can locally and reversibly control protein activities, each system has several disadvantages limiting their general use. An ideal optogenetic system would encompass small genetically encoded light-induced dimerization domains, which lack the requirement of exogenous co-factors, and are highly responsive to illumination with minimal background activity. To obtain precise subcellular control, this system would use a photosensitive domain that is responsive to a specific wavelength of light which can be locally controlled using commercial available equipment (micropoint, mosiac, and confocal systems). In order to examine a wide variety of signaling pathways which may be more or less responsive to light-mediated activation, the ability to finely tune the optogenetic probes is also desirable.

When I joined the Glotzer lab, a post-doc Devin Strickland, was developing a novel optogenetic system that fits all of the criteria listed above and will be discussed in detail in Chapter 2. For my thesis, I was interested in using this optimized optogenetic system to investigate the role of RhoA in directing cleavage furrow formation during cytokinesis.

### 1.6 Thesis Objectives

It has been well established that cytokinesis in animal cells is controlled by the mitotic spindle which directs furrow formation by directing a local zone of RhoA activation. Additionally, the molecular components required to generate the local zone of RhoA activation during cytokinesis are quite well-defined. Nonetheless, there are several fundamental questions concerning Rho-mediated furrow formation that remain unanswered. Is the local activation of RhoA sufficient to

generate a cleavage furrow? Or are there additional factors required for furrow formation? Is RhoA activity self-sustaining during anaphase? We know the precise location and timing of furrow formation are highly regulated to ensure division occurs properly. Is this spatial and temporal regulation of furrow formation occurring at the level upstream regulators or directly on active RhoA or its downstream effectors? Answers to these questions required the ability to spatially and temporally manipulate RhoA activation. The goal of my thesis was to gain light-mediated regulation of the small GTPase RhoA via the novel optogenetic system, TULIPs, which was developed in our lab. Using this tool to manipulate RhoA activity with high spatial and temporal precision, I sought to determine whether local RhoA activation can induce contractile ring assembly and ingression and if so, how might this activity be regulated by cell cycle progression and position of the mitotic spindle, a potential source of many regulatory mechanisms.

## 1.7 Appendix 1

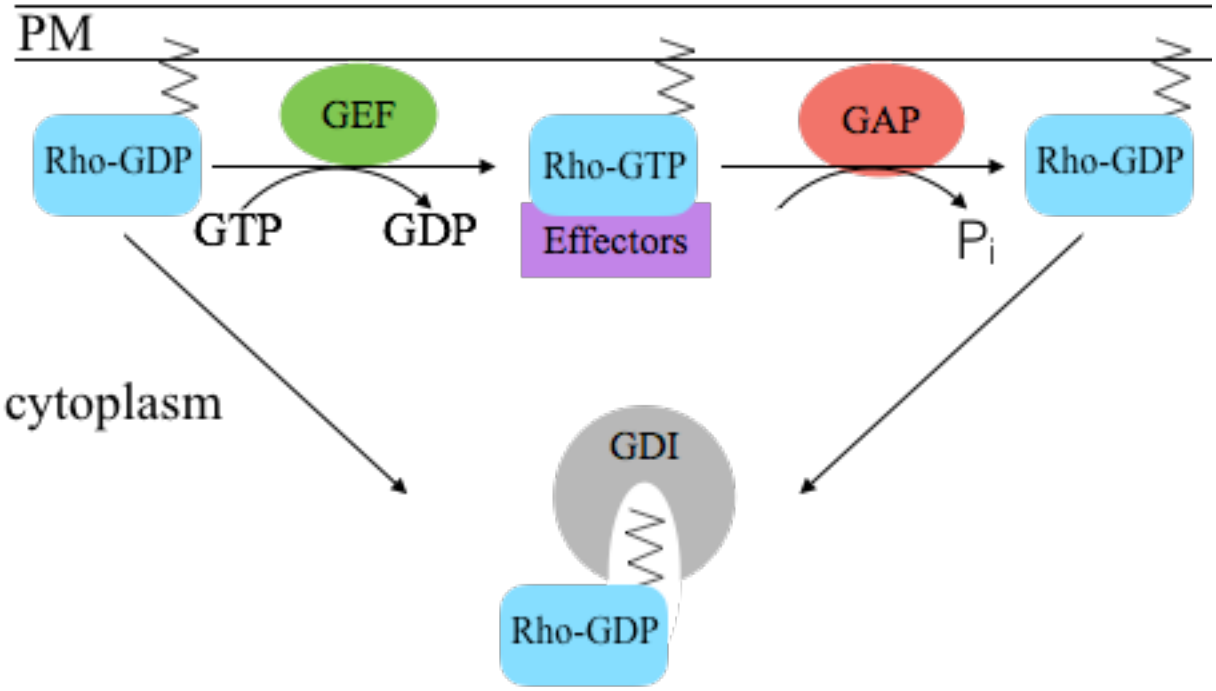


Figure1: Schematic of a Rho GTPase anchored to the membrane with a prenyl group near the carboxyl terminus (zigzag line). The GTPase binds either GDP or GTP. Guanine nucleotide exchange factors (GEFs) catalyse the release of GDP from the GTPase, allowing GTP to bind. GTPase-activating proteins (GAPs) increase the intrinsic GTPase activity of the Rho proteins, causing GTP to be hydrolysed to GDP and phosphate ($P_i$). GDP-bound Rho proteins can be sequestered by Rho guanine nucleotide dissociation inhibitors (GDIs), which bind to the prenyl group and thereby inhibit membrane binding of the GTPase. GTP-bound Rho proteins transduce signals by binding to effector proteins.

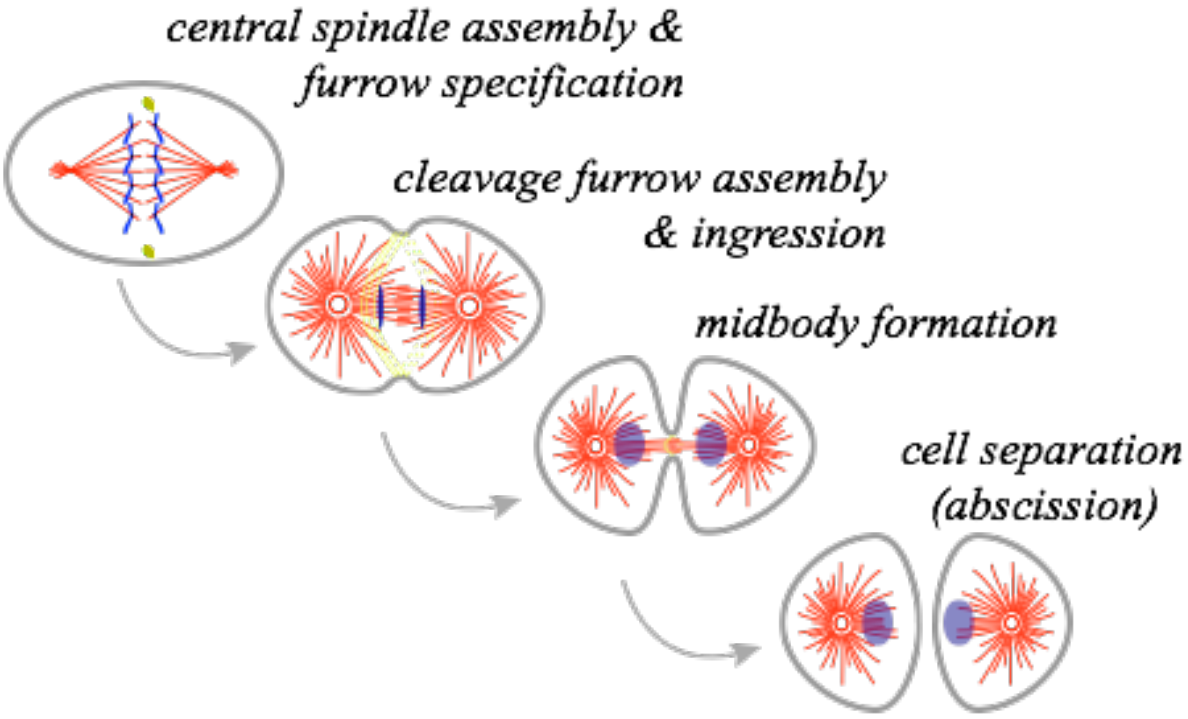


Figure 2: Schematic of stages of cytokinesis in animal cells. In early anaphase a subset of non-kinetochore microtubules become bundled to form the central spindle. The central spindle, together with the microtubule asters specify the position of local GTPase RhoA activation (yellow asterisk). RhoA activation promotes assembly of the actomyosin based contractile ring which ingresses until it reaches and forms the midbody. The last stage the midbody structure assembles factors required for abscission, which is the physical cutting of the cell into two.

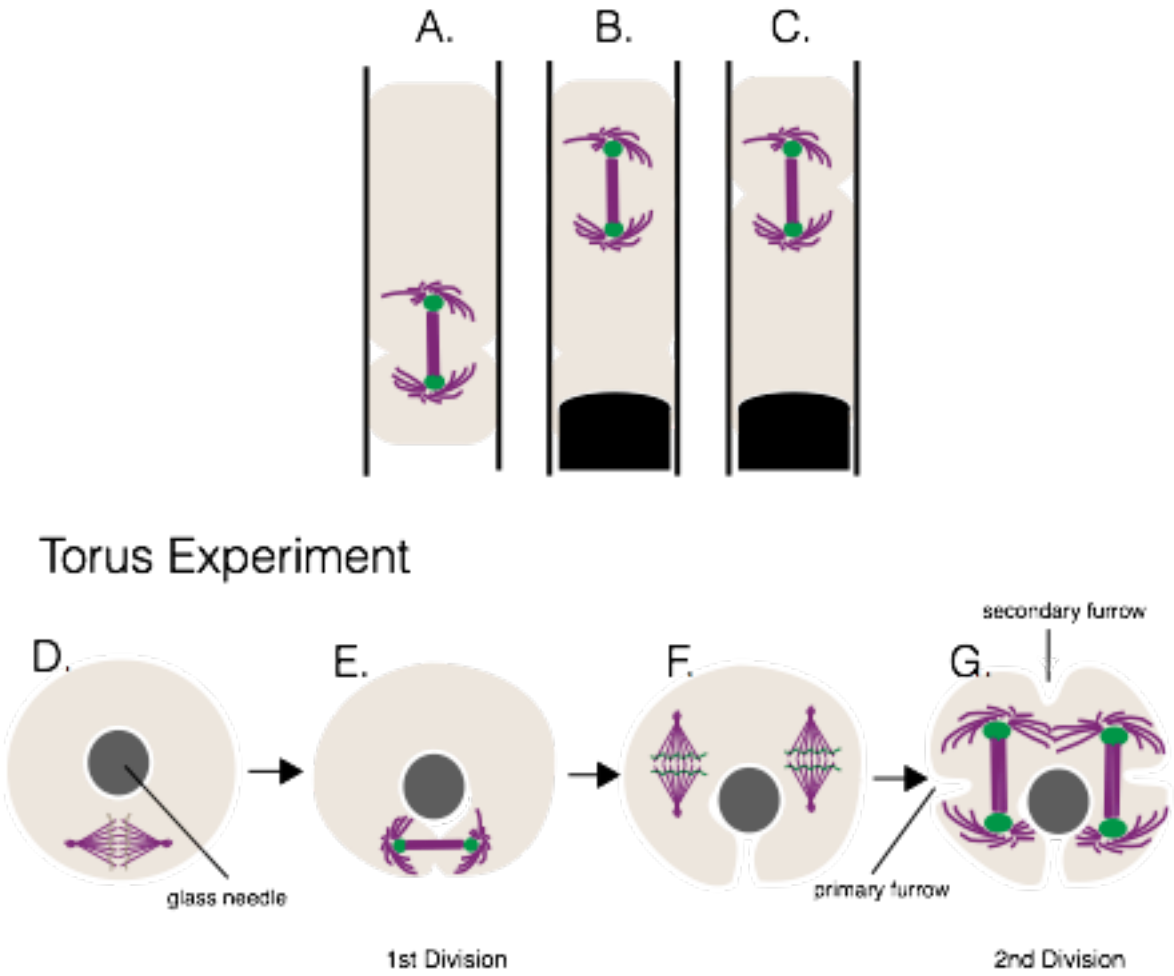


Figure 3: Rappaport Experiments 1. Cylinder Experiment. Sand dollar embryos were confined in silicone tubes (A).Furrow initiation occurs relative to the position of the mitotic spindle (B) Using a glass ball the mitotic apparatus is shifted within the embryo and depending on the timing the initial furrow either regressed or persisted. (C) A new furrow is initiated relative to where the mitotic apparatus has been shifted. 2. Torus Experiment (D) A sand dollar embryo was deformed into a torus (donut) using a glass needle. (E,F) The first cell division occurred between segregating chromosomes, generating a horseshoe-shaped binucleate cell. (G) At the second division, in addition to the furrows dividing the segregating chromosomes (primary furrows), another furrow appeared between the asters that were not connected by a spindle (secondary furrow).

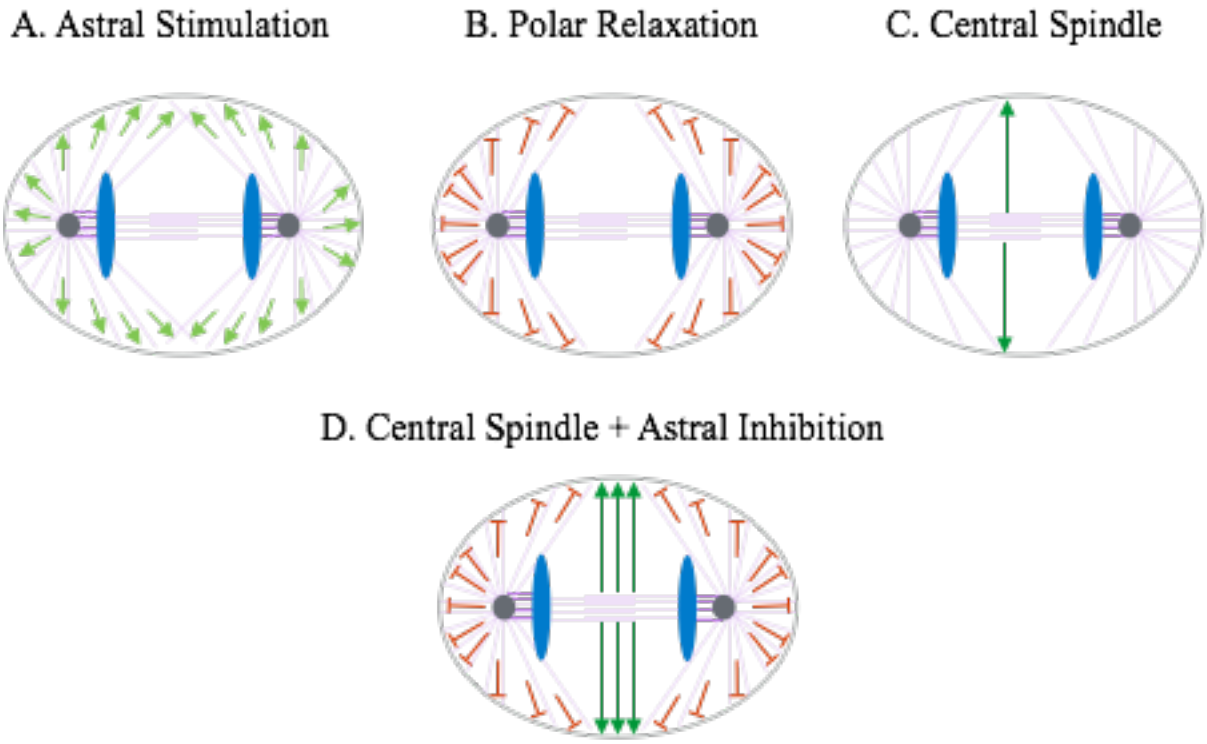


Figure 4: Schematic representation of models for cleavage furrow induction. Models of cleavage furrow induction differ based on the part of the mitotic apparatus responsible for delivering and the nature (stimulating or relaxing cortical contractility) of the hypothetical cleavage signal.

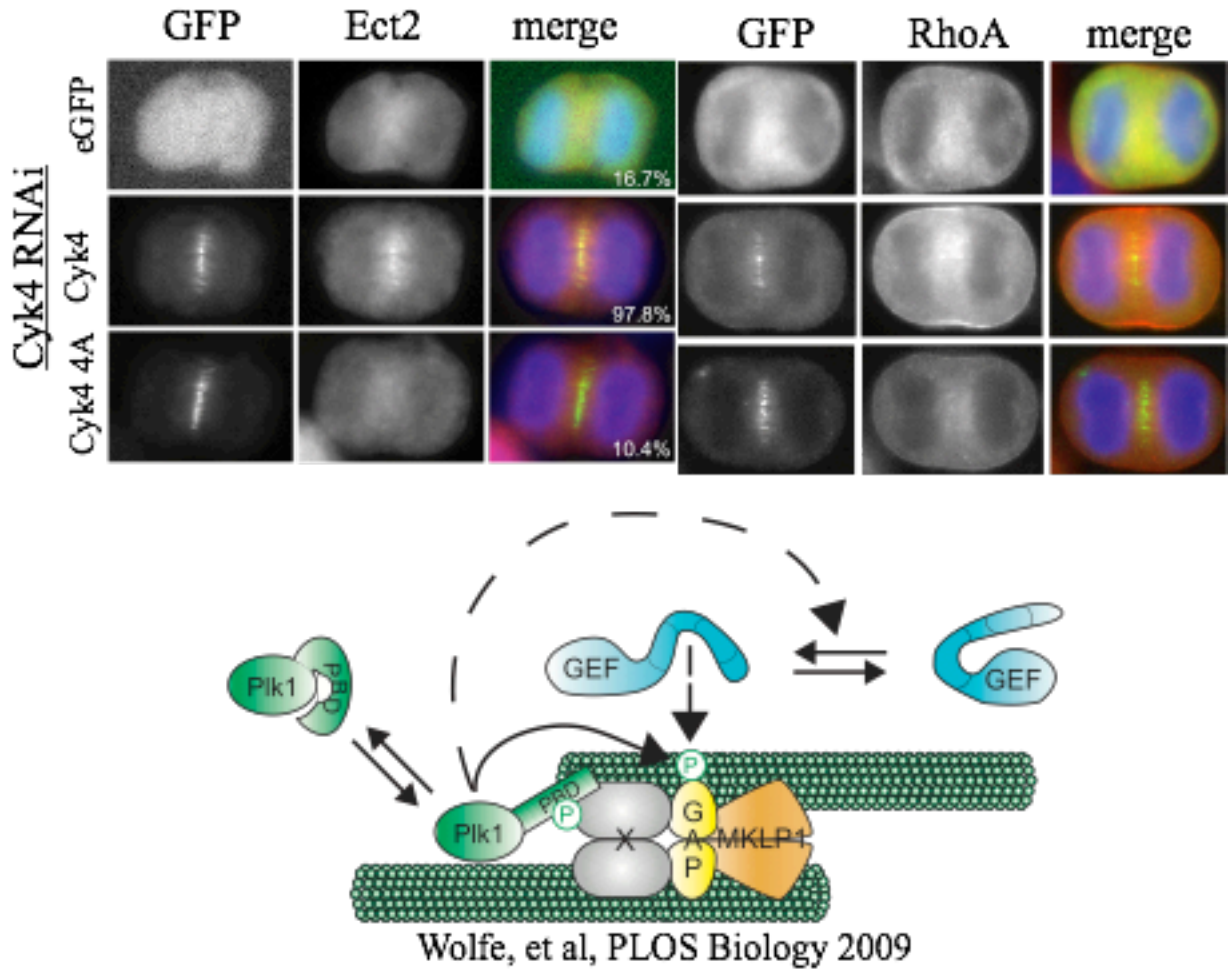


Figure 5. Phosphorylation of Cyk4 is necessary for Ect2 association. (A) The indicated stable cell lines transfected with siRNA to deplete endogenous Cyk4 were fixed and stained with Ect2 and GFP antibodies, and DNA was stained with DAPI. Percentages indicate the fraction of anaphase cells displaying "positive" Ect2 central spindle localization. (B) The indicated stable cell lines transfected with siRNA to deplete endogenous HsCyk-4 were fixed and stained with antibodies to RhoA and GFP, and DNA was stained with DAPI. (C) Proposed model. At the central spindle, microtubules are bundled through the combined efforts of the centralspindlin complex and Prc1. Prc1, Mklp2, centralspindlin, or an unknown factor, recruits Plk1 to the central spindle through association with its PBD, freeing the kinase domain to phosphorylate substrates at the central spindle (e.g., Cyk-4, Ect2). Phosphorylated Cyk4 binds to tandem BRCT domains of Ect2. Cyk4:Ect2 interaction is required for localizing Ect2 to the central spindle as well possibly relieving autoinhibition.

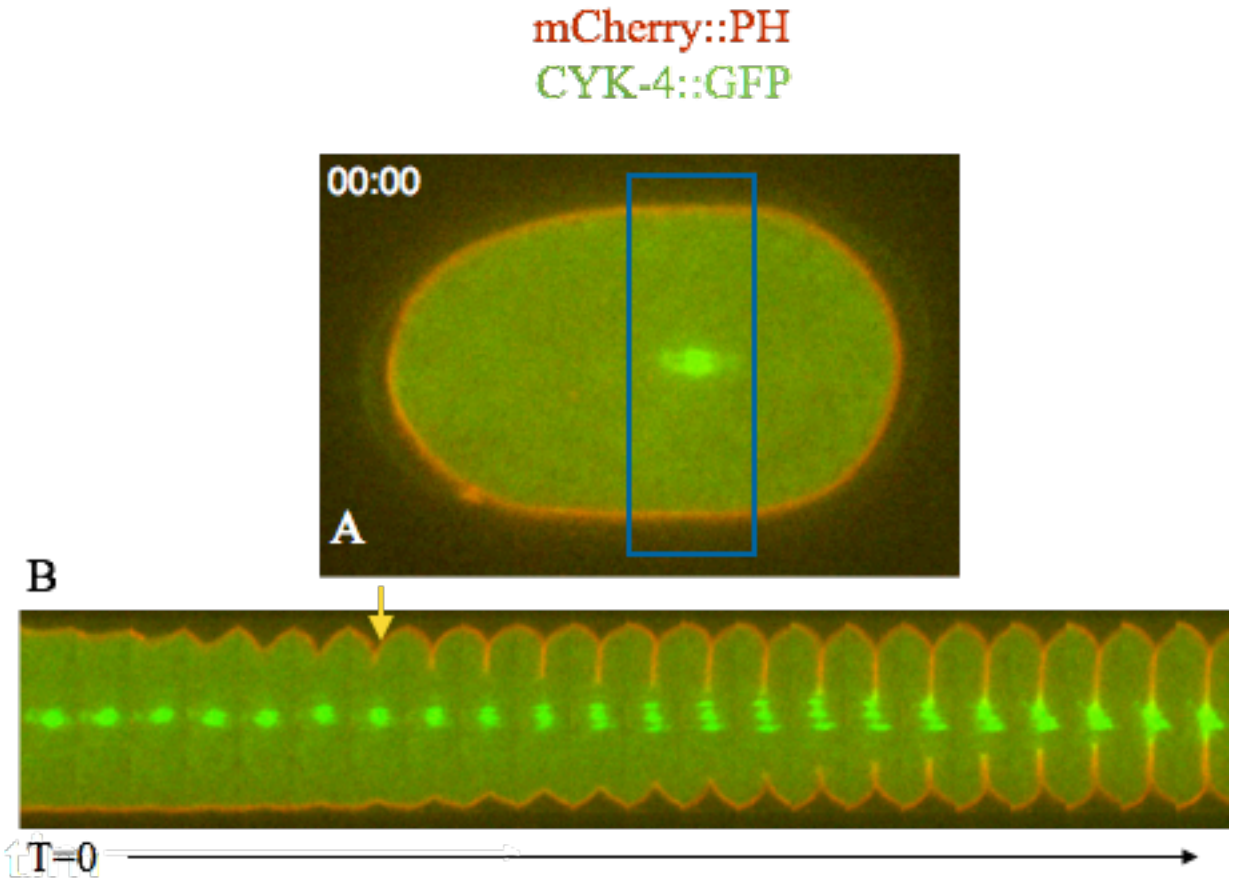


Figure 6: Cortical accumulation of Centralspindlin (A) C. elegans embryo expressing a mCherry::PH membrane marker with an RNAi-resistant wild-type CYK-4::GFP transgene was depleted of endogenous CYK-4 by RNAi. This embryo was filmed starting at metaphase in the first division cycle. (B) Shown are montages of the equatorial region (blue box) as the cell divides. The arrow indicates the appearance of cortical CYK-4::GFP under wild-type conditions. Scale bar, 10 μm.

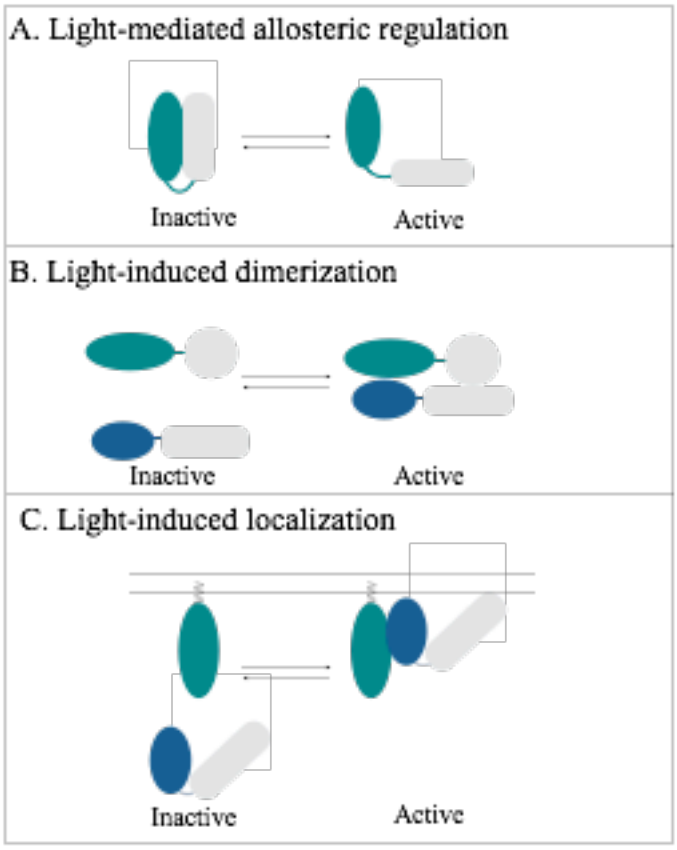


D.

| Photoactivatable Protein | Size (amino acid) | Cofactor | Association/ dissocation wavelength(nm) | Association/ Dissoction time |
|---|---|---|---|---|
| PhyB/PIF | 908/100 | PCB ** | 650/750 | s/s |
| Cry2/CIB | 498/170 | FAD | 450/dark | s/6-10min |
| LOV | 150 | FMN | 450/dark | s/1-2 min |

Figure 7 Models of light-regulated Protein Activity (A) Protein activity can be put directly under light control by fusion to light-responsive domains or residues (Blue). Upon stimulation with light, allosteric inhibition is removed, leading to activation. (B,C) Protein activity can be indirectly controlled using light-dependent anchoring to a subcellular compartment (B) or dimerization (C).(D) Characterization of photosensitive proteins or protein pairs utilized in optogenetic systems.

## Chapter 2: Design and validation of the optogenetic tool TULIPs in yeast and mammalian cells

### 2.1 Preface/Abstract

The development and optimization of the opotogenetic tool, TULIPs, in yeast was performed by a previous post-doc Devin Strickland. This chapter is his work, which was published in Nature Methods (2012). My contribution to the paper was to transition and demonstrate the functionality of the TULIP system in mammalian tissue culture cells. Although this was a relatively small part of the paper, it was a critical requirement of the reviewers for publication.

Title: TULlIPs: tunable, light-controlled interacting protein tags for cell biology

Devin Strickland[1], Yuan Lin[2], Elizabeth Wagner[1], C Matthew Hope[1], Josiah Zayner[3], Chloe Antoniou[3], Tobin R Sosnick[3–5], Eric L Weiss[2] & Michael Glotzer[1]

[1]Department of Molecular Genetics and Cell Biology, The University of Chicago, Chicago, Illinois, USA. [2]Department of Molecular Biosciences, Northwestern University, Evanston, Illinois, USA. [3]Department of Biochemistry and Molecular Biology, The University of Chicago, Chicago, Illinois, USA. [4]Institute for Biophysical Dynamics, The University of Chicago, Chicago, Illinois, USA. [5]Computation Institute, The University of Chicago, Chicago, Illinois, USA.

**Abstract:**

Cells integrate intra- and extracellular cues to move, form tissues, and divide by assembling protein–protein complexes at specific times and locations. Naturally photoswitchable proteins offer a means of directly manipulating the formation of these complexes. We have developed tunable light-inducible dimerization tags (TULIPs) based on a synthetic interaction between the LOV2 domain of Avena sativa phototropin 1 (AsLOV2) and an engineered PDZ domain (ePDZ). TULIP tags can recruit proteins to diverse structures in living yeast and mammalian cells, either globally or with precise spatial control using a steerable laser. The equilibrium binding and kinetic parameters of the interaction are tunable by mutation, making TULIPs readily adaptable to signaling pathways with varying sensitivities and response times. We demonstrate the utility of TULIPs by conferring light sensitivity to functionally distinct components of the yeast mating pathway and by directing the site of cell polarization.

## 2.1 Introduction

Cells commonly interpret developmental cues through assemblies of structural and signaling proteins that are built up from a combination of transient protein-protein and protein-membrane interactions(Hartman and Groves, 2011). These interactions can enforce the proximity of reactant species (for example, a kinase and its substrate) or spatially constrain molecules in the cell to create a polarized response. Designed photoactivatable proteins offer unprecedented spatial and temporal control of cellular signaling processes(Toettcher et al., 2011). For example, a fusion of the small GTPase Rac1 and the photosensor AsLOV2 allows direct control of Rac1

activity in living tissues and has led to ground-breaking experiments on polarity and motility (Wang et al., 2010b; Wu et al., 2009; Yoo et al., 2010). Nevertheless, direct fusion does not always confer photoactivatable control on proteins of interest, even with case- by-case optimization (Wu et al., 2009).

The ubiquity and modularity of protein-protein and protein- membrane interactions suggests that light-inducible interactions should be an especially flexible tool for triggering cellular signaling events precisely in space and time, thereby obviating the need to optimize the caging of individual proteins. Several groups have adapted light-inducible protein-protein interactions that occur naturally in Arabidopsis thaliana for use as cell-biological reagents (Kennedy et al., 2010; Levskaya et al., 2009; Yazawa et al., 2009). Whereas each of these methods has attractive features, all have drawbacks. For example, a method based on FKF1 and GIGANTEA requires a large photosensory protein (1,173 amino acids) and has slow association (minutes) and dissociation (hours) kinetics (Levskaya et al., 2009). Another method, based on the large photosensory domain (908 amino acids) of phytochrome B and its interacting factor PIF6, dimerizes within seconds upon illumination with 650-nm light, but recovery requires hours unless dissociation is accelerated by 750-nm light, and precise spatial control requires simultaneous, two-wavelength illumination (Yazawa et al., 2009). A third method, based on cryptochrome 2 and CIB1, features small domains (498 amino acids and 170 amino acids, respectively) that dimerize in 10 s upon illumination and dissociate in 10 min(Kennedy et al., 2010). However, it remains unclear whether the proteins can be used for spatially resolved control of cell signaling (Kennedy et al., 2010). More broadly, the basis of all three light-mediated interactions remains poorly characterized, and the ability to tune important physical parameters is limited.

An ideal light-inducible protein-protein interaction for optogenetics should use small, genetically encoded interacting domains that do not require exogenous cofactors. It should exhibit switching between biologically relevant binding affinities on a range of timescales. Its components should be compatible as fusions to a variety of subcellular markers, and it should be possible to confine photoactivation to a small region of the cell. We set out to create optogenetic dimerization tags with these properties using small, well-characterized interacting domains. We show that the resulting system, TULIPs, is a versatile and tunable optogenetic tool to localize proteins to specific regions of yeast or mammalian cells and to trigger specific cellular-signaling pathways. TULIPs can regulate the activity of nucleotide-exchange factors, scaffold proteins and kinases, all by recruitment to the plasma membrane.

**2.2 Photoswitch Design**

As a photosensor, we chose the second light-oxygen-voltage (LOV) domain of A. sativa phototropin 1 (AsLOV2) (Christie et al., 1998). LOV domains are small (~125-residue) photosensory domains based on a Per-ARNT-Sim (PAS) core that binds a flavin cofactor. Like many PAS domains, AsLOV2 features flanking N- and C-terminal α helices (the A′α and Jα helices, respectively) (Halavaty and Moffat, 2007; Harper et al., 2003). Upon photo- excitation with blue light (<500 nm), the Jα helix undocks from the LOV core and unfolds(Harper et al., 2003; Yao et al., 2008). This conformational change is critical to phototropin signaling and has been exploited in designed photosensors (Harper et al., 2004; Strickland et al., 2008; Wu et al., 2009). Many mutational (Christie et al., 2007; Strickland et al., 2010; Zoltowski et al., 2009)and chemical (Alexandre et al., 2007) methods of tuning the physical properties of AsLOV2 have been reported.

Following a broadly successful approach for making engineered photoreceptors (Möglich and Moffat, 2010), we reasoned that fusion of a peptide epitope to the C terminus of the Jα helix would allow the LOV2-Jα interaction to sterically block or cage the epitope from binding to a cognate PDZ domain (Fig. 8a and Supplementary Fig. 1). We anticipated that caging would require sequence overlap so that part of the epitope would adopt a binding-incompetent α-helical conformation in the dark, Jα-docked state (Strickland et al., 2008) (Supplementary Note 1). As a binding partner, we used high-affinity, high-specificity engineered variants of the Erbin PDZ domain (Huang et al., 2008). These clamshell-like 'ePDZ' chimeras (194 amino acids) are highly tunable; mutational variants of ePDZ and its cognate peptide vary in interaction affinity from ~0.5 nM to >10 μM(Huang et al., 2009).

We designed five AsLOV2-peptide fusions for initial screening (Supplementary Fig. 2a and Supplementary Note 1) by appending a peptide epitope (–SSADTWV–COOH) to serial truncations of the Jα helix. We fused these with GFP (the GFP(S65T) variant) and the transmembrane protein Mid2 and expressed the constructs with monomeric (m)Cherry-tagged ePDZ (Fig. 8b). We assayed recruitment of ePDZ-mCherry to the plasma membrane in the dark and immediately after photoexcitation with a 473-nm laser. To quantify the plasma membrane association of ePDZ-mCherry, we measured the ratio of plasma membrane and cytoplasmic fluorescence, averaged over a population of cells ($\langle R_{obs} \rangle$; Supplementary Fig. 3 and Online Methods). For the longest AsLOV2-peptide fusions (registers 1–3; Supplementary Fig. 2a), $\langle R_{obs} \rangle$ was relatively high in both the dark and photoexcited states, and photoswitching was slight (Supplementary Fig. 2b). Binding was diminished for the shorter fusions (registers 4 and 5; Supplementary Fig. 2a), probably because more of the epitope was masked in the Jα-docked

conformation. Both constructs exhibited greater binding in the lit state than in the dark, indicating light-directed plasma membrane recruitment of ePDZ-mCherry.

### 2.3 Subcellular Recruitment

We modified the register 4 construct to make the sequence more favorable for ePDZ binding and LOV-Jα docking, and named the construct LOVpep (Supplementary Fig. 2a and Supplementary Note 1). Using this construct, plasma membrane recruitment to Mid2 was reversible on minute timescales and capable of repeated cycles of photoexcitation (Supplementary Fig. 4). Using a steerable 440-nm laser to illuminate small (~250 nm) regions, we could reliably and reversibly recruit ePDZb1-mCherry (a high-affinity ePDZ variant fused to mCherry) to a cortical patch (Fig. 7c). After localized recruitment, global plasma membrane recruitment could be stimulated by global photoexcitation (Fig. 8c).

We used LOVpep fusions to recruit ePDZb-mCherry (a low affinity ePDZ variant fused to mCherry) to various subcellular compartments. We tethered GFP-LOVpep to proteins with distinctive localizations, including Hof1 (bud neck), Pil1 (eisosomes) and Pma1 (plasma membrane) (Huh et al., 2003). The GFP-LOVpep fusions localized as expected (Fig. 8d). ePDZ-mCherry was predominantly cytoplasmic in the dark and localized with GFP-LOVpep upon global photoexcitation.

We also tested TULIPs in cultured HeLa cells. We fused GFP-LOVpep to the plasma membrane localization signal from Lyn kinase(Inoue et al., 2005) and to the mitochondrial outer membrane protein Tom70 (Huh et al., 2003), and expressed each of these with ePDZb1-mCherry. In the dark, ePDZb1-mCherry was diffuse in the cytoplasm and nucleoplasm (Fig. 8e and

Supplementary Fig. 5). Upon global blue-light stimulation, ePDZb1-mCherry localized with GFP-LOVpep (Fig. 8e). The translocation was reversible for at least three cycles of illumination and recovery. Using spot photoexcitation, we could recruit ePDZb1-mCherry to the mitochondria or plasma membrane in a confined region of the cell (Fig. 8e).

**2.4 Mutational Tuning of affinity and kinetics**

The docking equilibrium of the LOV–Jα interaction can be changed by mutations, which enables modulation of the dynamic range of effector activity (Strickland et al., 2010). We tested previously described AsLOV2 mutations that either decrease (V529N) (Yao et al., 2008) or increase (I532A(Strickland et al., 2010) and T406A,T407A (J.Z., C.A. and T.R.S., unpublished data)) helix docking (Fig. 9a). In addition to ePDZb and ePDZb1, we also evaluated recruitment of PDZ-mCherry to explore lower binding affinities. For most recruited proteins, the V529N mutation increased both the lit- and dark-state values of $<R_{obs}>$, indicating increased binding (Fig. 9b). In the case of PDZ-mCherry recruitment, dark-state binding was effectively undetectable for LOVpep and the V529N mutant. The T406A,T407A double mutation, which stabilizes the N-terminal A′α helix of AsLOV2 and increases Jα docking affinity, decreased $<R_{obs}>$ for ePDZb- mCherry recruitment, in both the lit and dark states. The T406A,T407A mutation increased $<R_{obs}>$ for ePDZb1-mCherry recruitment (and slightly for dark-state PDZ-mCherry recruitment), perhaps owing to adventitious interactions between the mutated LOV domain and ePDZb1. When paired with ePDZb or ePDZb1, the I532A mutation decreased $<R_{obs}>$ relative to that of the T406A,T407A variant. We also tested mutations in the peptide epitope that have been shown to diminish binding to ePDZ (Supplementary Note 1 and Supplementary Fig. 6). Most previously described mutations in AsLOV2, ePDZ and the peptide

epitope exhibited predictable effects on the LOVpep-ePDZ interaction, thereby supporting our design principle (Fig. 9b and Supplementary Fig. 6). The variants provide a range of experimentally accessible dimerization affinities.

The maximum temporal resolution of experiments using ePDZ-LOVpep depends on the lifetime of the light-recruited complex. When photoexcitation ceases, light-recruited ePDZb fully dissociates from LOVpep within a few minutes in vivo (observed rate constant, $k_{obs}$ = 0.041 $s^{-1}$; Supplementary Table 1). We investigated whether this observed dark-state dissociation rate ($k_{obs}$) follows the LOVpep dark-state recovery rate ($k_{phot}$) or the intrinsic ePDZ-peptide dissociation rate ($k_{diss}$). The rate $k_{diss}$ is slower for ePDZb1 than for ePDZb when binding to model peptide substrates in vitro (~$10^{-4}$ $s^{-1}$ and ~$10^{-2}$ $s^{-1}$, respectively) (Huang et al., 2008). However $k_{obs}$ was remarkably similar for ePDZb-mCherry and ePDZb1-mCherry (Supplementary Table 1). Using a mutated LOVpep(V416I) with approximately tenfold slower dark-state recovery (Zoltowski et al., 2009), $k_{obs}$ was again similar for the ePDZb- mCherry and ePDZb1-mCherry, and both rates were similar to the slower $k_{phot}$. To test whether $k_{obs}$ can be increased, we chemically accelerated $k_{phot}$ by adding imidazole to the medium (Alexandre et al., 2007). As with mutational tuning, changes in $k_{obs}$ generally tracked changes in $k_{phot}$ (Fig. 9c). Taken together, the data indicate that mutational or chemical modulation of the dark-state recovery of LOVpep also controls $k_{obs}$.

These data are compatible with two models: either the ePDZ- LOVpep complex persists as long as the lit state, or the bound ePDZ rapidly exchanges with the unbound pool. To distinguish between these, we observed ePDZ-mCherry dissociation from a locally photoexcited spot. Spot

recruitment did not deplete the unbound pool; therefore the LOVpep occupancy was higher than during global recruitment (Fig. 8c). The dissociation of spot-recruited ePDZ-mCherry followed single-exponential kinetics with a rate similar to $k_{phot}$ when left unperturbed but followed biphasic kinetics when the cytoplasmic pool was rapidly depleted by global photoexcitation after a few seconds (Fig. 9d, Supplementary Table 2). Most of the bound ePDZ-mCherry dissociated quickly, but the remainder dissociated slowly with a rate matching $k_{obs}$ and $k_{phot}$. Taken together, the data suggest that bound ePDZ rapidly exchanged with the unbound pool. When the unbound pool was quickly depleted by global recruitment, the amount of spot-recruited ePDZ was above the new equilibrium value. Re-equilibration occurred with the rapid dissociation of ePDZ, whereas the equilibrium itself changed slowly as the LOVpep reverted to the low affinity dark state with the rate $k_{phot}$. Fast dissociation kinetics and a continuously tunable photoexcitation lifetime are potentially desirable features for an optogenetic tool because together they allow precise temporal control in biological experiments.

**2.5 Optical control of MAPK activation and polarity**

We asked whether TULIPs can be used for light-activated cellular signaling. The yeast mating pathway normally is initiated by binding of a peptide pheromone to a G protein–coupled receptor (GPCR) (Fig. 10a). Downstream, components of two conserved signaling modules are recruited to the plasma membrane by the activated G protein: one comprising a mitogen activated protein kinase (MAPK) cascade organized by the scaffold Ste5 and the other comprising the GTPase Cdc42 and its associated scaffolds, guanine nucleotide exchange factor and effectors. The MAPK module, whose activation leads to G1 arrest and transcription of mating-specific genes, has been extensively engineered in attempts to elucidate its workings(Pryciak, 2009). Notably,

tethering Ste5 or Ste11 to the plasma membrane robustly activates the pathway(Pryciak and Huntress, 1998; Winters et al., 2005). The Cdc42 module is required for polarized growth in budding yeast, and its activation is usually constrained by intrinsic or extrinsic spatial cues(Park and Bi, 2007). Disruption of Cdc42-mediated polarization in vegetatively growing cells prevents budding, but not isotropic growth, and leads to an enlarged terminal phenotype(Park and Bi, 2007).

We screened a variety of MAPK- and Cdc42-associated proteins for growth defects upon plasma-membrane recruitment. We performed initial experiments with a constitutively active LOVpep variant (LOVpep$^{CA}$) fused to Mid2 and under control of the galactose-inducible GAL1 promoter. Several proteins, when fused to ePDZb caused growth arrest upon galactose- induced expression of LOVpep$^{CA}$ (Supplementary Fig. 7).We next asked whether light-dependent recruitment of ePDZb- Ste5ΔN (Ste5ΔN is a truncated protein deficient in G-protein binding(Pryciak, 2009)) and ePDZb-Ste11 could cause MAPK pathway activation (Fig. 9a). There was little or no detectable dark-state growth arrest upon galactose induction over a range of expected affinities (Supplementary Fig. 8), indicating that the ePDZb-LOVpep interaction is well caged in the dark with respect to biological activity. However, continuous illumination caused growth arrest in some strains and the extent of arrest corresponded with the expected affinity of the LOVpep variant (Supplementary Fig. 8).

To characterize the phenotype, we illuminated cells for 4 h in liquid culture and then examined them by microscopy and flow cytometry. As expected, αF-stimulated control cells formed mating projections (shmoos) and transcribed a FUS1 promoter driven DsRed-Max reporter gene(Strack et al., 2008); these cells also did not show light-stimulated pathway activation (Fig.

10b and Supplementary Fig. 9). For ePDZb-Ste5ΔN recruitment, highly caged LOVpep variants did not measurably activate the pathway (Fig. 9b and Supplementary Fig. 9). This level of dark-state suppression is consistent with our previous observation that strong Jα docking can suppress effector activity even under full photoexcitation(Strickland et al., 2010). In contrast, less strongly caged LOVpep variants allowed more robust light-dependent cell-cycle arrest and polarized growth, presumably because the weaker peptide caging leads to greater Ste5ΔN recruitment. Conversely, more caging was required to bring ePDZb-Ste11 recruitment into a sensitive range, with the less caged variants causing constitutive activation (Fig. 10b and Supplementary Fig. 9). Light-stimulated cells were less polarized than αF-stimulated cells, even though both had stopped forming buds (Fig. 10b).

To determine whether TULIPs can also control GTPase signaling pathways, we examined light-directed recruitment of Cdc24- ePDZb1 to Mid2-GFP-LOVpep. Global recruitment caused a growth arrest with a terminal phenotype of large, round cells that depended on the strength of the ePDZ–peptide interaction (Supplementary Fig. 10). The ability of full-length Cdc24 to block polarization upon global recruitment was surprising as earlier work indicated that the protein was autoinhibited(Shimada et al., 2004). This discrepancy could result from the efficiency with which the protein was recruited (Supplementary Fig. 10).

To determine whether plasma membrane–localized Cdc24 is active, we locally recruited Cdc24-ePDZb1 to specify the direction of polarized growth. Indeed, we could specify the orientation of mating projection growth in αF-arrested cells (Fig. 10c), suggesting that the GEF was intrinsically active. This result demonstrated that the TULIPs system can be used to control the activity of signaling molecules with high spatial precision, even in small (~5 μm diameter) cells.

## 2.6 Discussion

Our approach, though conceptually similar to other strategies 6–8 including alterations of the intrinsic affinity, the stability of Jα helix docking and the photocycle time, are available and can be easily incorporated into experiments (Online Methods and Supplementary Note 2). In principle, many activation mechanisms should be light-controllable using TULIPs, such as transcriptional regulation, enzyme-substrate enforced proximity and protein-fragment complementation.

Even in simple engineered systems, small changes in binding affinity can greatly impact function(Dueber et al., 2003). A failed or suboptimal implementation can be due to either design flaws or a poor choice of a parameter value, yet it is usually not obvious a priori which parameter values will be best. Just as electronics prototyping requires a ready assortment of resistors, capacitors and transistors with different characteristics, our experiments demonstrate that biological prototyping requires protein modules that are quantifiably tunable to ensure robust activation of a pathway of interest.

## 2.7 Methods

Plasmid and strain construction. S. Koide (University of Chicago) provided plasmids encoding ePDZ variants. B. Glick (University of Chicago) provided plasmids encoding PMA1 and DsRedMax. F. Cross (Rockefeller University) provided a plasmid encoding the Gal4-rMR construct. All ARS/CEN plasmids used in this study were from the pGREG series(Jansen et al., 2005). All integrating plasmids were of the YIplac series(Gietz and Sugino, 1988). The MET25, TEF, and ADH promoters were from the PCR Toolbox plasmids(Janke et al., 2004). All other

yeast CDS were obtained by PCR from the Yeast Genomic Tiling Collection (Open Biosystems) or from genomic DNA.

DNA manipulations were simulated with a pre-release version of the SnapGene software (GSL Biotech). Plasmids were generated using a combination of conventional ligation, InFusion cloning (Clontech) and recombination in yeast(Jansen et al., 2005). Yeast were transformed using LiAc/SS-DNA/PEG(Gietz and Woods, 2002). All plasmids and strains were verified by colony PCR or DNA sequencing.

We constructed the background strain YLS1254 by integrating a Gal4-rMR expression cassette(Picard, 2000) into W303 MATa so as to delete the endogenous TRP1 coding sequence using a URA3 marker, which was itself subsequently deleted(Storici and Resnick, 2006). We then integrated a C-terminal mCherry tag at the endogenous ABP1 coding sequence using a HIS3MX marker(Longtine et al., 1998).

Affinity, caging and switching. We use the term “intrinsic affinity” to denote the intrinsic affinity of binding between a photoactivated, helix-undocked LOVpep and free ePDZ (Supplementary Fig. 1). We use the term “caging” for the diminishment of LOVpep–ePDZ binding in the dark state. Quantitatively this is the ratio of the dark-state dissociation constant to the intrinsic dissociation constant. We use the term “switching” to refer to the ratio of the dark- and lit-state dissociation constants. Because it is possible for a highly stabilized helix to remain substantially docked to the LOV core even in the lit state, caging and switching may have different values.

However, caging is always numerically greater than or equal to switching. We use the term "overall affinity" to refer to the observed affinity of the reaction scheme depicted in Fig. 8a.

Peptide epitope design considerations. The Erbin PDZ domain binds specifically to the last four amino acids of a peptide (–3 to 0). In ePDZ fusions the specificity is extended to include the last eight amino acids (–7 to 0), but most of the binding energy derives from specific interactions with the last five amino acids(Huang et al., 2009). Notably, the sequence specificity of ePDZ is somewhat relaxed in the –4 to –7 positions, and we reasoned that these amino acids should be selected to be compatible with both Jα docking and ePDZ binding.

One important limitation of the current implementation is that ePDZ proteins only bind to C-terminal peptides; thus, LOVpep must be used as a C-terminal tag. However, ePDZ is functional as either an N- or C-terminal tag. A second potential limitation is that ePDZ or the peptide epitope may interact with endogenous PDZ domains or targets(Huang et al., 2008). However, we have not detected such interactions in HeLa cells (Supplementary Fig. 5) and future implementations of TULIPs may be able to circumvent both limitations.

Plasma membrane recruitment assay. We used a plasma-membrane recruitment assay in living yeast to assess the lit- and dark-state binding between ePDZ and the LOV–peptide fusions. We fused GFP–AsLOV2–peptide constructs to the C-terminus of the integral plasma membrane protein Mid2(Huh et al., 2003). We expressed the $P_{TEF}$–Mid2–GFP–LOVpep constructs from ARS/CEN plasmids maintained with a LEU2 or KanMX marker. Generally, GFP fluorescence was cleanly and evenly localized to the plasma membrane and accumulation in endocytic

compartments was minimal. Sometimes GFP fluorescence was also localized to the vacuole or nuclear periphery, but this was always less intense than the plasma membrane signal.

We co-expressed the LOV–peptide constructs with mCherry-tagged ePDZ (Fig. 8b). To ensure that binding affinity was in a sensitive range for the assay, we used moderate- and high-affinity ePDZ variants (ePDZb and ePDZb1, respectively, having a 10-fold difference in affinity for model peptides) (Huang et al., 2008). We expressed $P_{TEF}$ –ePDZ–mCherry or $P_{TEF}$ –PDZ–mCherry constructs from a plasmid integrated at the URA3 locus. We found that this combination of ARS/CEN and integrating plasmids provided the most consistent expression levels as judged by GFP and mCherry fluorescence levels. Diploid JK9-3d strains harboring both plasmids were constructed by mating singly transformed haploids and selecting on SD –LEU –URA.

We grew cells in liquid culture (YPD + G418), then pelleted and resuspended in minimal media. We plated 3 μL on a 2 × 2 × 0.1 cm, 1.2% agar pad made with the same media. We then placed a #1.5 coverslip over the pad and sealed the edges with petroleum jelly(Gibson et al., 2009). We imaged the cells on an Axiovert 200M microscope (Zeiss) equipped with a spinning disk confocal (CSU10, Yokogawa) and an EMCCD camera (Cascade 512B, Photometrics) using a 63 ×, 1.4 NA objective. The microscope was controlled using MetaMorph (Molecular Devices). We placed a 550 nm long pass filter (Edmund Optics) in the transmitted light path to avoid photoexciting the LOV domain when using phase contrast.

We assayed recruitment of ePDZ–mCherry to the plasma membrane in the dark and immediately after photoexcitation with a 473 nm laser. To quantify the plasma membrane association of ePDZ–mCherry, we measured the ratio of plasma membrane and cytoplasmic fluorescence, averaged over a population of cells ($<R_{obs}>$, below & Supplementary Fig. 3). We used an ImageJ macro to quantify recruitment with minimal user intervention. Because the algorithm works best with individual cells or mother-daughter pairs that are well-separated from other cells, we searched for fields of well-separated cells using Nomarski illumination. We then took a 500 ms image of mCherry fluorescence, and a 125 ms image of GFP fluorescence. We used an additional 1 s pulse (473 nm) to ensure the LOV domain was fully photoexcited (see below for more on light requirements). For basic recruitment assays, we took a single 500 ms image of mCherry fluorecence after a 1–10 s delay to allow recruitment to reach the maximum level. For kinetic assays, we acquired a time lapse of 500 ms images.

Quantification included the following steps: First, a stack registration plugin (StackReg(Thorn, 2010)) corrected for stage drift. This was especially important for long time lapse imaging in kinetic assays. Second, a thresholding method automatically defined regions of interest (ROIs) for the plasma membrane, cytoplasm, and background based on the GFP image (Supplementary Fig. 9a). There was no user intervention in defining the ROIs, but cells that were not thresholded accurately (e.g. because of nearby dust particles) were discarded. Third, for each frame of a given cell the average, background-subtracted intensities were measured in the plasma membrane, cytoplasm ROIs. The ratio of the plasma membrane and cytoplasm intensities ($R_{obs}$) were also calculated. Notably, the background autofluorescence of the media and the cellular mCherry fluorescence have different photobleaching properties. Because $R_{obs}$ is a ratio of two

background-subtracted values it is somewhat sensitive to this difference, and this sensitivity is especially apparent when photoexciting over multiple cycles. However, we have not attempted to correct for this phenomenon in any assays. We collated the data and calculated the mean, denoted $\langle R_{obs} \rangle$, and standard error for populations of cells using Excel (Microsoft), and plotted the data using Igor Pro (Wavemetrics).

Register series. We designed a series of five AsLOV2–peptide fusions for initial screening (Supplementary Fig. 2a). Because increased Jα docking affinity improves switching in designed AsLOV2-based photoswitches, we used an AsLOV2 variant with two helix stabilizing mutations, G528A and N538E, as a starting point for our fusions(Strickland et al., 2010). We used a seven amino-acid peptide epitope (SSADTWV–COOH) that retains the last four amino acids of the high affinity sequence (GSIDTWV–COOH) (Huang et al., 2009) but has more "neutral" amino acids in the –6 to –4 positions. In particular, we were concerned that the glycine at –6 would disrupt helix formation in the docked state, thereby uncaging the peptide. We therefore substituted a serine at this position, which selection experiments have shown to also have high-affinity binding(Huang et al., 2009). We were also concerned that the bulky isoleucine at –4 would interfere with helix docking in shorter constructs. We substituted an alanine at this position, which is known to substantially reduce affinity. However, we felt that this concern was outweighed by the benefit of avoiding potential uncaging. We appended the peptide epitope (–SSADTWV–COOH) to serial truncations of the Jα helix. In the longest of these fusions (Register 1), one amino acid overlaps the end of the Jα helix. We did not explore AsLOV2–peptide fusions shorter than Register 5 because mutation of Ile539 constitutively undocks the Jα helix(Harper et al., 2004).

For the longest AsLOV2–peptide fusions (Registers 1–3), $\langle R_{obs} \rangle$ was relatively high in both the dark and photoexcited states, and photoswitching was slight (Supplementary Fig. 2b). The notable exception was the case of Register 1 paired with ePDZb1. Binding was diminished for the shorter fusions (Registers 4 & 5), probably because more of the epitope is masked in the Jα-docked conformation. Both constructs exhibited greater binding in the lit state than in the dark, indicating light-directed plasma membrane recruitment of ePDZ–mCherry. Register 5 showed less binding than Register 4, suggesting that masking larger regions of the epitope leads to greater caging. It is unclear why the Register1–ePDZb1 construct undergoes photoswitching; potentially it is because adventitious interactions between ePDZb1 and Jα-derived residues increase the effective size of the epitope beyond eight residues.

Sequence of LOVpep. Once settling on the Register 4 construct, we modified it so as to make the sequence more favorable for ePDZ binding and LOV–Jα docking (LOVpep, Supplementary Fig. 2a). In particular, at position –4 valine is strongly favored over alanine for ePDZ binding(Huang et al., 2009). Because the corresponding position in the LOV domain (543) is conserved as either valine or alanine, we reasoned that this mutation would not affect helix docking very much. Conversely, ePDZ binding shows little discrimination at position –5 and –6(Huang et al., 2009). We therefore mutated the serine at –5 to alanine because alanine is conserved at this position (542) in LOV2 domains, and we mutated the serine at –6 to lysine to introduce a potentially helix-stabilizing i, i – 4 salt bridge with the glutamate at LOV2 position 537(Strickland et al., 2010). Specifically, “LOVpep” comprises residues 404–540 of AsLOV2, including the G528A and N538E mutations, fused to the C-terminal peptide KAVDTWV–COOH.

Mutational tuning of affinity. We asked whether mutations in the peptide epitope that weaken binding of model peptides in vitro (V–4A and T–2S(Huang et al., 2009)) would also show lower $<R_{obs}>$ in our in vivo assay (Supplementary Fig. 6). As in the register series assay, we used ePDZb1–mCherry and ePDZb–mCherry as the recruited proteins. Although the mutations behave somewhat differently in ePDZb and ePDZb1, the V–4A and T–2S mutations usually showed diminished binding; the V–4A,T–2S double mutant showed less than either single mutation. For any given peptide mutation, ePDZb1 usually showed higher binding than ePDZb. In in vitro assays, ePDZb1 binds to model peptides an average of 10-fold more tightly than ePDZb, and the V–4A mutation diminishes binding by 110-fold on average(Huang et al., 2009). Although we clearly detect the expected trends in binding affinity, the magnitude of the change in $<R_{obs}>$ is comparatively small. This difference may reflect an inherent insensitivity in our assay, or it may indicate that ePDZ interacts with LOVpep differently than with model peptides.

Interpretation of $<R_{obs}>$. Empirically, $<R_{obs}>$ ranges from ~ 0.35 to ~ 2.5. We estimated the lower value by globally evaluating multiple data sets. We found that $<R_{obs}>$ is never less than ~ 0.30, and all data approach a value of ~ 0.35 as the expected affinity decreases. We confirmed the assignment of ~ 0.35 as 100% cytoplasmic fluorescence by inspecting a subset of cells with individual $R_{obs}$ of 0.34–0.36. mCherry fluorescence was strongly cytoplasmic in these cells (Supplementary Fig. 3b). In Fig. 9 and Supplementary Fig. 2b, we indicate that $<R_{obs}> = 0.35$ is estimated to be 100% cytoplasmic. In Supplementary Fig. 6, the lowest observed $<R_{obs}>$ is ~ 0.30, and we adjusted the 100% cytoplasmic estimate to this lower value. While not ideal, this

adjustment is needed due to a small amount of systematic variation in $\langle R_{obs} \rangle$ seen across experiments (data not shown).

We designed our thresholding algorithm to analyze large and variable populations of cells quickly and with minimal user intervention. In settling on an automated thresholding algorithm we favored robustness and a high signal-to-noise ratio. However, this robustness comes at the expense of capturing the true extremes of plasma membrane and cytoplasmic fluorescence, and the method tends to compress the numerical range of $\langle R_{obs} \rangle$. Furthermore, a given $\langle R_{obs} \rangle$ value should not be interpreted as representing a clearly defined ratio of bound and unbound molecules. For example, $\langle R_{obs} \rangle = 1$ should not be taken to mean that 50% of the molecules are plasma membrane-bound, and 50% are cytoplasmic.

Global illumination during live-cell microscopy. We used the same 473 nm laser as for GFP imaging. The light intensity measured at the back of the objective was 750 $\mu J \cdot s^{-1}$. Using the conservative assumption that all of this light was evenly distributed across the area imaged by the camera ($1.23 \times 10^{-4}$ $cm^2$), the irradiance was 6.1 $J \cdot cm^{-2} \cdot s^{-1}$. We generally used 1.125 seconds total blue light photoexcitation (6.9 $J \cdot cm^{-2}$) for ePDZ–mCherry recruitment assays. For comparison, a recent study examining the effects of phototoxicity in budding yeast(Thévenaz et al., 1998) used 4 s blue light pulses of 4.9 $J \cdot cm^{-2}$ every 20 s for GFP image acquisition (i.e., in addition to constant illumination used as the experimental source of phototoxicity). Imaging illumination itself was well below the apparent threshold for a detectable stress response in their experiments(Thévenaz et al., 1998).

We assessed whether lower levels of illumination could elicit ePDZ–mCherry recruitment. We clearly detected recruitment after a 0.063 s pulse with a 10% transmission filter in the excitation path (0.038 $J \cdot cm^{-2}$, Supplementary Fig. 10a). This is considerably less power than would be used for routine GFP imaging.

Spot illumination. We used a galvanometer-steerable 440 nm dye laser (Micropoint, Photonics Instruments) to locally photoexcite Mid2-localized LOVpep. We controlled the illumination intensity using an adjustable internal attenuator plate and an external 1.0 OD absorptive neutral density filter (Thor Labs) placed in the beam path.

We did not measure the Micropoint laser intensity directly. However, with the attenuator plate set to ~ 30% transmission, three pulses of the laser were just sufficient to ablate the reflective coating on the calibration slide provided with the instrument. We used this setting as the reference power for experiments. Five pulses at the reference power was sufficient to slightly bleach Mid2-GFP (Supplementary Fig. 10b). After five pulses at 10–11% of the reference power (attenuated with either the attenuator plate or the external filter), Mid2–GFP bleaching was nearly undetectable. For spot photoexcitation experiements we used five pulses at ~1% of the reference power (i.e., with the attenuator set at 3% and the external filter in place). Five pulses at this power was more effective than a single higher power pulse for spot recruitment.

Spot photoexcitation kinetics. We manually defined ROIs corresponding to the recruited spot, cytoplasm, and background, and measured the average pixel intensities for these regions over all timepoints. We fit background-subtracted spot intensities to one- and two-exponential functions

using IgorPro (Wavemetrics). For the spot only experiments, a two-exponential function did not offer any improvement over a one-exponential function. For the spot + global experiments both data sets were better approximated by a two-exponential function (not shown). Nevertheless, we have provided the rate constant for the one-exponential fit for wild-type cycling LOVpep.

HeLa culture and transfection. We grew Hela cells in Dulbecco's Modified Eagle Medium (DMEM) supplemented with 10%FBS, 100 U penicillin and 0.1 mg/ml streptomycin at 37C in 5% CO2. We transfected cells using Lipofectomine 2000 (Invitrogen) according to standard protocols. We grew cells overnight on glass coverslips and transfected with 0.5–1 μg of plasmid DNA the next day. The following day, we transferred the cells to phenol-free DMEM, laid the coverslips directly on a microscope slide and sealed the edges with petroleum jelly.

For HeLa experiments we used LOVpep with either the K–6R, T–2S mutations (Lyn and Tom70 global) or the T406A, T407A and I532A mutations (Tom70 spot). The choice of the first allele was arbitrary, and we have no reason to expect that any of the mutations are optimal for mammalian cells. Indeed, we fount the more highly caged T406A, T407A, I532A variant superior in the Tom70 spot recruitment experiment. We performed global and spot recruitment assays essentially as described for yeast.

Blue LED illumination. Blue AlGaInP LEDs (http://theledlight.com, 20° viewing angle, 8,000 millicandela, 468-nm λmax at 3.4 V) were arranged into 6 × 8 arrays by pressing into an empty

pipet tip rack and soldered together in parallel. The entire array was powered with a 3.3 V, 1.2 A power supply (Phihong PSA05R-033).

The unfiltered light intensity from the LED arrays was ~ 0.005 $J \cdot cm^{-2} \cdot s^{-1}$. A considerably higher intensity ( > 0.037 $J \cdot cm^{-2} \cdot s^{-1}$) is required to elicit nuclear shuttling of the transcription factor Msn2, an indicator of environmental stress in budding yeast(Thévenaz et al., 1998). For MAPK activation and polarity disruption experiments, we attenuated the light intensity with either colored plastic notebook dividers (Avery) or transparency sheets laser printed with a uniform gray tone. In either case, we determined the transmission at 465 nm spectroscopically. In these experiments, 10% of the raw LED intensity was sufficient to elicit a strong biological response.

Growth arrest assay. For all signaling assays, we used a modified Mid2 construct, Mid2(SS/TM), in which the extracellular serine-and-threonine rich and cytoplasmic domains were deleted. To assay growth arrest on solid media, we made 1:10 serial dilutions of cells (grown in liquid culture or resuspended from plates) in water. We spotted the dilutions onto YP + 2% Dextrose or 2% Galactose, with G418 to maintain CEN plasmids. We grew the plates at room temperature, either foil wrapped for dark plates, or under an LED array with filters for 10% transmission for lit plates. We wrapped the edges of the plates with parafilm to prevent drying, and kept the plates with the growth surface facing down. For lit plates, we positioned fans to blow across the plates to dissipate heating from the LED array, and placed the plates on a foil surface to reflect transmitted light back onto the growth surface.

Assay for light-dependent mating pathway activation. We grew overnight cultures (YLS2067 background with plasmids as indicated) in 5 mL YP + 2% galactose + G418. If the overnight cultures were above $OD_{600}$ = 0.8, then we diluted the cultures with the same media to $OD_{600}$ = 0.2 and grew them for an additional 2 hours. We diluted the log-phase cultures to $OD_{600}$ = 0.1 to 0.2 and aliquoted 100 µL into standard clear 96-well microtiter plates. For alpha factor stimulation, we added 5 µL media + 20X alpha factor.

We incubated the cultures at room temperature with shaking for 4 hours. Dark plates were foil wrapped, and lit plates were under an LED array with filters for 10% transmission.

For microscopy, we spun down 50–100 µL and resuspended in 5–10 µL SC. We spotted 2 µL onto 10 mm × 10 mm × 1 mm thick agarose pad made with SC (4 pads per slide) and sealed the edges with vaseline(Gibson et al., 2009). We imaged with a 40 × objective (Zeiss).

For flow cytometry, we pelleted the cells and resuspended in phosphate buffered saline. We collected DsRedMax(Strack et al., 2008) fluorescence intensities on a BD Biosciences LSR II flow cytometer using a 561 nm excitation laser and a 610 nm ± 20 nm emission filter, and analyzed the data using FlowJo (Tree Star).

Assay for light-dependent polarity disruption. We grew overnight cultures (YLS1254 background with plasmids as indicated) in 5 mL YP + 2% galactose. We aliquoted 100 µL into standard clear 96-well microtiter plates and incubated at room temperature with shaking for 5

hours. Dark plates were foil wrapped, and lit plates were under an LED array with filters for 10% transmission.

For microscopy, we spun down 50–100 uL and resuspended in 5–10 uL SC. We spotted 2 µL onto 10 mm × 10 mm × 1 mm thick agarose pad made with SC (4 pads per slide), placed a coverslip on the pad and sealed the edges with vaseline. We imaged with a 40 × objective.

Assay for light-dependent polarity specification. We grew overnight cultures (YLS2446) in SC –HIS –LEU –MET –URA +2X ADE with 20 µM deoxycorticosterone (DOC(Picard, 2000)) in foil-wrapped tubes. We spun down 1–1.5 mL of the overnight culture and resuspended in 20 µL of the same media with 10 µM DOC and 10 µg / mL αF, and incubated in the dark for 30 min. We spotted 2 µL onto 10 mm × 10 mm × 1 mm thick agarose pad made with the same media, including DOC and αF, placed a coverslip on the pad and sealed the edges with vaseline.

We imaged the cells on the same microscope used for recruitment assays. We used a 550-nm long pass filter (Edmund Optics) in the transmitted light path to avoid photoexciting the LOV domain when using phase contrast. Once per minute we took a 1 s confocal image of mCherry fluorescence and a 100 ms confocal phase contrast image, and photoexcited the cells using the Micropoint laser. We used the same photoexcitation duration and intensity as for spot recruitment. For "– Photoexcitation", the experiment was performed identically, except with the laser switched off.

A MetaMorph journal recorded the laser targets directly into a stack of phase contrast images. Using ImageJ, we made composites of the phase contrast and mCherry images, and measured the angle between the laser target and the incipient polarized growth. We binned the measured angles using Excel, and plotted the results using Igor Pro. We also performed a two-sample Kolmogorov–Smirnov test using Igor Pro.

We estimate the uncertainty in laser targeting to be 0.6–0.8 μm, and the corresponding angular uncertainty to be ~ 15° for a 5 μm yeast cell. This uncertainty limits the precision with which we can measure the angle between photoexcitation and polarized growth. Furthermore, this uncertainty is compounded by human error in updating targets in real time. Thus it is likely that the laser narrowly missed some cells during some photoexcitation cycles, although we do not know to what extent a near miss by the laser would photoexcite LOVpep.

We also note a slight tendency of polarization towards the mock photoexcitation target (Fig. 10c). To facilitate interpretation of the data, we avoid placing the laser target at points of cell-cell contact. This may have the unintended effect of biasing target placement towards the default polarization cue or away from regions of higher pheromone degradation.

TULIPs plasmid system

We have deposited a set of plasmids for the TULIPs system, along with maps and sequences, at Addgene (www.addgene.org, Supplementary Table 3). The plasmids allow cloning of protein coding sequences with GFP–LOVpep, cpPDZ, ePDZb, and ePDZb1 as tags. We have provided

integrating versions, based on the YIplac series of plasmids, and centromeric versions, based on the pGREG series of plasmids.

Our cloning scheme is based on in vitro recombination cloning such as the InFusion system (Clontech), or the method of Gibson et al. (Bodvard et al., 2011). Cloning by recombination in yeast can also be used with the centromeric plasmids(Jansen et al., 2005). See Supplementary Table 5 for primer details.

Suggested workflow for using the TULIPs system. Because tagging can interfere with function for unexpected and unknown reasons, we suggest using the TULIPs system in an initially exploratory way based on few assumptions. We favor tagging multiple potential targets in parallel, in case the tagging inactivates the first choice target. We suggest testing whether GFP–LOVpep tags are functional and accessible for binding by testing recruitment of ePDZ–mCherry constructs. We also suggest testing the effects of recruitment using a constitutively active LOVpep allele expressed from an inducible promoter. This strategy makes it unnecessary to do light-dark experiments initially, and can demonstrate whether a particular configuration is capable of activating a pathway by recruitment.

Once particular tagging strategies have been proven functional, we suggest screening a range of affinity and caging mutations for the best activity. It is important to realize that background binding in the dark state may not be eliminated. We therefore suggest using inducible or repressible promoters whenever there is a possibility that the effects of recruitment will be selected against during strain propagation. Expression levels can affect the degree of binding in

both light and dark. If no light dependent effect is observed, try increasing the level of expression. Conversely, if dark activation is too great, try reducing the expression level. We have found that high expression of plasma membrane-bound LOVpep and low expression of cytoplasmic ePDZ–mCherry generally works well for achieving strong recruitment. However, we note that the Mid2(SS/TM)–GFP–LOVpep constructs used in our signal transduction experiments (Fig. 10) recruit ePDZ–mCherry very weakly (data not shown) compared to the full-length Mid2–GFP–LOV constructs used in the visual recruitment assays (e.g., Fig. 9b).

## 2.8 Appendix 2

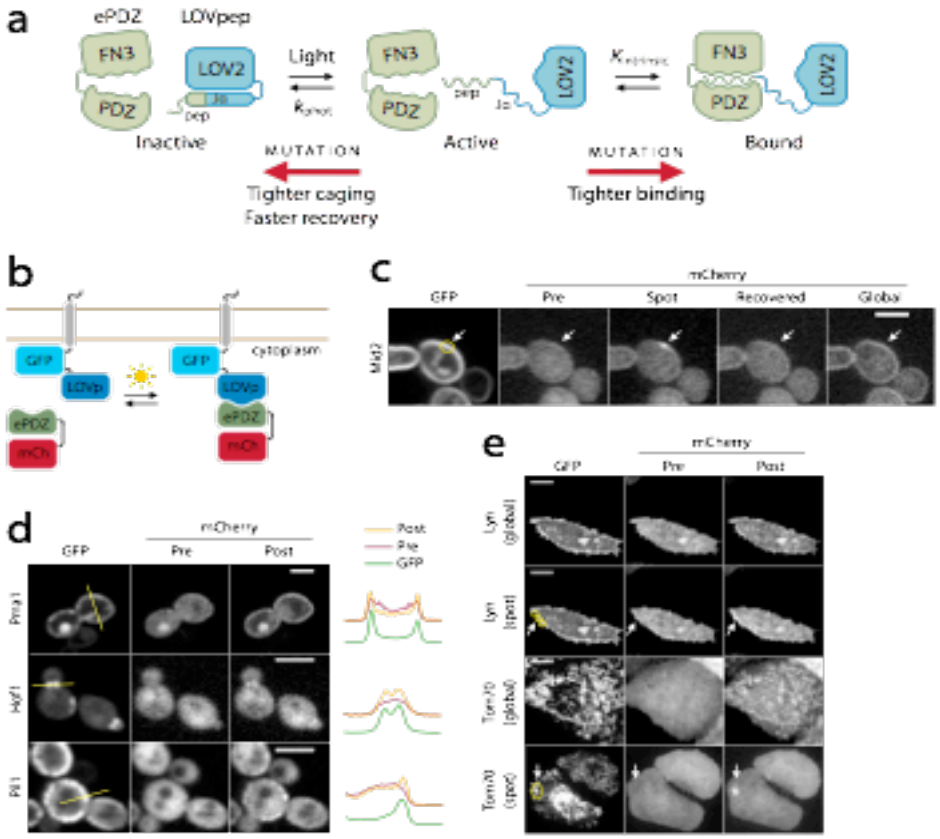


Figure 8 Design and characterization of TULIPs. (a) Schematic design of TULIPs. In the dark, a peptide epitope is caged by docking of the Jα helix to the LOV2 core (blue). Upon photoexcitation, the Jα helix undocks and exposes the peptide epitope for binding by ePDZ (green). The caging, intrinsic ePDZ–peptide affinity ($K_{intrinsic}$) and lifetime of the photoexcited state ($k_{phot}$) can all be tuned by mutations. (b) Schematic of the assay used to measure ePDZ–LOVpep binding in living yeast. (c) Recruitment of ePDZb1–mCherry to the integral plasma membrane protein Mid2 in yeast using spot (arrow) and global photoexcitation. Scale bar, 5 µm. (d) Recruitment of ePDZb–mCherry to diverse subcellular markers in yeast by global photoexcitation. Scale bars, 5 µm. The plots depict pixel intensities measured along the yellow lines indicated in the GFP images. (e) Recruitment of ePDZb1–mCherry to the plasma membrane and mitochondria of HeLa cells by global and spot (arrow) photoexcitation. Scale bars, 10 µm.

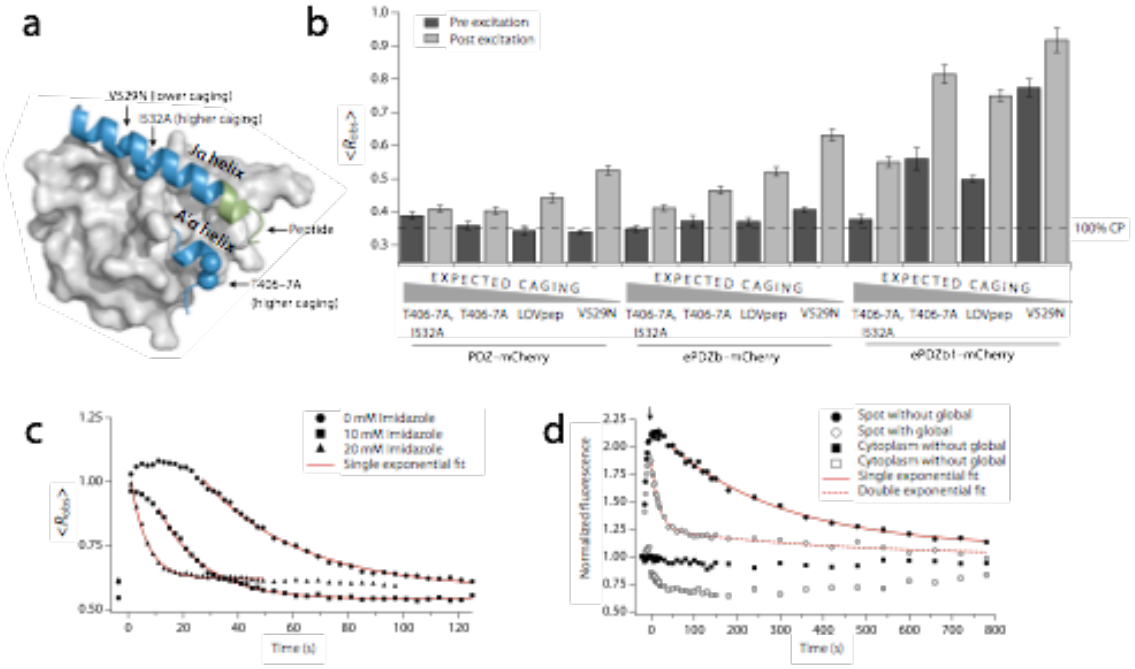


Figure 9 Mutational and chemical control of binding. (a) AsLOV2 structure (Protein Data Bank: 2v0u) showing the location of the ePDZ epitope (green) and the caging mutations used in this study. (b) Lit- and dark-state $\langle R_{obs} \rangle$ using LOVpep with caging mutations. Data are the means from a population ($n \geq 34$) of cells; error bars show s.e.m. The dashed line represents $\langle R_{obs} \rangle$ for ~100% cytoplasmic ePDZ–mCherry. (c) Kinetics of global recruitment and dissociation of ePDZb1–mCherry for LOVpep with wild-type dark-recovery kinetics. Imidazole is added to the media in the concentrations indicated. Data are the means from a population ($n \geq 8$) of cells. Red lines are exponential fits of the dissociation phase ($k_{obs}$). (d) Kinetics of spot recruitment and dissociation of ePDZb1–mCherry using slow-cycling (V416I) LOVpep. ePDZb1–mCherry is recruited to a spot as in Fig. 1c. For the closed symbols, the recruited molecules are allowed to recover without further illumination. For the open symbols, the cell is globally photoexcited at the time indicated by the arrow so as to deplete the unbound cytoplasmic pool (open squares) of ePDZb1–mCherry. Data are the means from a population ($n \geq 13$) of cells. Red lines are exponential fits of the dissociation phase.

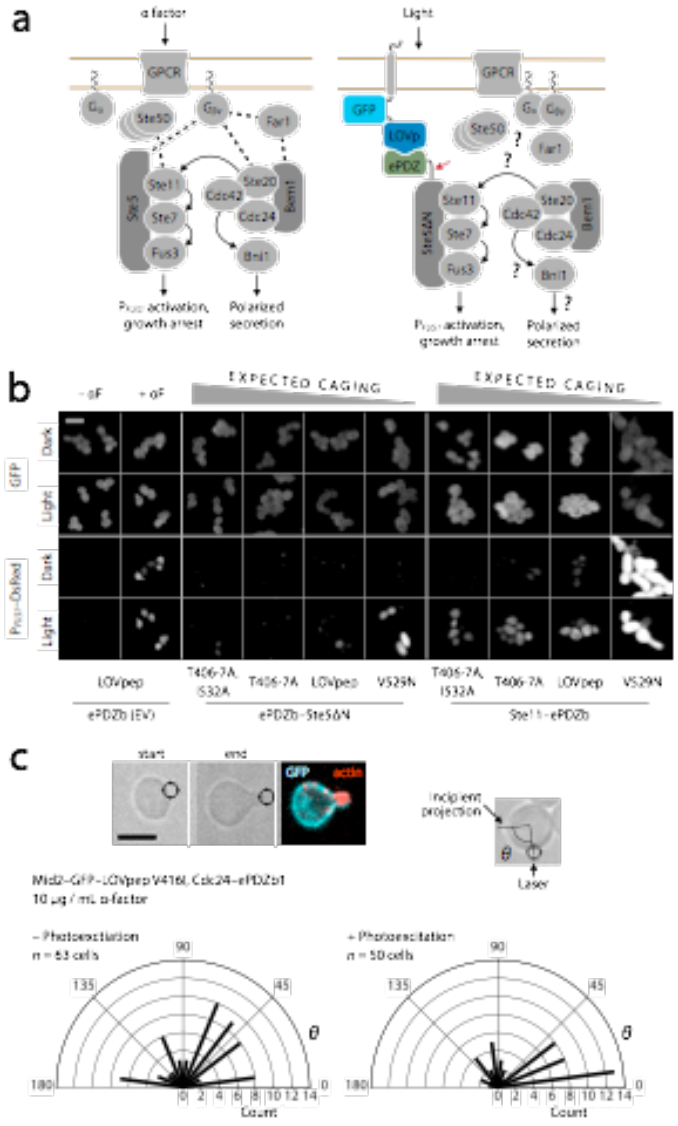


Figure 10 Optical control of MAPK activation and polarity establishment in yeast. (a) The wild-type mating pathway in budding yeast (left), and a scheme for light-dependent plasma membrane recruitment of Ste5ΔN (right). The red arrow indicates the fusion between ePDZ and Ste5ΔN. Dashed lines indicate wild-type binding interactions, many of which may be absent in Ste5ΔN recruitment. (b) $P_{FUS1}$ promoter activation, cell cycle arrest and polarized growth in light- and dark-grown cells. ePDZb–Ste5ΔN or ePDZb–Ste11 are globally recruited to plasma membrane-tethered LOVpep variants as indicated. Scale bar, 10 μm. (c) Light-directed polarized growth. Cells are exposed to mating pheromone to induce cell cycle arrest, then stimulated with spot photoexcitation to recruit Cdc24–ePDZb1 to plasma membrane-tethered LOVpep. Radial plots show quantification of light-directed polarized growth. θ is the angle between the spot of laser photoexcitation, the center of the cell and the incipient projection. Radial bars depict the number of polarization events of angle θ in each 15° sector. "– Photoexcitation" denotes a negative control experiment in which the spot photoexcitation laser was switched off. $P < 0.01$ for a comparison of experimental and control distributions (two-sample Kolmogorov–Smirnov). Scale bar, 5 μm.

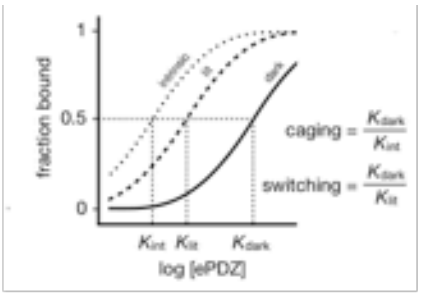


**Supplementary Figure 1** Definition of caging and switching. The schematic plot depicts the fraction of LOVpep bound vs. ePDZ concentration for a photoswitchable interaction. Caging is the dark-state diminishment of binding affinity relative to the intrinsic binding affinity. Switching is the dark-state diminishment of binding affinity relative to the lit-state binding affinity.

a

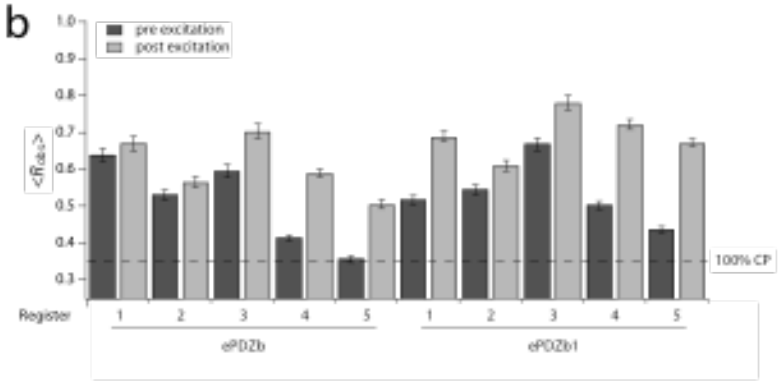


**Supplementary Figure 2** Register series of LOV–peptide fusions. (**a**) Partial sequences of AsLOV2 (blue), a high-affinity ePDZ epitope (green), and LOV–peptide fusion constructs in 5 different registers used in **b**. AsLOV2 positions are numbered as in phototropin 1. In the fusion constructs, LOV2-derived amino acids are blue, and peptide epitope amino acids are green. (**b**) Lit- and dark-state $<R_{obs}>$ for fusions in registers 1–5. Data are the means from a population ($n \geq 37$) of cells. Error bars, s.e.m. The dashed horizontal line represents the estimated $<R_{obs}>$ for ~100% cytoplasmic ePDZ–mCherry.

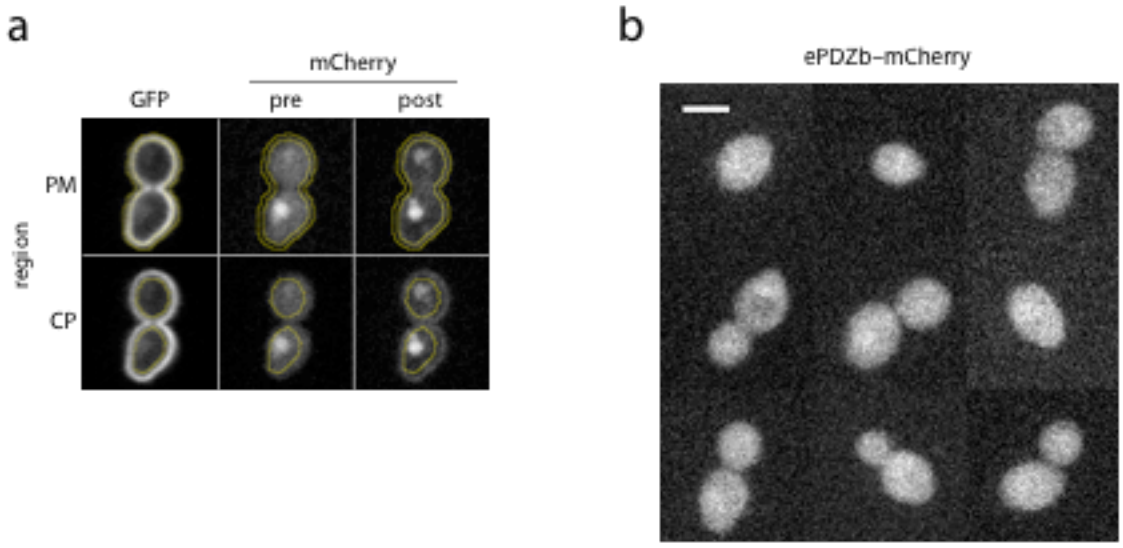


**Supplementary Figure 3** Thresholding of cells for the PM recruitment assay. (**a**) Representative examples of plasma membrane (PM) and cytoplasm (CP) thresholded regions. $\langle R_{obs} \rangle$ is the ratio of PM:CP mCherry fluorescence, averaged over a population of cells. (**b**) A montage of representative cells with $R_{obs} \simeq 0.35$. Scale bar, 5 µm.

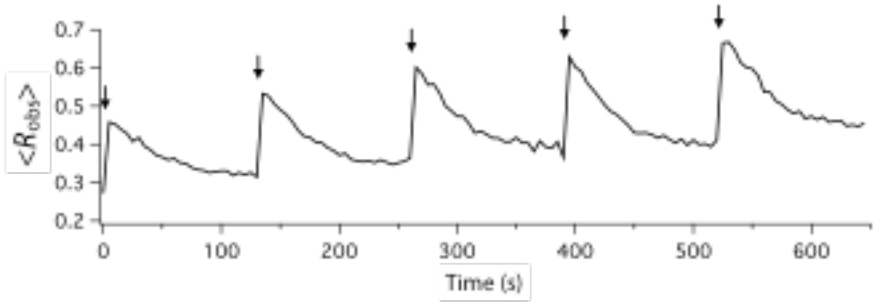


**Supplementary Figure 4** Reversible light-triggered recruitment of ePDZb by LOVpep. A population of cells ($n = 6$) was repeatedly photoexcited for 1.125 second (arrows), and allowed to recover.

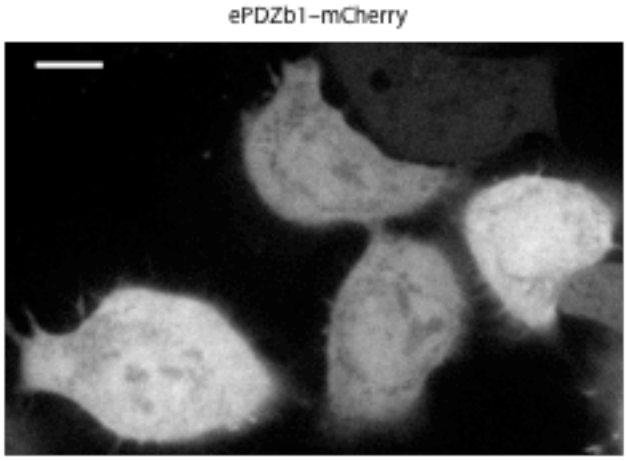


**Supplementary Figure 5** ePDZ–mCherry localization in HeLa cells in the absence of LOVpep. Scale bar, 10 µm.

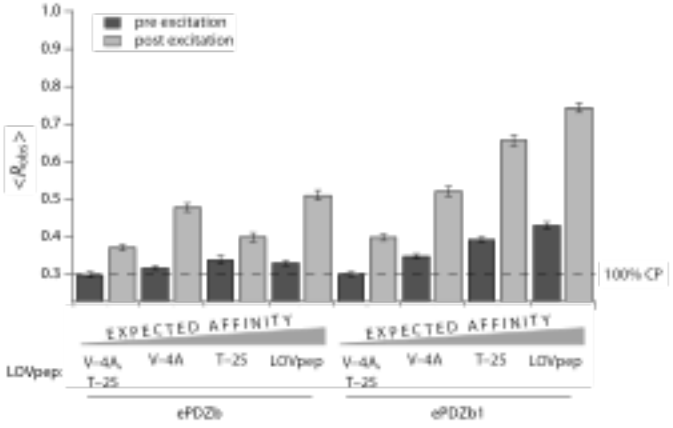


**Supplementary Figure 6** Lit- and dark-state $\langle R_{obs} \rangle$ using LOVpep mutations in the peptide epitope. Data are the means from a population ($n \geq 31$) of cells; error bars, s.e.m. The dashed line represents $\langle R_{obs} \rangle$ for ~100% cytoplasmic ePDZ–mCherry.

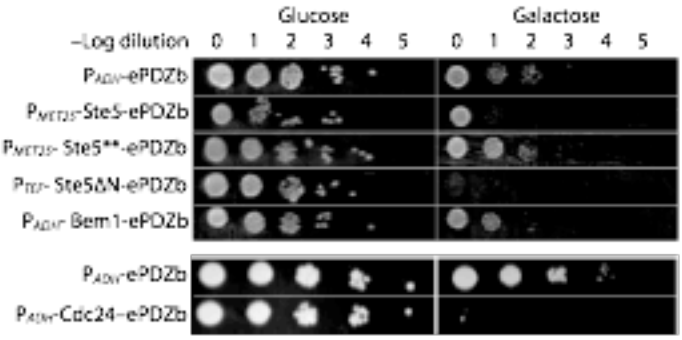


**Supplementary Figure 7** Growth arrest assay for ePDZ fusions. Serial dilutions of cells were spotted onto solid media. Expression of Mid2–GFP–LOVpep$^{CA}$ was induced or repressed with 2% galactose or 2% glucose, respectively.

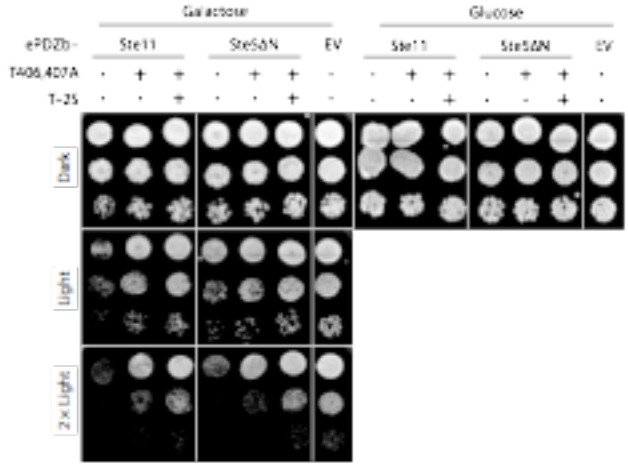


**Supplementary Figure 8** Light induced growth arrest by MAPK activation. (**a**) Growth arrest by recruitment of Ste11–ePDZ and ePDZb–Ste5ΔN to Mid2(SS/TM)–GFP–LOVpep. LOVpep constructs have the T406A, T407A, and T–2S mutations as indicated. All LOVpep constructs are slow cycling (V416I). 3 dilutions (10-fold) are shown for each condition, arranged vertically.

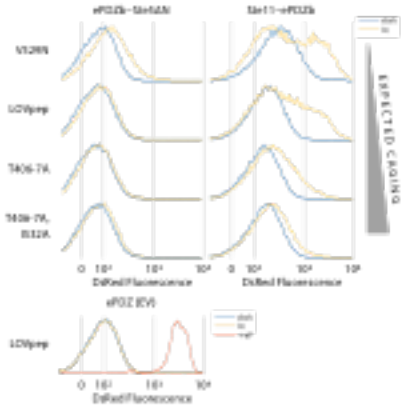

**Supplementary Figure 9** $P_{FUS1}$–DsRed reporter activation for ePDZb–Ste5ΔN and Ste11–ePDZb constructs measured using flow cytometry. Mid2(SS/TM)–GFP–LOVpep constructs have the T406A, T407A, V529N and I532A mutations as indicated. All LOVpep constructs are slow cycling (V416I).

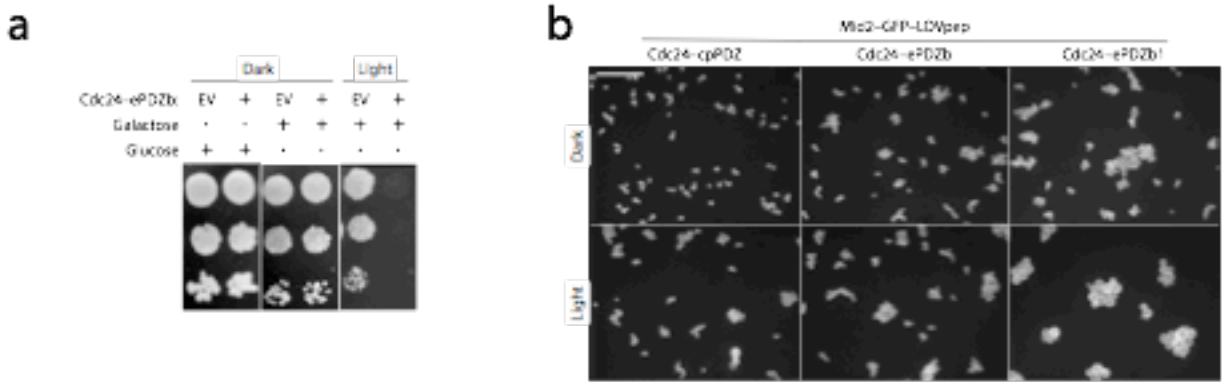


**Supplementary Figure 10** Light induced growth arrest by polarity disruption. (**a**) Growth arrest on solid media by recruitment of Cdc24–ePDZb to Mid2–GFP–LOVpep. 3 dilutions (10-fold) are shown for each condition, arranged vertically. (**b**) Terminal phenotype in liquid culture caused by light-dependent global recruitment of the Cdc42 GEF Cdc24. Cdc24 is fused to PDZ, ePDZb, or ePDZb1 as indicated and globally recruited to PM-tethered LOVpep. Scale bar, 50 µm.

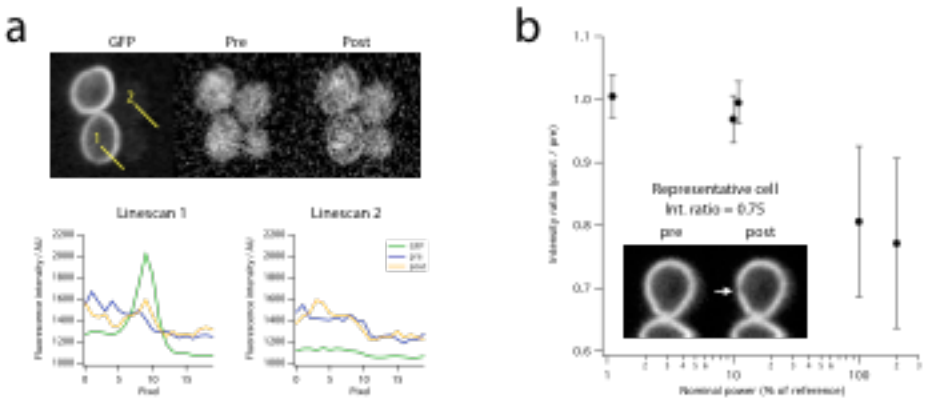


**Supplementary Figure 11** Photoexcitation requirements. (**a**) Global recruitment using minimal global illumination. Cells were illuminated with a 0.063 s pulse of 0.038 J·cm$^{-2}$. The plots show pixel intensities measured along the yellow lines in the image. (**b**) GFP bleaching vs. Micropoint laser power. The *y*-axis is the fraction of GFP fluorescence remaining after spot illumination. The *x*-axis is the laser power. 100% nominal power is the minimal power required to ablate a thin-metal-coated slide when calibrating Micropoint steerable laser. GFP bleaching (white arrow) is nearly undetectable at 10% of this power. Spot photoexcitation experiments were conducted using 1% of the reference power.

## Chapter 3: Optimization of TULIPs system in mammalian cells and Light-mediated regulation of RhoA in mammalian cells

### 3.1 Abstract

The goal of my thesis was to obtain optogenetic control of the small GTPase RhoA to investigate the spatiotemporal regulatory logic of cleavage furrow formation in mammalian cells. To accomplish this goal, I needed to transition and optimize the TULIP system in mammalian cells. To optically control activation of RhoA, we decided to mimic how cells do this endogenously by inducing membrane localization of a RhoA specific GEF with light. This requires tethering the photosensitive LOVpep to the plasma membrane and the generation of a recruitable RhoA GEF. Although this seemed relatively straight forward there were several technical complications that arose, including modifications to the recruitment tag, identifying optimal illumination system, and the generation of a GEF whose activity could be controlled by light-mediated recruitment to the membrane. The next section will discuss this and other work I did in order to gain light-mediated control of RhoA activity with high spatial and temporal precision.

### 3.2 Optimal membrane tether

To first validate the TULIP system in mammalian cell culture, we initially fused GFP-LOVpep to TOM70 mitochondrial targeting sequence to target LOVpep to mitochondria. This was co-expressed with ePDZb1-mCherry and examined in the mCherry channel pre- and post-photoexcitation. Both global and local illumination using the micropoint system successfully recruited ePDZb1-mCherry to the mitochondria. We were interested in using TULIPs to study light-directed plasma membrane signaling and therefore needed to identify an appropriate

membrane tether for GFP-LOVpep. An ideal tag would localize exclusively to the plasma membrane (PM) throughout the cell cycle and exhibit minimal exchange or lateral diffusion. The N-terminal fragments of proteins that are co-translationally modified by the addition fatty acids are effective in mediating membrane localization and are compatible with the LOVpep system which requires a free C-terminus. We generated a hybrid protein containing the N-terminal 13 amino acids (MLCCMRRTKQVEK) of GAP-43 linked to GFP-LOVpep(GAP-$43_{N13}$-GFP-LOVpep). GAP-43 binds membranes via palmitoylated cysteine residues at positions 3 and 4. GAP-$43_{N13}$ -GFP-LOVpep localized well to the PM in both interphase and mitotic Hela cells. This fusion protein supported global and local recruitment of ePDZb1-mCherry upon photoexcitation (Figure 11A). In addition to GAP-$43_{N13}$, the N-terminus of the C. elegans PEF-1, which undergoes palymitoylation and myristoylation, was examined as well and showed similar localization and recruitment results as GAP-$43_{N13}$-GFP-LOVpep. However, both of these tags were found to bind promiscuously to internal membranes. Additionally, we were concerned these would have the potential to diffuse on and off and laterally within the membrane.

We next examine integrated plasma membrane tags, including CD8, yeast Mid2, Beta2-adrenergic receptor ($Beta_2AR$), and Stargazin. Both CD8 and yeast Mid2 fused to GFP-LOVpep were trapped in the Golgi and failed to localize to the PM. $Beta_2AR$, which is a seven transmembrane GPCR, localizes well to the plasma membrane during interphase and both global and local illumination of $Beta_2AR$-GFP-LOVpep successfully recruited ePDZb1-mCherry (Figure 11C). However, upon examining the distribution of $Beta_2AR$ in mitotic cells (monopolar arrested cells), we found the $Beta_2AR$-GFP-LOVpep no longer localizes to the PM, therefore it is not an ideal tag for future experiments (Figure 11D). Stargazin-GFP-LOVpep expressed at high

levels, localized well to the PM throughout the cell cycle, and supports recruitment of PDZ-tagged mCherry (Figure 1E,F) and therefore was used for all future 74experiements.

### 3.3 Optimal recruitment tag (ePDZb1 vs. 2X PDZ)

Although we expected the bioengineered clamp ePDZ to have a high affinity for lit state conformation of LOVpep, this construct does not always appear to behave well in vivo. During the construction of a light-recruitable RhoA RhoGEF, we noticed TULIPs mediated expression and recruitment of the ePDZ-mCh-GEF were relatively low. In addition, we discovered that the orientation of the ePDZ-tagged GEF affected membrane recruitment. Constructs with ePDZ tag placed on the N-terminus recruit well, while placement on the C-terminus abolishes detectable recruitment. Based on the crystal structure of ePDZ, we suspect this may be due to the proximity of ePDZ's N-terminus to the peptide binding pocket. Fusing the GEF constructs to the N-terminus of ePDZ  may weaken or disrupt the binding interaction with LOVpep. To improve recruitment we reasoned we could improve the avidity of a weak interaction by multimerizing PDZ. We replaced the FN3 domain of ePDZ with a second PDZ domain creating a tandem PDZ-mCherry construct (2XPDZ-mCh). Compared to ePDZ the 2X-PDZ constructs have improved recruitment and expression levels with and without and the GEF (Fig 12).

### 3.4 Subcellular recruitment (Micropoint vs Mosiac illumination systems)

Although, the micropoint illumination was suitable for subcellular recruitment in small yeast cells, we were concerned this system may not be optimal for larger mammalian cells in which we would require local illumination of much larger regions.  The micropoint system we were using is a highly focused laser, which pulses sub-micron regions of the desired region of interest

(ROI). For comparison we used a Mosiac system, which is a digital micro mirror device that uses epi-illumination to activate arbitrarily sized ROI's in a single pulse and is more diffuse in Z (activating through cell) . Using the Mosiac to locally illuminate either Hela or NIH3T3 cells, we observe much stronger recruitment of mCherry-tagged GEF(Fig 13). Using the Mosiac system we determined the minimal light intensity required for maximum photoactivation to be ~1μJ/s, which is considerably below the intensity levels associated with phototoxicity. Furthermore, by electronically attenuating the laser power or the duration of the illumination pulse, the levels of GEF recruitment can be titrated giving us another way to tune our optogenetic system.

### 3.5 Light-mediated control of RhoA activation

To control RhoA activity with light, we can use TULIPs system to induce membrane localization of its activator a RhoGEF. This requires the construction of a genetically encoded, tandem PDZ-tagged GEF variant which will be inactive in the cytosol and active upon light-mediated membrane recruitment. We first examined the RhoA GEF Ect2, as it is normally required for RhoA activation during cytokinesis and the regulation of Ect2's activity is relatively well-understood.

To construct a light-regulated GEF, we first needed to incapacitate the endogenous regulatory mechanisms of Ect2's GEF activity creating a latent construct which would remain inactive in the absence of TULIPs-directed membrane recruitment. By removing the N-terminal tandem BRCT domains, we disrupted Ect2's ability to interact with Cyk4, which is normally required for Ect2's activation of RhoA during cytokinesis. As a proxy for RhoA activation, we expressed the constructs in HeLa cells and examined their ability to induce stress fiber formation during

interphase. Expression of the Ect2 C-terminus containing the catalytic DHPH domains and PBC tail induced by pronounced stress fiber formation. By removing the N-terminus, we had also disrupted autoinhibition and this construct localized well to the PM on its own where it could constitutively active RhoA (Figure 14A). To cripple Ect2's inherent ability localize to the PM and activate RhoA we introduced two separate point mutations T815D and G668D, both reported to weaken Ect2's PM localization during cytokinesis (Frenette et al., 2012; Su et al., 2011). Both mutants had little to no effect on preventing PM localization or stress fiber formation in interphase Hela cells. In addition to its PH domain, Ect2 also contains a polybasic cluster (PBC) in its C-terminal tail which has been shown to contribute to PM localization(Su et al., 2011). Upon deletion of the PBC tail, Ect2's PM localization and activation of RhoA were dampened, however this construct was still able induce stress fiber formation relatively well (Figure 14B). It was not until we further truncated the construct removing the entire PH domain, that we created a construct that remained cytosolic and did not induce RhoA activation when expressed on its own (Fig 14C). To ensure this minimal construct still retained its GEF functionality, we tethered it to the PM using and the PH domain of PLC delta. Exogenous PM tethering of Ect2 DH induced stress fiber formation and cell rounding of Hela cells (Figure 14D). TULIPs-mediated membrane tethering via constitutively active LOVpep variant also induces stress fiber formation. These results suggested that the 2XPDZ-mCh-Ect2 DH construct should be ideal for TULIPs-mediated activation of RhoA because it is inactive in the cytosol, but is able to activate RhoA and induce stress fiber formation upon constitutive PM recruitment. To examine the effects of light-mediated recruitment of 2XPDZ-Ect2 DH, we co-expressed various markers to detect increases in RhoA activation including the RhoA biosensor (AHDPH-mcherry), and the downstream effects on actin (mApple-actin) and myosin (mApple-MLC). Although the RhoA

biosensor has been previously validated and works during cytokinesis, during interphase the probe is rather punctate and cortically localized. Its unclear if this is due to non-specific aggregation or dependent on RhoA activity. Upon local PM recruitment of 2XPDZ-Ect2 DH, the effects on RhoA activation, actin polymerization, and myosin accumulation were minimal and often hard to detect (Figure 15A). As a more quantitative measure to examine RhoA activation, in collaboration with Patrick Oakes a post-doc from Margaret Gardel's lab, we used traction force microscopy to observe changes in cellular contractility upon local recruitment of 2XPDZ-Ect2 DH. In interphase NIH3T3 cells, TULIPs-mediated recruitment of 2XPDZ-Ect2 DH induces local increases in traction forces, yet we still observed minimal changes on actomyosin cytoskeleton.

Although we were able to generate light-regulated version of Ect2, the levels of RhoA activation upon light-mediated membrane recruitment appear to be relatively low. We therefore examined if we could use the RhoA specific GEF LARG, which is reported to have high GEF activity towards RhoA(Jaiswal et al., 2011). Similar to our strategy for Ect2, by systemically truncating LARG we determined using the minimal catalytic DH domain had the lowest background levels of RhoA activation (Fig 14 E,F). However, the levels of background activation were still considerable as moderate stress fiber formation was observed. Upon local recruitment of 2XPDZ-LARG DH, robust local increases in RhoA activation was observed, yet only moderate increases in actin and myosin accumulation (Fig 15B). For comparison we also examined how this construct behaved in NIH3T3 cell lines. Expression of 2XPDZ-LARG DH had little effect on actomyosin cytoskeleton compared to control cells suggesting the background levels of RhoA activation may be lower and upon local illumination rapid and robust increases in RhoA

activation, actin, and myosin II accumulation were observed (Chapter 4, Figure 16 D,E). It is unclear why expression of 2XPDZ-LARG DH gives rise to different background levels of RhoA activation between HeLa and NIH3T3 cell lines, but one possibility could be differences in endogenous levels of RhoGAP activity.

Although we initially validated our ability to generate a light-regulated GEF in interphase cells, the goal of my thesis was to use this tool to manipulate RhoA activity during mitosis. To generate mitotic cells, NIH3T3 cells were incubated with a low dose of nocodazole to arrest cells in metaphase. However, we observed that the mitotic index is low for this cell line and the majority of the metaphase arrested cells detached making it very difficult to examine the effects in light-mediated RhoA activation in NIH3T3 mitotic cells. On the other hand, it is relatively easy to generate a high number of metaphase arrested HeLa cells which remain attached to the coverslip. Although there was evidence 2XPDZ-LARG DH may have some degree of background RhoA activation during interphase, we did not detect higher cortical levels of RhoA activation, actin, or myosin in mitotic arrested HeLa cells compared to control cells. Furthermore, upon local illumination we observe local activation of RhoA, actin polymerization, and myosin II accumulation (Chapter 4, Figure 18 E,G,I). Additionally, in weakly adherent, rounded interphase HeLa cells, which will be discussed in further detail in Chapter 4, we observe light-mediated activation of RhoA and downstream effectors upon recruitment of 2XPDZ-LARG DH. It is unclear why in HeLa cells the levels of actin and myosin accumulation upon light-mediated recruitment of 2XPDZ LARG DH vary between adherent interphase and rounded interphase or mitotic cells, but we were interested in controlling RhoA activity during mitosis when this construct appears to function well. Therefore, we used the 2XPDZ-mCherry-LARG

DH, which we refer to as photorecruitable GEF (PR_GEF) to investigate spatiotemporal regulation of RhoA-mediated furrow formation in mitotic HeLa cells.

### 3.6 Appendix 3

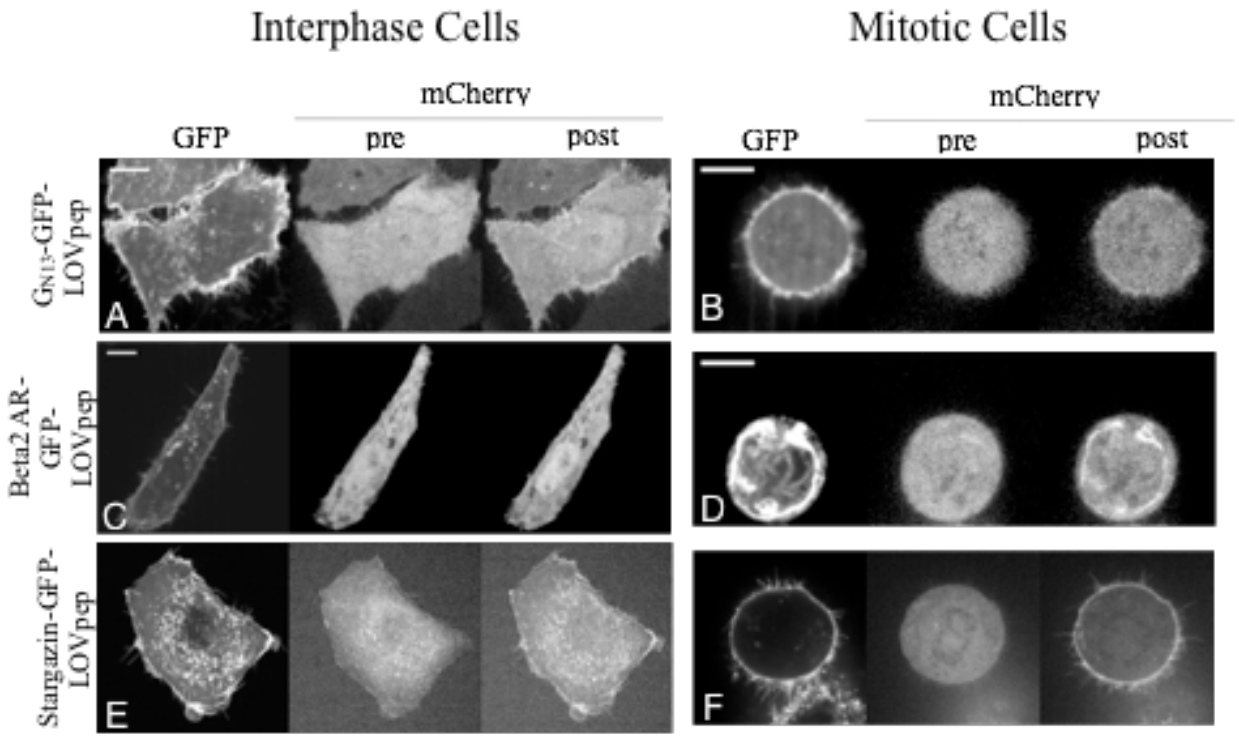


Figure 11:Light-mediated PM recruitment: (A,C,E) Fluorescence images tracking recruitment of ePDZb1-mCherry to the indicated PM tags in Hela cells before and after global photoexcitation. (B,D,F) Fluorescence images of mitotic Hela cells expressing indicated membrane-tag fused to GFP-LOVpep before and after global photoexcitation. Scale bars 10 µm.

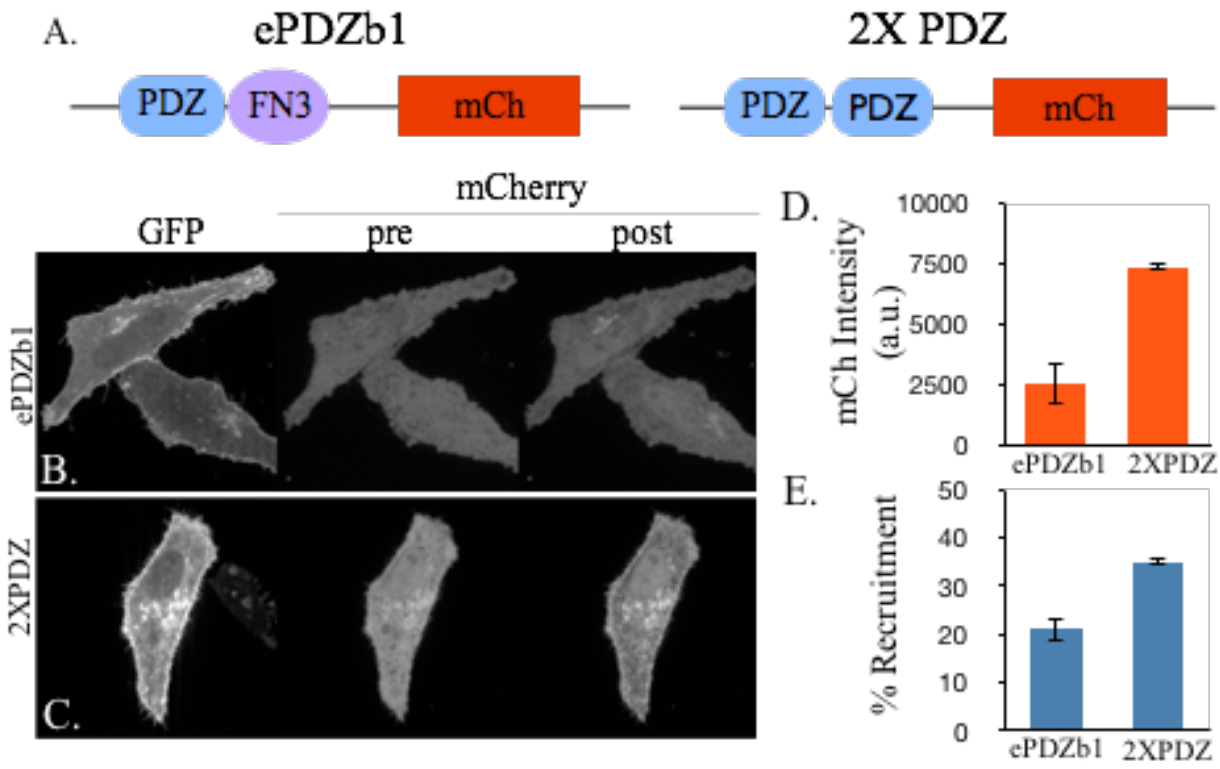


Figure 12: Expression and light-mediated recruitment of ePDZb1 versus 2XPDZ (A) Schematic of ePDZb1 and 2XPDZ recruitment tags (B,C) Fluorescence images tracking recruitment of ePDZb1-mCherry (B) or 2XPDZ (C) to the PM in Hela cells before and after global photoexcitation. (D) Average expression level of ePDZb1-mCherry (n=12 cells) or 2XPDZ (n=15 cells). (E) Average percent recruitment for ePDZb1-mCherry (n=12 cells) or 2XPDZ (n=15 cells) was determined by drawing a linescan across the PM and calculating the percent increase in PM localized mCherry intensity post global photoactivation relative to PM localized mCherry pre photoactivation.

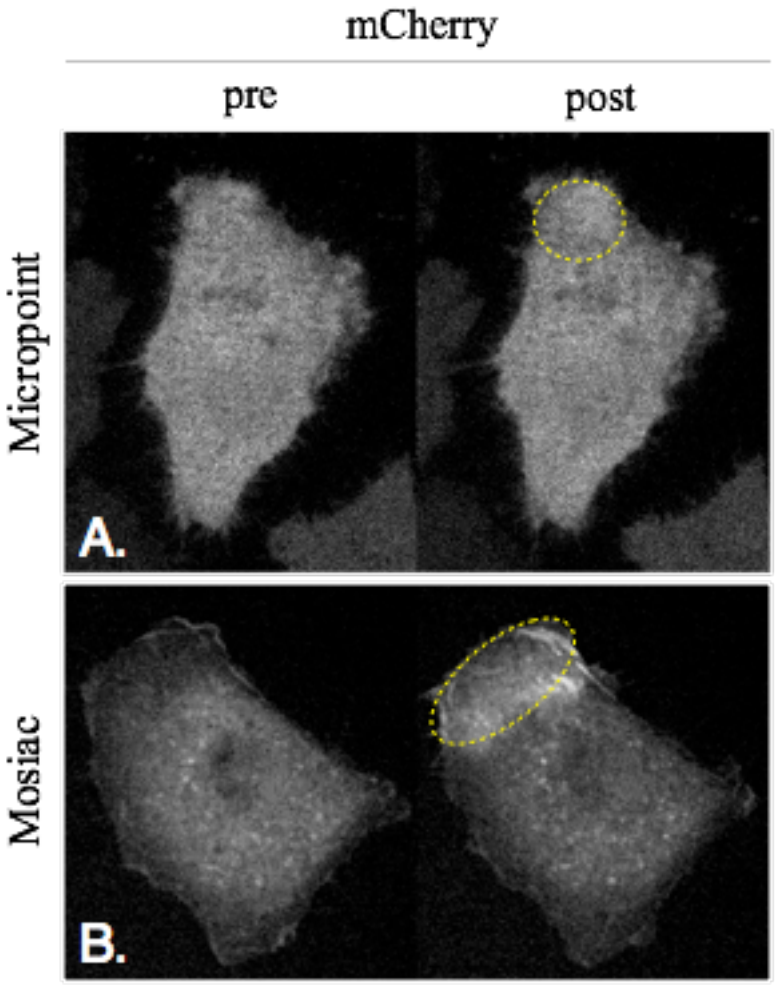


Figure 13: Micropoint vs. Mosaic local illumination (A,B) Fluorescence images tracking PM recruitment of 2XPDZ-mCherry in Hela cells before and after local photoexcitation (yellow circles) with either the Micropoint (A) or Mosaic (B) illumination system. Cells were locally illuminated every 20 secs for 5 mins.

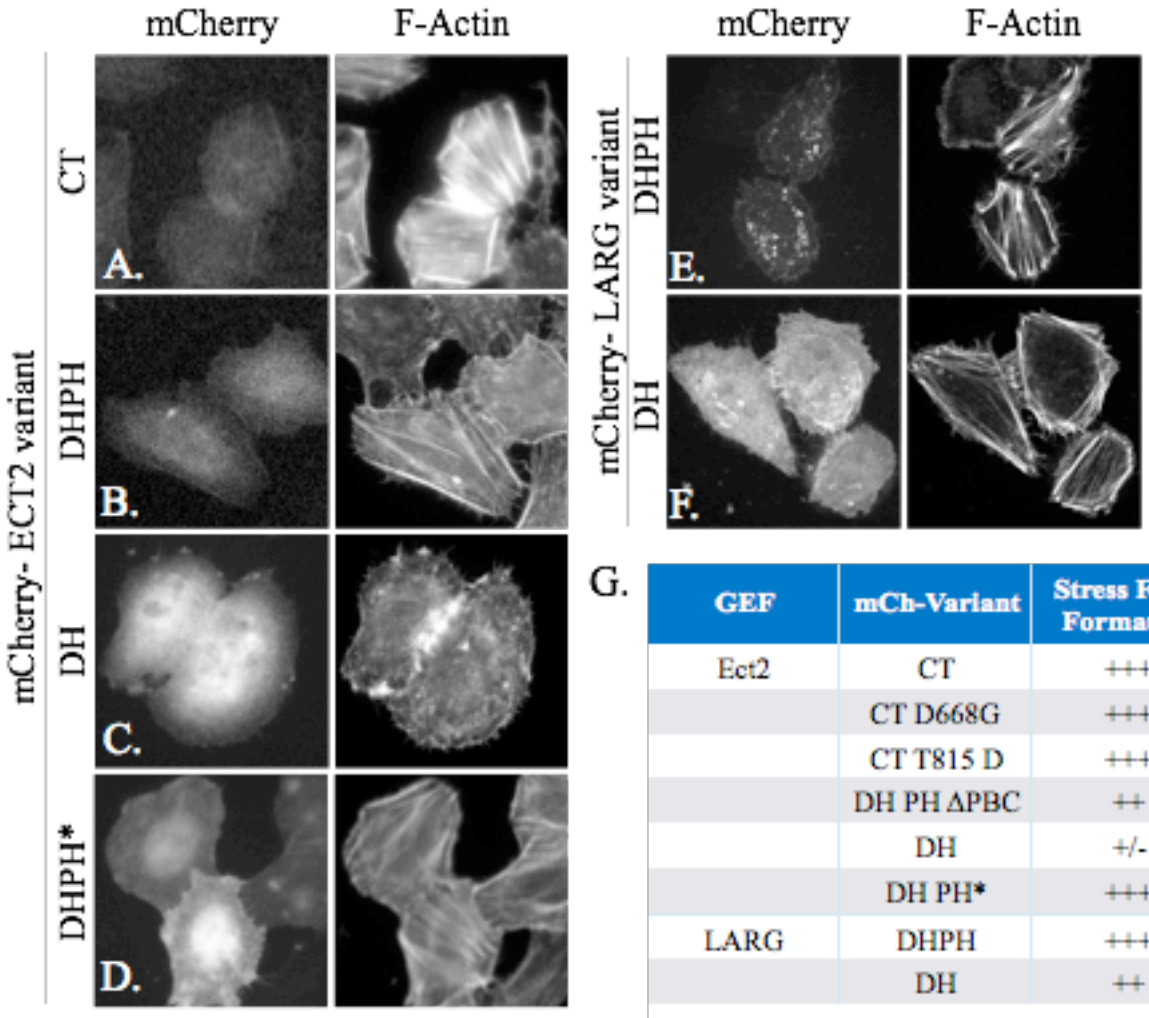


G.

| GEF | mCh-Variant | Stress Fiber Formation |
|---|---|---|
| Ect2 | CT | +++ |
| | CT D668G | +++ |
| | CT T815 D | +++ |
| | DH PH ΔPBC | ++ |
| | DH | +/- |
| | DH PH* | +++ |
| LARG | DHPH | +++ |
| | DH | ++ |

Figure 14: Construction of Latent RhoA GEF (A-F) Fluorescences images of fixed Hela cells expressing indicated mch-tagged GEF construct (mCherry) and stained with Cy-5 labeled phalloidin (F-actin).(G) Summary of all Ect2 (DHPH* is Ect2 DH domain tagged with PH domain of PLCδ) and LARG constructs expressed in Hela cells and the relative levels of background RhoA activation as indicated by the presence of stress fiber formation (+++ pronounced, ++ moderate, and + minimal levels of stress fiber formation observed)

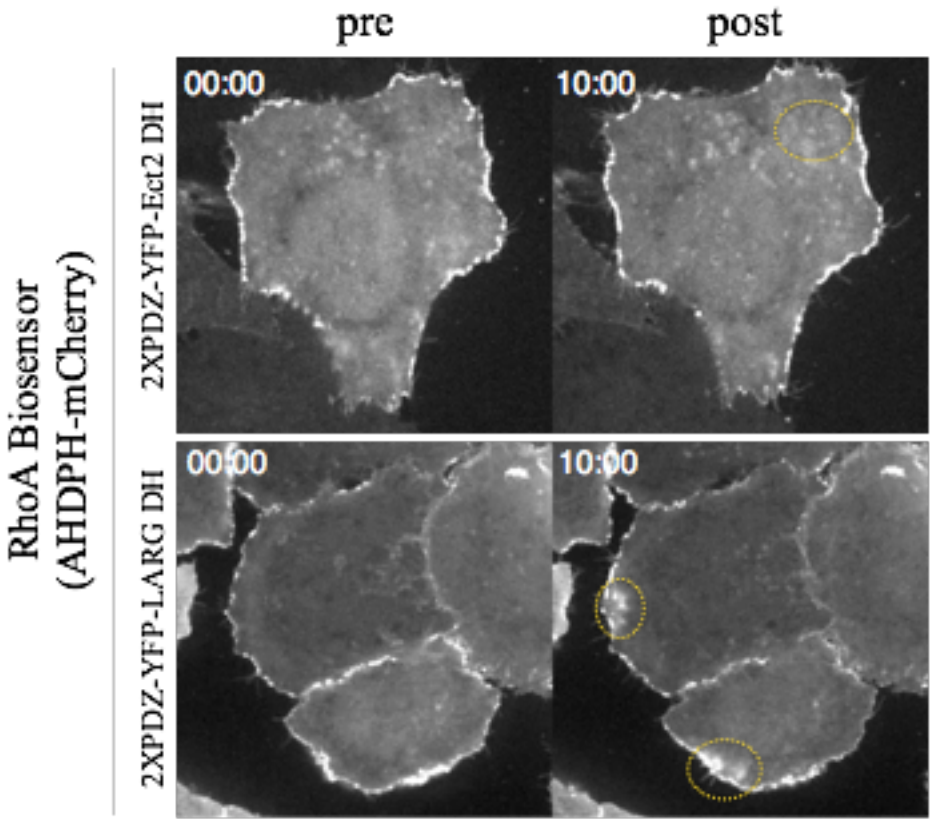


Figure 15: Light-mediated RhoA activation with Ect2 DH vs LARG DH. Hela cells co-expressing Stargazin-GFP-LOVpep, AHDPH-mCherry, and either 2XPDZ-YFP-Ect2DH (A) or 2XPDZ-YFP-LARGDH (B) were locally (yellow circles) photoactivated using the Mosaic system every 20 sec for 5 mins and pre- and post-photoactivation mCherry images are shown.

**Chapter 4: Local RhoA Activation Induces Cytokinetic Furrows Independent of Spindle Position and Cell Cycle Stage**

Elizabeth Wagner and Michael Glotzer

Department of Molecular Genetics and Cell Biology

The University of Chicago

Chicago, IL 60637

**Recently accepted for publication in Journal of Cell Biology

## 4.1 Abstract

The GTPase RhoA promotes contractile ring assembly and furrow ingression during cytokinesis. While many factors that regulate RhoA during cytokinesis have been characterized, the spatiotemporal regulatory logic remains undefined. Here, we have developed an optogenetic probe to gain tight spatial and temporal control of RhoA activity in mammalian cells and demonstrate that cytokinetic furrowing is primarily regulated at the level of RhoA activation. Light-mediated recruitment of a RhoGEF domain to the plasma membrane leads to rapid induction of RhoA activity, leading to assembly of cytokinetic furrows that partially ingress. Furthermore, furrow formation in response to RhoA activation is not temporally or spatially restricted. RhoA activation is sufficient to generate furrows at both the cell equator and at cell poles, in both metaphase and anaphase. Remarkably, furrow formation can be initiated in rounded interphase cells, but not adherent cells. These results indicate RhoA activation is

sufficient to induce assembly of functional contractile rings and that cell rounding facilitates furrow formation.

### 4.2 Introduction

Cytokinesis is the final stage of cell division in which an actomyosin-based contractile ring physically divides the cell into two genetically equivalent daughter cells. Our understanding of cytokinesis has been greatly influenced by classical experiments in which spindles and/or cells were repositioned or micromanipulated. These perturbations demonstrated that the spindle induces furrow formation during a specific time interval following anaphase onset (Rappaport, 1985). At a molecular level, the small GTPase, RhoA, serves as an essential, dosage-sensitive regulator of cleavage furrow formation in metazoan cells (Kishi et al., 1993). RhoA serves as a molecular switch that is active when bound to GTP. Once active, RhoA binds to effectors including a diaphanous-related formin to induce F-actin assembly (Otomo et al., 2005; Watanabe et al., 2008) and Rho Kinase, ROCK, to activate non-muscle myosin II {Kosako:2000cm}. Through these and other effectors, RhoA regulates the dynamic changes in actomyosin required for contractile ring assembly and cleavage furrow formation.

RhoA activation during cytokinesis is spatially and temporally regulated and dependent upon the RhoGEF Ect2 (Tatsumoto et al., 1999). Ect2 localization and activation are regulated by phospho-dependent interactions with centralspindlin, a protein complex that accumulates on the spindle midzone during anaphase (Wolfe et al., 2009; Yüce et al., 2005; Zhang and Glotzer, 2015)(Fig. 16A). This complex also accumulates on the cortex where it directs local RhoA activation (Basant et al., 2015). Despite extensive research, several questions concerning the

regulation of cytokinesis remain unanswered. Is local activation of RhoA sufficient to generate a cleavage furrow or are other factors required in parallel to RhoA for furrow formation? Are there spatial or temporal requirements for RhoA-mediated contractile ring assembly and furrow formation?

Answers to these fundamental questions require the ability to spatially and temporally manipulate cytokinesis at the molecular level, in particular, at the level of RhoA activation. Optogenetic tools provide of precise control of protein localization. In many cases, control of localization allows control of protein activity (Strickland et al., 2012; Toettcher et al., 2013). We have engineered an optogenetic tool to manipulate RhoA activity and have used it to demonstrate that local activation of RhoA is sufficient to direct cleavage furrow formation.

### 4.3 Light-mediated control of RhoA

Previous iterations of the two component optogenetic system TULIPs utilized a membrane-targeted photosensitive domain, LOVpep, in conjunction with a second tag, ePDZ-b1, that binds to LOVpep in a light-dependent manner (Strickland et al., 2012). Here, we substituted the ePDZ-b1 tag with a tandem PDZ tag which is functional in more diverse protein fusions. To manipulate RhoA activation with light, we fused the tandem PDZ tag to the highly specific RhoA guanine nucleotide exchange factor (GEF) LARG (Jaiswal et al., 2011), creating a construct we refer to as photorecruitable GEF (PR_GEF) (Fig. 16B ). To reduce basal activity, only the catalytic GEF DH domain was included. GFP-tagged LOVpep was localized to the plasma membrane by fusion to the transmembrane receptor Stargazin. A digital micro mirror device was used to illuminate

arbitrarily defined regions of the cell with 405 nm light. Illumination of adherent cells expressing these constructs resulted in light-mediated local recruitment of PR_GEF (Fig. 16C-D). Recruitment also leads to local accumulation of myosin and F-actin within 20-40 secs (Fig. 16 E-H). When illumination ceases, the local increase in GEF recruitment is rapidly lost, consistent with the thermal reversion of LOVpep into the dark state (Strickland et al., 2012) ($t_{½}$ = 80 sec)(Fig. 16D). The local increases in actin and myosin are lost with roughly similar kinetics (Fig. 16F,H), suggesting that RhoA activation is not self-sustaining and suggest the existence of RhoGAPs that rapidly inactivate ectopically activated RhoA.

**4.4 Local activation of RhoA is sufficient to initiate furrow formation at the midzone of anaphase cells**

A central question we sought to answer was whether a local zone of RhoA activation is sufficient to form a cleavage furrow. The least stringent test of this model is to determine whether, in a cell progressing normally through anaphase, light-induced RhoA activation can substitute for the endogenous pathway at the equator. Polo-like kinase 1 (Plk1), is required for the phospho-dependent interaction between centralspindlin and Ect2; Plk1 inhibition therefore precludes RhoA activation and furrow formation (Petronczki et al., 2007; Wolfe et al., 2009). This provides an appropriate context for examining whether light-mediated activation of RhoA is sufficient to induce furrow formation.

To generate non-contractile anaphase cells, HeLa cells were arrested in metaphase using a low dose of nocodazole (30 ng/ml) for 4-5 hrs. Release of the block allows cells to initiate mitotic exit. Plk1 inhibitor (BI 2536, 200 nM) was added 30 min after release to block endogenous RhoA activation while permitting anaphase onset (Fig. 17A) (Petronczki et al., 2007). In the

absence of PR_GEF recruitment, cells remain non-contractile and furrows do not form (Fig. 17C). Light-mediated activation of RhoA at the equator was sufficient to initiate formation of a cleavage furrow (Fig. 17D). The initial rate of ingression was similar to that of cells dividing normally in the absence of BI 2536 (Fig. 17J). This photoactivation protocol zone induced recruitment of PR_GEF to a finely limited region around the entire cell circumference (Fig 17G). Notably, light-induced furrows do not fully ingress (~34% , n=32). Furrows resulting from PR_GEF recruitment require the RhoA pathway as the extent of furrowing was inhibited by Rho kinase inhibitor (5.6 +/- 4%; n=4) (Fig. 2F) and recruitment of $PDZ_2$-mCherry failed to induce furrow formation (Fig. 17E). In the absence of continued photoactivation, furrows regress, indicating that RhoA activation during cytokinesis is not self-sustaining under these conditions.

Furrowing activity is restricted to sites of PR_GEF recruitment. Recruitment of PR_GEF to one side of the cell generates a unilateral furrow and recruitment of PR_GEF to a wide equatorial zone induces equatorial flattening rather than an ingressing furrow (Fig. 17H-I).
In addition to regulating the Ect2:centralspindlin interaction, Plk1 may promote furrow ingression through other substrates (Liu et al., 2004; Lowery et al., 2007; Neef et al., 2003; Niiya et al., 2006; Wolfe et al., 2009). To generate non-contractile anaphase cells without inhibiting Plk1, cells were depleted of HsCyk4. Light-mediated activation of RhoA in Cyk4-depleted cells induces furrow ingression to 33 +/- 5 % at 4.2 +/- 1.76 μm/min (n=6) (Fig. 3 A,B). Thus, light induced furrowing is similar in Cyk4-depleted and Plk1-inhibited cells, indicating Plk1 functions primarily upstream of RhoA activation.

To test whether incomplete ingression might be a consequence of the mode of RhoA activation, we induced light-mediated RhoA activation at the equator of cells in which the endogenous pathway for furrow formation was intact. Cells treated in this manner ingressed significantly further than cells induced to furrow by light alone, though they did not fully ingress during 20 min of observation (78.8 +/- 9.29 % at 3.9 +/- 1.56 μm/min, n=6) (Figure 18C).

To examine if limited ingression was due to insufficient levels of RhoA activation, we used a RhoA biosensor (Piekny and Glotzer, 2008) to compare the levels of active RhoA in cells furrowing in response to PR_GEF recruitment and in normally dividing cells. The distribution and level of active RhoA are comparable to those in normally dividing cells (Fig. 18D, E, J). In addition, two downstream effectors of RhoA, F-actin and myosin, accumulate at levels comparable to those observed in normally dividing cells (Fig. 18F-J). Thus, incomplete ingression does not appear to caused by dramatically reduced activation of RhoA or its key effectors.

**4.5 The anaphase cortex is uniformly responsive to RhoA activation**

We exploited the flexibility that optogenetic tools provide to determine whether the response to RhoA activation is spatially modulated in the anaphase cortex. The anaphase spindle has been shown to play both positive and negative roles in directing RhoA activation and cleavage furrow formation. The central spindle promotes local RhoA activation and cleavage furrow formation at the midzone {Fededa:2012cb}. Conversely, dynamic astral microtubules play a role in inhibiting cortical contractility in the polar regions (van Oostende Triplet et al., 2014; Werner et al., 2007). The spindle may provide additional positive cues in addition to locally regulating RhoA, such as directed membrane trafficking (Drechsel et al., 1997) and local accumulation of mitotic kinases

{Golsteyn:1995wj}{Adams:2001ue}. Thus, induction of active RhoA at cell poles provides a stringent test of whether RhoA activation is sufficient to induce furrowing.

Using the same experimental design where endogenous RhoA activation pathway is suppressed by the Plk1 inhibitor, we induced local RhoA activation in a zone spanning the cell poles. RhoA activation is sufficient to initiate furrow formation at this site. These furrows behave similarly to those at induced at the midzone, ingressing ~36% at a constriction rate of 4.5 μm/min (Fig. 19A-C). To directly compare the response to RhoA activation in the midzone vs. poles we simultaneously activated both regions in the same cell. Concurrent illumination of the midzone and poles induces furrows in both regions that ingress at similar rates and to similar extents (Fig. 19D-F). To rule out the possibility that excessive PR_GEF recruitment overwhelms the inhibitory effects of astral microtubules, we compared the response at the equator and poles with shorter pulses of light. The duration of the illumination pulse permits tuning of the levels of GEF recruitment and RhoA activation (Supplemental Fig. 12). We observe simultaneous and similar degrees of furrow induction in the equatorial and polar regions at short activation pulses (Figure 19G). We conclude that RhoA activation alone is sufficient to induce cleavage furrow ingression and the entire cortex is equally responsive to RhoA activation. Furthermore, astral inhibition does not principally act at the level of active GTP-bound RhoA or its downstream effectors, but rather appears to act upstream of RhoA activation.

As PR_GEF can induce furrowing at the poles, we also assessed the ability of exogenous RhoA activation to compete with the endogenous pathway. Polar recruitment of PR_GEF dramatically slows ingression of the endogenous furrow; in some cases blocking furrow initiation altogether

(Fig. 19G-I). Although we do not observe deep furrows in the poles in these perturbations, we observe local flattening and suppression of blebbing in the zone of activation, indicating polar activation. This provides additional evidence that the level of RhoA activation induced by PR_GEF is roughly comparable to that of the endogenous furrow.

**4.6 The response of RhoA activation is not strongly regulated during the cell cycle**

We next sought to determine if the response to RhoA activation is temporally regulated. Because the upstream RhoA activation pathway is largely suppressed by Cdk1 activity in metaphase (Yüce et al., 2005), it is not known whether active RhoA or its downstream effectors are subject to cell cycle regulation. Cells were arrested using a low dose of nocodazole (30 ng/ml) for 4-5 hrs and released for 20 mins to allow assembly of astral microtubules. Prior to mitotic exit, PR_GEF was locally recruited, resulting in furrow formation. The response to local RhoA activation was similar to that seen during anaphase. Furrows ingressed ~33% at a rate of ~4.8 μm/min (Fig. 19A,B, Supplemental Fig. 13). Thus, there does not appear to be potent metaphase-specific regulation of active RhoA or its downstream effectors. PR_GEF-induced furrow formation occurs irrespective of whether the zone of illumination was parallel or perpendicular to the metaphase plate, indicating that the response to RhoA activation during metaphase is not spatially regulated.

The consistent response to RhoA activation irrespective of mitotic stage or spindle position prompted us to investigate whether local activation of RhoA can induce furrow formation during interphase. As shown in Figure 16 C,E,G, local activation of RhoA in adherent interphase cells promotes F-actin and myosin II accumulation but does not induce furrowing. However, cells entering mitosis remodel their adherence to the substrate and to neighboring cells, allowing them

to round (Stewart et al., 2011). We hypothesized that a decrease in cell adhesion would alter the response to local RhoA activation in interphase cells. To induce cell detachment and rounding we treated NIH3T3 cells with trypsin-EDTA prior to replating. Upon local illumination, cells rapidly form furrows which ingress to 72 % of completion (Fig. 20D). Similar results were observed in non-adherent interphase HeLa cells (Supplemental Fig. 14). These results demonstrate that local activation of RhoA is sufficient to induce assembly of a contractile ring and no mitosis specific factors downstream of RhoA are required for cleavage furrow formation.

**4.7 Cortical tension modulates furrow ingression in response to local RhoA activation**

Exogenous activation of RhoA is sufficient to initiate furrow formation throughout the cell cycle, however, furrows ingress further in non-adherent interphase cells as compared to those in metaphase or anaphase. The distinct mechanical properties of mitotic vs rounded interphase cells may contribute to this differential response. Mitotic entry induces an isotropic increase cortical tension and hydrostatic pressure concomitant with cell rounding; the rounding pressure is approximately 3-fold higher in metaphase as compared to non-adherent interphase cells (Stewart et al., 2011). Enhanced furrow ingression in non-adherent interphase cells could therefore reflect their increased compliance relative to mitotic cells.

We therefore modulated the levels of global cortical tension and assessed whether this altered the response to local RhoA activation in non-adherent interphase cells. In addition to the normal local photoactivation pulse (960 ms) cells were also globally illuminated cells with a short (10 ms) pulse to modestly increase global cortical tension. In comparison to local activation alone, global activation induces a 1.5-fold decrease in both the extent of ingression and the constriction

rate (Fig. 20E-G). Conversely, a global decrease in cortical tension in mitotic cells would be predicted to enhance light-mediated furrow ingression. Upon treatment of non-contractile anaphase cells with the Na/H exchange inhibitor EIPA, which has been shown to decrease cortical tension levels of mitotic cells(Stewart et al., 2011), we observed an increase in the extent of furrow ingression (Fig. 20B,C) (45.6 +/- 10 % ingression at rate 3.84 +/- 1.44 μm/min, n=8) compared to untreated cells (33.9 +/- 13.3 % ingression at a rate of 3.7 +/- 1.8 μm/min). These results demonstrate that cortical compliance impacts furrow ingression.

**4.8 Discussion**

RhoA activation is necessary for contractile ring assembly and cleavage furrow formation during cytokinesis {Fededa:2012cb}. However, whether RhoA activation is the primary control point for cleavage furrow assembly has not been previously examined. An optogenetic approach to control RhoA activation has allowed us to molecularly dissect the regulatory logic underlying furrow formation. Exogenous activation of RhoA is sufficient to rescue furrow formation and the anaphase cortex is uniformly responsive to RhoA activation. These results demonstrate that neither the spindle midzone nor astral microtubules directly regulate active RhoA or its downstream effectors during furrow initiation. Rather, these structures regulate cytokinesis by promoting or inhibiting RhoA activation, respectively.

RhoA activation is also sufficient to induce contractile ring assembly in non-adherent interphase cells. Decreased cell adhesion and rounding are commonly observed in dividing cells {Meyer:2011ec}. As active RhoA does not induce furrows in adherent cells, our results suggest

furrowing requires both mitotic cell rounding and the ability to generate an equatorial zone of active RhoA.

The response to RhoA activation is not strongly cell cycle regulated, as we observe equal furrow formation in metaphase and anaphase cells. The enhanced furrow ingression observed in non-adherent interphase cells may be due, at least in part, to their reduced cortical tension as compared to mitotic cells (Stewart et al., 2011). Thus, we propose that cytokinesis is normally restricted to anaphase because of cell cycle regulation of cell rounding and the formation of an equatorial zone of active RhoA. We speculate that the central spindle provides a pool of Ect2-centralspindlin that drives complete furrow ingression by activating RhoA with high spatial precision. Accumulating evidence indicates centralspindlin, Ect2, and RhoA are engaged in a positive feedback loop that may strengthen and sharpen the zone of RhoA activation (Bement et al., 2015; Zhang and Glotzer, 2015) which may contribute to complete furrow ingression during anaphase.

## 4.9 Methods

### Cell culture and Drug Treatment

HeLa and NIH3T3 (ATCC) cells were grown in Dulbecco's modified Eagles medium (Sigma) supplemented with 10% fetal bovine serum (Hyclone; Thermo Fisher Scientific), 0.2 mM L-glutamine (Invitrogen), and 1% penicillin/streptomycin (Invitrogen). Where indicated, endogenous HsCyk4 was depleted as described previously (Yüce et al., 2005). For HeLa cell experiments, cells were plated onto glass coverslips one day before transfection with plasmid DNA and siRNAs (where applicable) using Lipofectamine 2000 (Invitrogen). For all mitotic cell

experiments, 24 h post transfection, HeLa cells were arrested in prometaphase with a 30 ng/ml Nocodazole (Sigma) for 4-6 hours. The nocodazole was then washed off and cells were incubated for 30 mins to allow them to recover and exit metaphase. BI-2536 (200 nM, generously provided by Norbert Kraut, Boehringer Ingelheim) was then added to block RhoA activation as cells entered anaphase. For NIH3T3 cell experiments, plasmids were transiently transfected using a Neon electroporation system (Invitrogen). For non-adherent HeLa and NIH3T3 cell experiments, cells were trypsinized using 0.05% trypsin-EDTA (Sigma), washed, replated onto glass coverslips and incubated for 5-10 mins to allow minimal adhesion prior to imaging. HeLa and NIH3T3 cells were differentially suited to the mitotic and interphase experiments. Detached interphase HeLa cells are too non-adherent and tend to move during experiments. Conversely, NIH3T3 cells are too weakly attached during mitosis for reliable imaging.

**Constructs**

The optogenetic membrane tether consists of a Stargazin-GFP-LOVpep fusion. Full-length Stargazin (a gift from A Karginov, University of Illinois Chicago, Chicago IL) was used. The LOVpep variant used contains the substitutions T406A, T407A, I532A (Strickland et al., 2012). The PR_GEF construct consists of a $(PDZ)_2$-mCherry-LARG(DH) fusion protein. The PDZ domain is derived from erbin {Skelton:2003ht} (a gift from S. Koide, University of Chicago, Chicago IL), which was fused to the DH domain (aa 766-997) of the RhoGEF LARG (NM_015313.2). Flexible linkers ($SAGG_3$ and $SAGG_5$, respectively) were placed between the PDZ domains and between mCherry and the LARG DH domain. $PR\_GEF^{YFP}$ was constructed in an identical manner to PR_GEF with YFP replacing mCherry. This construct was used in experiments where the effects on various downstream markers were visualized. To examine the

levels of RhoA activation we used the RhoA biosensor (AHDPH-mCherry) (Piekny and Glotzer, 2008). To examine effects on the actin and myosin networks, we used mApple-Actin and mApple-MLC constructs (gifts from M Davidson, U. Florida, Gainesville FL).

**Live Cell Imaging and Photoactivation**

Glass coverslips were placed into an imaging chamber with media supplemented with 10 mM HEPES and 3% Oxyrase (Oxyrase Inc., Mansfield, OH) and maintained at 37°C. Cells were imaged using a 60X 1.49 NA ApoTIRF oil-immersion objective on a Nikon Ti-E inverted microscope (Nikon, Melville, NY). The microscope is fitted with a spinning disk confocal (CSU-X1; Yokogawa Electric, Musashino, Tokyo, Japan), illuminated with a laser merge module containing 491 nm and 561 nm lasers (Spectral Applied Research, Richmond Hill, Ontario, Canada). Images were acquired with Coolsnap HQ2 CCD camera (Photometics). A Mosaic digital micromirror-based device (DMD) equipped with a 100 mW 405 nm laser (Photonic Instruments) was used for photoactivation. MetaMorph acquisition software (Molecular Devices, Eugene, OR) was used to control the microscope hardware. The photoactivation laser was electronically attenuated and optically filtered such that the total incident light if the entire DMD was illuminated was < 1 μJ/s. For all photoactivation experiments unless designated otherwise, the defined ROI was illuminated for 960 ms every 20 secs for 20 min. In some cells, Stargazin-GFP-LOVpep hyperaccumulates in a photoactivation-dependent manner. This hyperaccumulation is not observed upon recruitment of a probe lacking the GEF (2X-PDZ-mCh). Therefore, we infer that cortical contractility can induce concentration of the membrane tethered probe. When the entire cell was globally activated, an additional 10 ms exposure was added. To select cells for study, confocal images were acquired with 491 nm light followed by 561 nm light and robust recruitment of PR_GEF was visually confirmed. To examine effects on

RhoA activation levels (AHD-mCherry), actin (mApple-actin), or myosin (mApple-MLC), these constructs were co-expressed with Stargazin-GFP-LOVpep and PR_GEF$^{YFP}$. Cells strongly expressing both the reporter and the membrane tether were chosen for study. In studies where Stargazin-GFP-LOVpep and PR_GEF were co-expressed, GFP and mCherry positive intracellular puncta were observed (Fig. 16) and the number of puncta appears to increase during photoactivation. We speculate that these are membrane-bound structures that form is response to RhoA activation. These puncta are also present in control experiments using the $PDZ_2$-mCh lacking the GEF, albeit at much lower frequencies and do not increase in response to photoactivation.

**Image Analysis**

To quantify the extent and rates of furrow ingression, the position of each side of the ingressing furrow was manually tracked at each time point. The extent of ingression was normalized by measuring the cell diameter between furrow tips and dividing by the initial cell diameter. To measure the accumulation of the RhoA biosensor, actin, and myosin II in furrowing cells, linescans were drawn through the furrow region. For each timepoint, the maximum intensity, reflecting the cortically localized signal, was measured as was an average cytoplasmic intensity; recruitment is defined as the ratio of these values. Results shown represent the average of the maximal recruitment for each cell. In adherent cells, the average intensity in the activation region was measured and normalized to the initial intensity.

## 4.10 Appendix 4

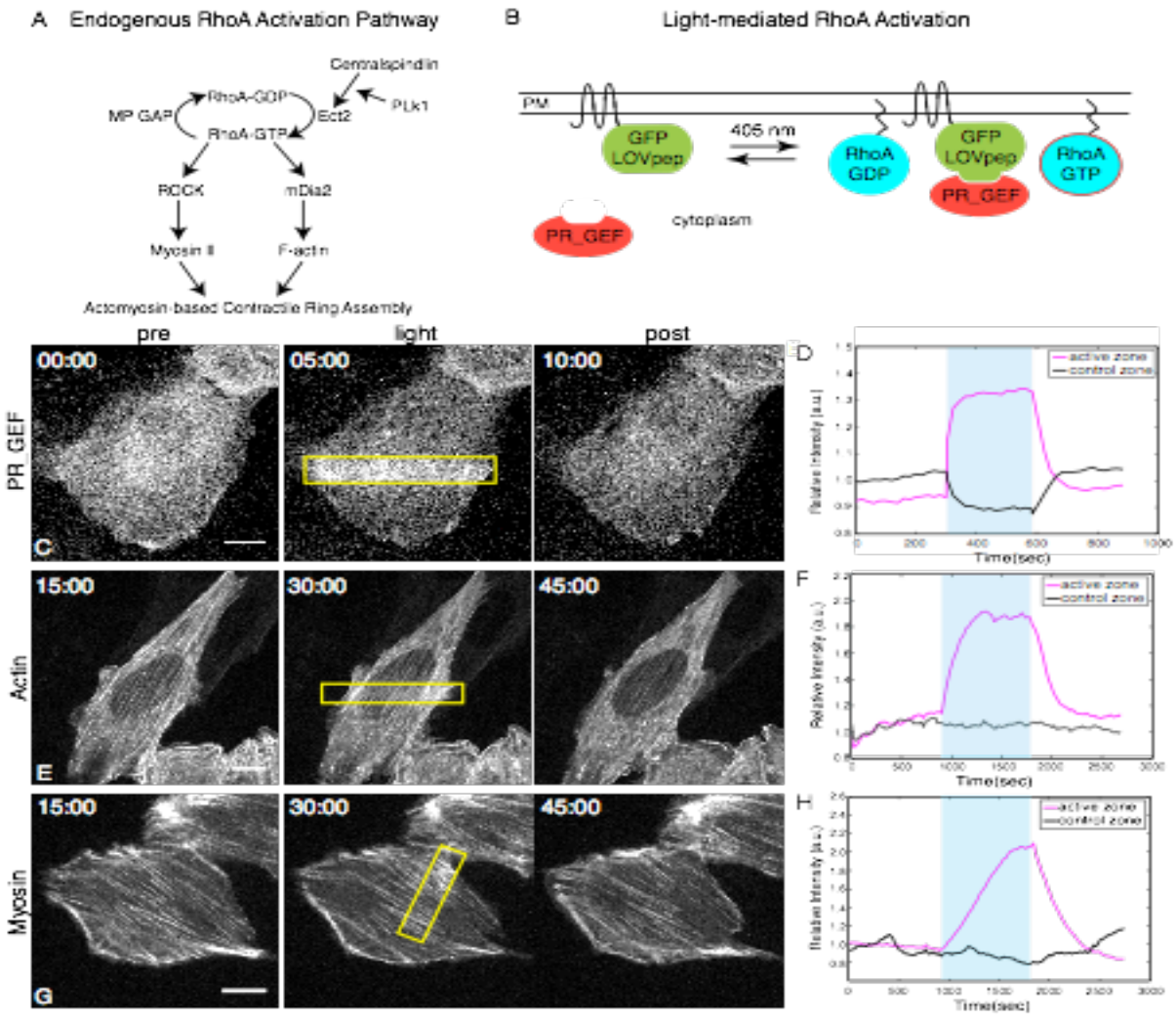


Figure 16: (A) Schematic depicting the pathway that promotes RhoA activation during cytokinesis. (B) TULIPs-mediated activation of RhoA by light-directed recruitment of PR_GEF. Photoactivation of NIH3T3 cells (yellow boxes) induces local recruitment of PR_GEF (n=9)(C), F-actin polymerization (n=7) (E), and myosin accumulation (n=15) (G). Quantification of the relative increase in intensity in the activation region (magenta) vs. a control region (black) for PR_GEF (D), mApple-actin (F), and mCherry-MLC (H) over time. During photoactivation, designated by the blue box, cells were locally illuminated (405 nm) with a 960 ms pulse every 20 sec. PR_GEF or effectors were imaged every 20 secs. Scale bar: 10 µm.

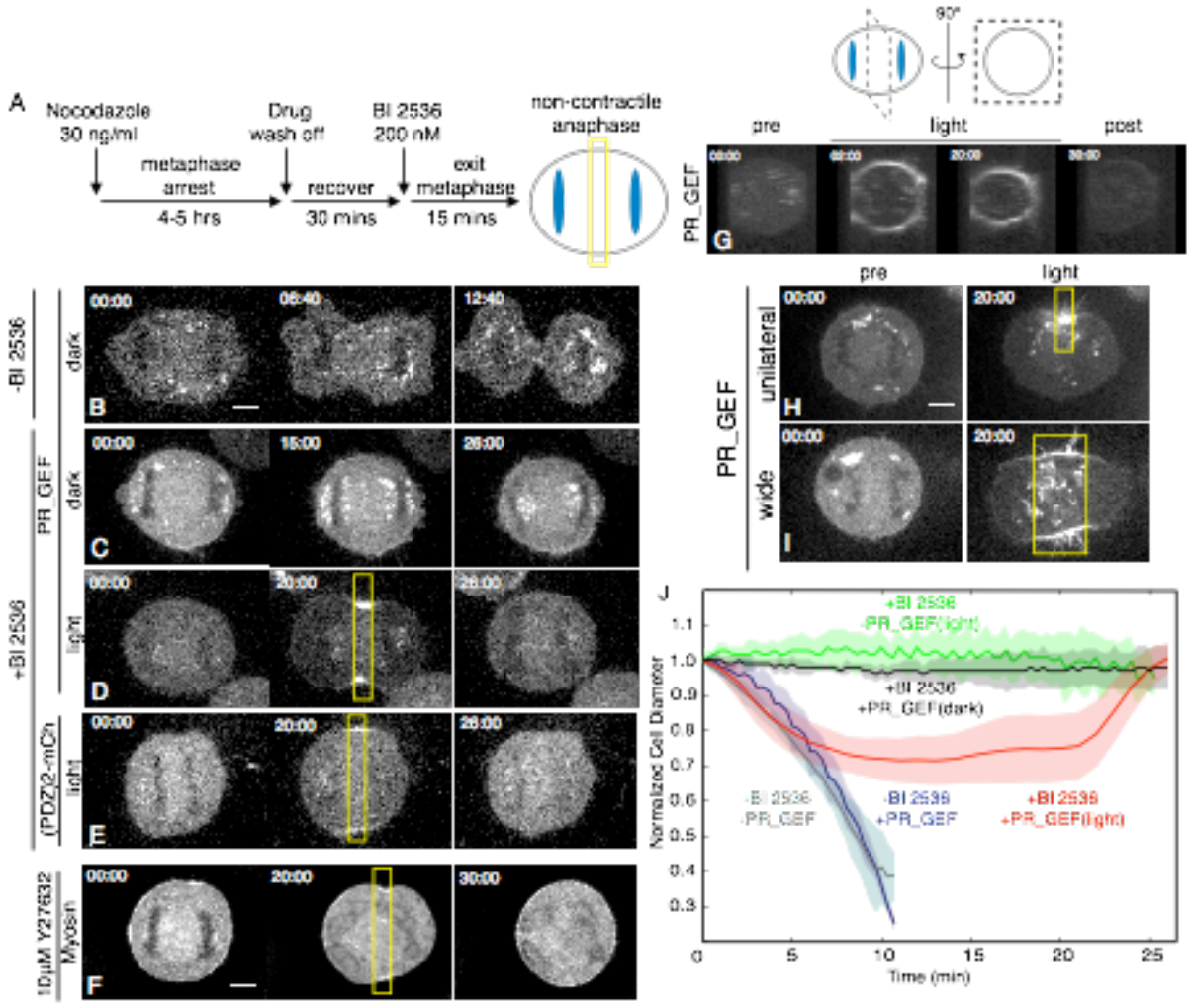


Figure 17: (A) Protocol for generating non-contractile anaphase HeLa cells. (B) Images of control HeLa cell expressing PR_GEF dividing normally without illumination (dark). Images of non-contractile anaphase HeLa cells (200 nM BI 2536) expressing PR_GEF (C,D) or $PDZ_2$-mCh (E) either with photoactivation (yellow boxes) (D,E) or without (C). (F) Cell treated as in (D) in presence of ROCK inhibitor (10 μM Y27632, 30 min.). (G) 3-D reconstruction of the midzone region of a non-contractile anaphase Hela cell expressing PR_GEF before (pre), during (light) and following (post) photoactivation. (H-I) Images of cells treated as in D in which the photoactivation zone is restricted (H) or expanded (I). (J) Time course of average (+/- S.E.M.) furrow ingression overtime of HeLa cells dividing normally (-BI 2536) with (blue, n=7) and without (grey, n=10) PR_GEF expression (T=0 is furrow initiation), non-contractile anaphase cells (+BI 2536) expressing PR_GEF with (red, n=32) and without local illumination (black, n=6), and local illuminated non-contractile anaphase cells (+BI 2536) expressing $PDZ_2$-mCherry (green, n=5) (T=0 start of photoactivation or start of imaging for dark controls). For all photoactivation experiments, cells were photoactivated for 20 mins followed by 10 mins without photoactivation. In all figures, cells are oriented so that the spindle axis is horizontal. Scale bar: 5 μm.

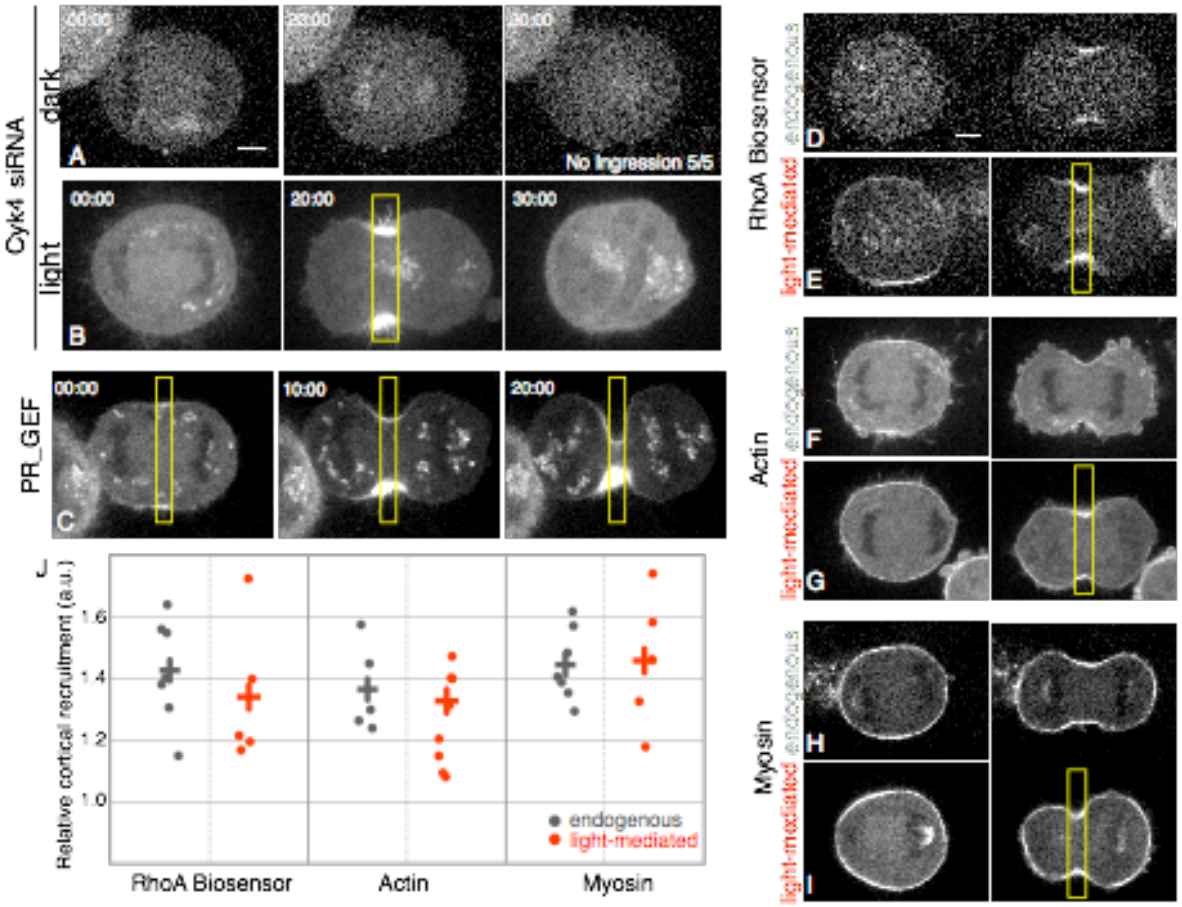


Figure18: Images of anaphase HeLa cells transfected with PR_GEF and Cyk4 siRNA without (A) or with (B) photoactivation. (C) Images of normally dividing Hela cell expressing PR_GEF just prior (t=0) and during (light) local illumination at the midzone. Comparison of RhoA biosensor (AHDPH-mCherry) (D-E), F-actin (mApple-actin) (F-G), and myosin (mApple-MLC) (H-I) in cells dividing normally and during light-induced furrow formation. (J) Quantification of recruitment of RhoA biosensor, actin, and myosin at endogenous (grey) or light-induced (red) furrows; each dot represents an individual cell, + indicates the average for that condition. For all photoactivation experiments, cells were locally illuminated for 20 mins. Scale bar: 5 µm.

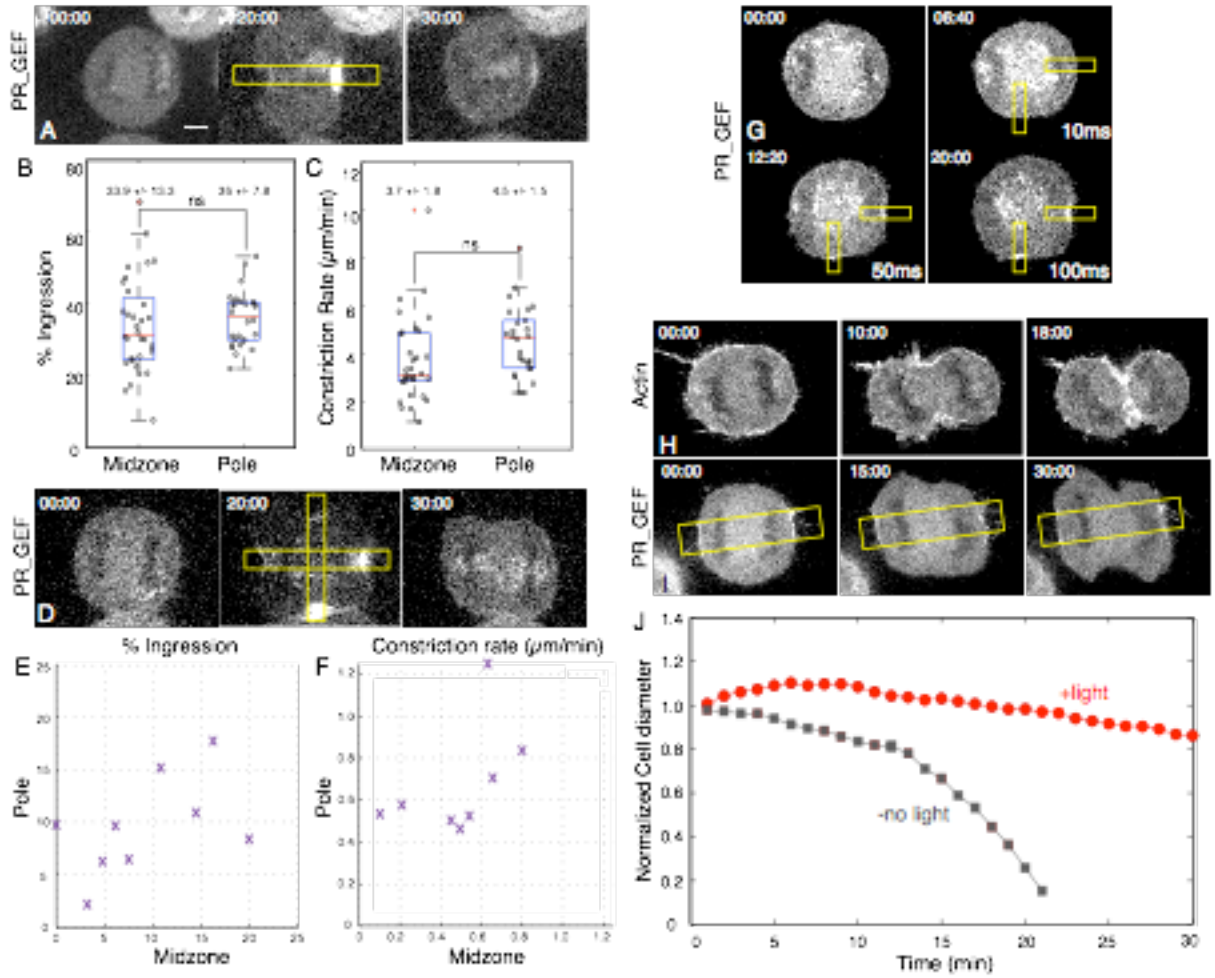


Figure19: (A) Images of non-contractile anaphase HeLa cells (200 nm BI 2536) expressing PR_GEF photoactivated (yellow boxes) parallel to the spindle axis. Quantification of the extent of ingression (B) and constriction rate (µm/min) (C) of light-induced furrows at cell midzone and poles. (D) Images of non-contractile anaphase HeLa cells (200 nm BI 2536) expressing PR_GEF photoactivated at both the midzone and polar regions. Comparison of the extent of ingression (%) (E) and constriction rate (µm/min) (F) at the midzone vs pole for individual cells (n=8). (G) Images of non-contractile anaphase HeLa cells expressing PR_GEF photoactivated with pulses of the indicated duration at the midzone and pole. (H) Images of HeLa cell expressing mApple-Actin undergoing cytokinesis (-BI 2536). (I) Images of a HeLa cell expressing PR_GEF undergoing cytokinesis (-BI 2536) with polar photoactivation. (J) Ingression kinetics of the endogenous furrow with polar photoactivation (red) and without (grey). In (H-I) cells were photoactivated for 30 min. Scale bar: 5 µm.

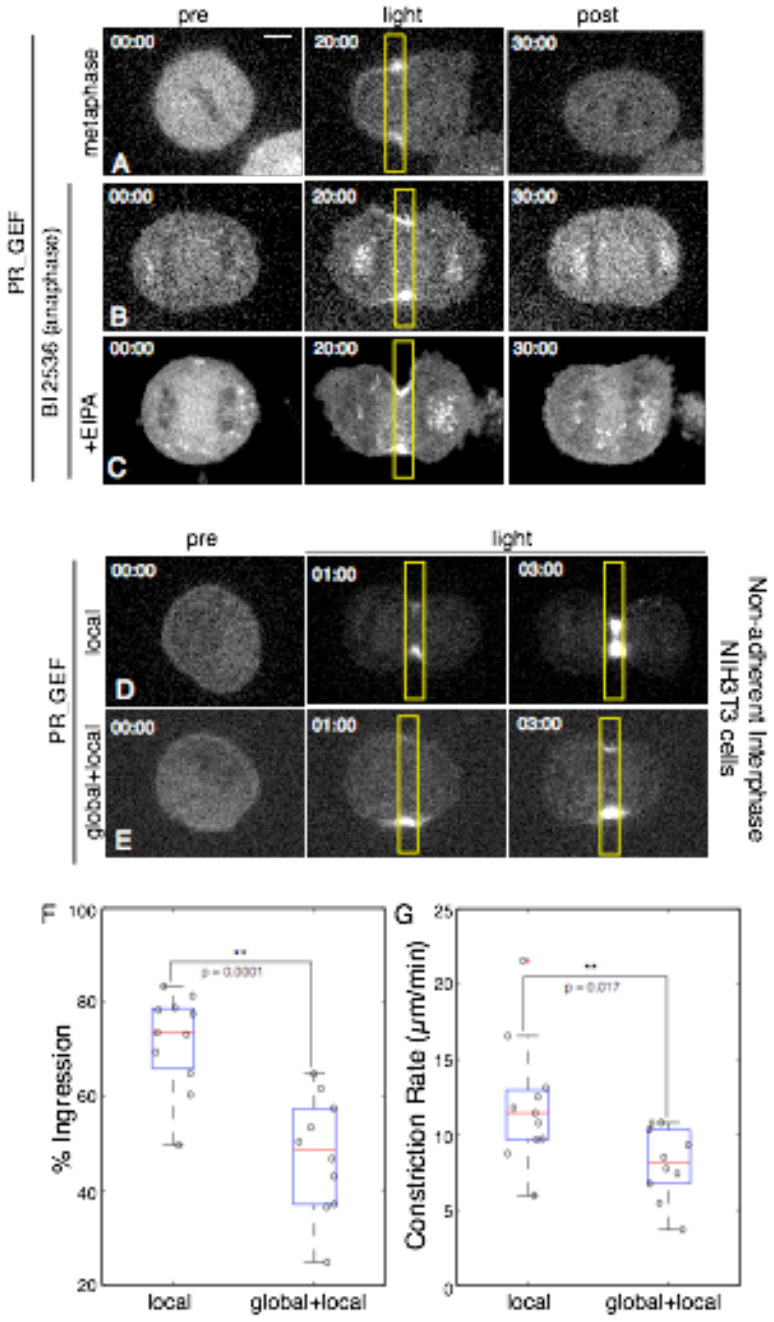


Figure20: Images of photoactivated metaphase HeLa cells (A), non-contractile (200 nM BI 2536) anaphase HeLa cells without (B) and with EIPA (37.5 µM, 30 min) (C). Non-adherent interphase NIH3T3 cells photoactivated only locally (960 ms pulse) (D) or supplemented with global illumination (10 ms pulse) (E). Quantification of ingression (%) (F) and constriction rate (µm/min) (G) of non-adherent interphase NIH3T3 cells illuminated as in D-E. Scale bar: 5 µm.

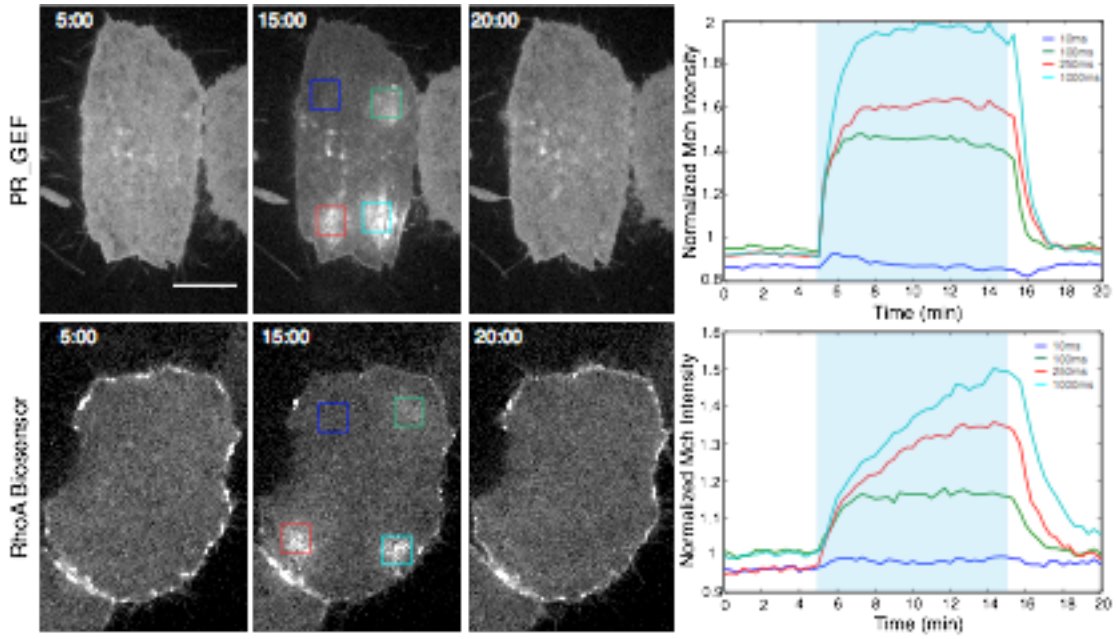


Supplementary Figure 12: (A) Images of a HeLa cell expressing PR_GEF or RhoA Biosensor just prior to (pre), during (light), and following (post) simultaneous local illumination at the designated regions (boxes) for varying pulse lengths. (B) Quantification of relative intensity of each region as a function of time. Cells were locally illuminated with 405 nm light every 20 secs for designated pulse length for the designated photoactivation period (blue-shaded region) and 561 nm images were taken every 20 secs. Scale bar is 10 μm.

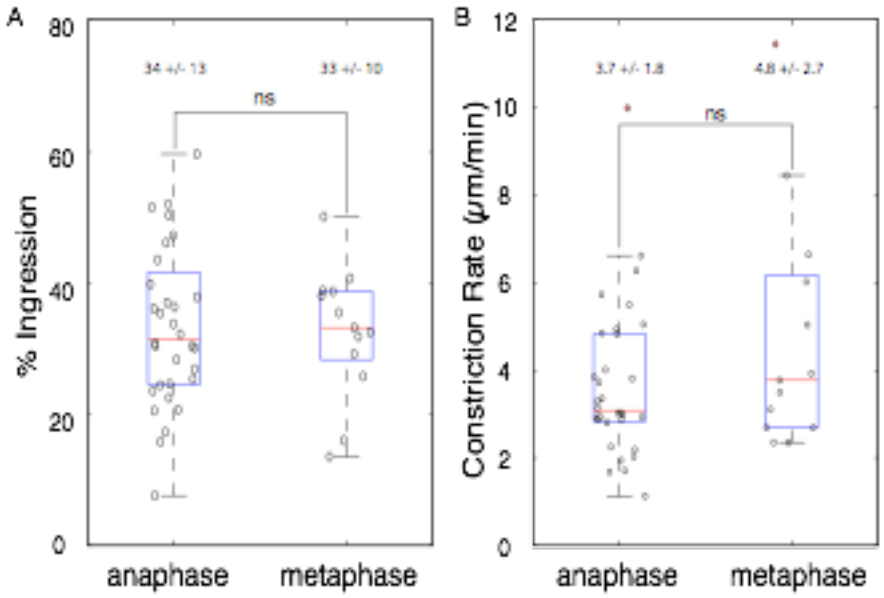


Supplementary Figure13: Quantification of extent of furrow ingression (A) and constriction rate (µm/min) (B) of HeLa cells locally illuminated at the midzone during metaphase cells (results with Plk1-inhibited anaphase cells from Figure 3B-C is shown for comparison).

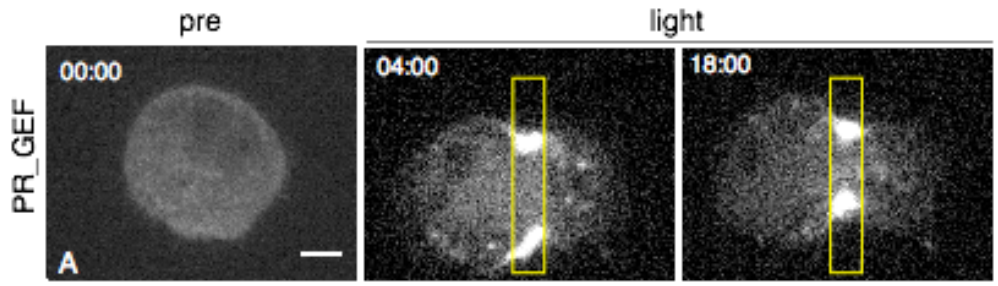


Supplementary Figure 14: (A) Images of locally illuminated,non-adherent interphase HeLa cell. For n= 4 cells, the mean % Ingression was 69 +/- 6.3% and the mean constriction rate was 7.34 +/- 4.59 µm/min. The increased adhesive nature of NIH3T3 cells when replated onto glass coverslips stabilized cells for imaging, while HeLa cells frequently moved out of the imaging field. Scale bar is 5 µm.

## Chapter 5: Spatial Regulation of RhoA Reveals Zyxin-mediated Mechanics of Stress Fibers

Patrick W. Oakes[1,4*], Elizabeth Wagner[2*], Christoph A. Brand[3+], Dimitri Probst[3+], Marco Linke[3+], Ulrich S. Schwarz[3], Michael Glotzer[2], Margaret L. Gardel[1]

[1]Institute for Biophysical Dynamics, James Franck Institute and the Department of Physics, University of Chicago, Chicago, IL 606037

[2]Department of Molecular Genetics and Cell Biology, University of Chicago, Chicago, IL 60637

[3]Institute for Theoretical Physics and BioQuant, Heidelberg University, Heidelberg, Germany

[4]Current address: Department of Physics & Astronomy, University of Rochester, Rochester, NY 14627

[*,+]Contributed equally

In addition to my main thesis project, I established a collaboration with the Gardel and Schwarz labs to utilized light-induced RhoA mediated contractility to probe mechanical properties of cells. This manuscript is currently being submitted to eLife for publication.

### 5.1 Abstract

The mechanics of the actin cytoskeleton regulates cell morphogenesis during essential physiological processes. While cellular contractility is known to be largely RhoA-dependent, how localized biochemical signals translate into cell-level responses is not well understood. Here, we use an optogenetic approach to spatiotemporally increase RhoA activity to probe the mechanics of the actin cytoskeleton in adherent fibroblasts. Local activation of RhoA results in

local increases in F-actin and myosin, but not *de novo* formation of stress fibers or focal adhesions. It also stimulates local contraction, leading to increased traction forces that rapidly propagate across the cell via stress fibers and drive actin flow towards the region of heightened RhoA. Surprisingly, the flow reverses direction when local RhoA activation stops. These data are explained with a physical model, which demonstrates that stress fibers are elastic-like, even at time scales exceeding turnover of constituent proteins. We identify zyxin as a regulator of stress fiber mechanics, as they are fluid-like in its absence. Such molecular control of mechanics likely plays critical roles in regulation of morphogenic events.

## 5.2 Introduction

A diverse array of essential physiological processes, ranging from the subcellular to the multicellular, depend on the spatial and temporal regulation of contractile forces(Iskratsch et al., 2014; Lecuit et al., 2011; Murrell et al., 2015; Paluch and Heisenberg, 2009). This regulation drives changes in cell shape(Martin et al., 2010; Wagner and Glotzer, 2016) and mediates interactions with the extracellular environment(Melvin et al., 2011; Plotnikov and Waterman, 2013). Changes in contractility can furthermore alter gene expression(McBeath et al., 2004) and impact development(Müller et al., 2011; Wang et al., 2010a). The molecular machinery required for generating contractile forces is well conserved and dominated by the actin cytoskeleton, myosin II activity and associated regulatory proteins(Blanchoin et al., 2014; Murrell et al., 2015; Schwarz and Gardel, 2012). Specifically, actin filaments dynamically organize into distinct contractile architectures, including the cortex and stress fibers(Fletcher and Mullins, 2010; Hotulainen and Lappalainen, 2006). Contractile forces are transmitted across the cell by actin

arrays and are ultimately to the extracellular matrix by focal adhesions(Blanchoin et al., 2014; Devreotes and Horwitz, 2015; Gardel et al., 2010; Schwarz and Gardel, 2012).

The regulation of cellular force transmission is controlled by the mechanical properties of actomyosin assemblies. Cellular mechanics has been explored extensively both experimentally(Fletcher and Mullins, 2010; Hoffman and Crocker, 2009; Stricker et al., 2010; Zhu et al., 2000) and theoretically(Broedersz and MacKintosh, 2014; Prost et al., 2015; Schwarz and Safran, 2013). Current understanding is that, at time scales comparable to those of typical kinetic processes, the actin cytoskeleton behaves like an elastic solid. Such elasticity enables rapid force transmission across the cell and reversible deformations to preserve cytoskeletal architecture. In contrast, at longer time scales, it is thought dynamic processes make the cytoskeleton predominately like a viscous fluid. Such viscosity enables cytoskeletal flows and remodeling. However, the molecular regulation of cell mechanics is not well understood.

Cellular contractility is largely controlled by the activity of the small GTPase RhoA (Chrzanowska-Wodnicka and Burridge, 1996; Ridley and Hall, 1992), which in adherent cells is preferentially active at the cell periphery(Machacek et al., 2009; Pertz et al., 2006). RhoA regulates contractility through the promotion of actin polymerization and myosin light chain phosphorylation via the downstream effectors Diaphanous-related formins and Rho-associated Kinase (ROCK), respectively. RhoA activity is required for stress fibers and focal adhesions(Chrzanowska-Wodnicka and Burridge, 1996; Ridley and Hall, 1992). Little, however, is known about how small changes in activity can regulate cell contractility, actin architecture and adhesion.

In this paper, we have used an optogenetic probe to locally activate RhoA in adherent fibroblasts. Plasma membrane recruitment of the RhoA specific guanine exchange factor (GEF) LARG induces local RhoA activation(Guilluy et al., 2011; Jaiswal et al., 2011; Strickland et al., 2012; Wagner and Glotzer, 2016). Local activation of RhoA leads to an increase in actin polymerization and myosin activity in the region of activation, but it does not stimulate de novo stress fiber formation or changes in focal adhesion morphology. We find that exogenous RhoA activation leads to an immediate increase in both the local and global contractility of the cell, followed by a rapid relaxation after GEF recruitment is stopped. The local increase in stress fiber contractility drives an actomyosin flow towards regions of increased RhoA activity. Surprisingly, these flows reverse direction as soon as GEF recruitment ceases. Using physical modeling, we show this behavior is consistent with stress fibers behaving as predominately elastic-like over hour time scales. We find that zyxin is necessary for this elasticity; in its absence, stress fibers become predominately fluid-like even at second time scales. These results suggest that stress fiber mechanics is sensitive to small changes in composition, which has significant implications for regulation of force transmission and cytoskeletal organization.

### 5.3 Spatiotemporal control of RhoA and its downstream effectors

To spatially and temporally control contractility in adherent cells, we adapted a previously established optogenetic probe(Strickland et al., 2012; Wagner and Glotzer, 2016) to act on the RhoA signaling pathway (Fig. 21a). During stimulation by blue light, a cytosolic fusion protein, photo-recruitable GEF (prGEF), consisting of tandem PDZ domains fused to the DH domain of the RhoA specific GEF LARG(Wagner and Glotzer, 2016), is recruited to the plasma membrane

where it activates RhoA (Fig. 21b). To illustrate the local recruitment of prGEF we tagged it with the fluorophore mCherry and imaged an NIH 3T3 fibroblast expressing the constructs on a glass coverslip (Fig. 21c). A digital micromirror device was used to spatially control the illumination of the blue activating light (orange box, Fig. 21c), and was pulsed before each image acquisition during the recruitment period. Recruitment of the prGEF to the activation region was rapid and reversible upon extinguishing the stimulating blue light (Fig. 21c,d).

To investigate whether recruitment of the prGEF resulted in activity of proteins downstream of RhoA, we tracked the dynamics of actin and myosin light chain (MLC) during recruitment (Fig. 1e,g). Both actin and myosin accumulated in the activation regions, resulting in an increase in fluorescence intensity during the 15 min activation period (Fig. 21e-h). Interestingly, local activation of RhoA did not lead to *de novo* stress fiber assembly in the activation region (Fig. 21e). At the end of the activation period, fluorescence intensities of both actin and myosin returned to baseline levels. These results indicate that exogenous RhoA activation via LARG recruitment is not sufficient to maintain elevated RhoA activity and the concomitant increases in local actin and myosin concentrations. To confirm that local activation of RhoA was acting on actin and myosin through its downstream effectors, formin and ROCK, the experiments were repeated in the presence of either SMIFH2, a pan formin inhibitor(Rizvi et al., 2009), or Y-27632, a Rho-associated Kinase inhibitor. Local recruitment of actin and MLC were significantly inhibited by the presence of SMIFH2 and Y-27632, respectively. These results illustrate that RhoA activity and recruitment of its downstream effectors can be spatially and temporally controlled via light.

### 5.4 Focal adhesion dynamics and morphology are unperturbed by local increases in RhoA activity

Previous work has suggested that focal adhesion formation and maturation are tension dependent processes driven by increased RhoA activity at adhesion sites (Balaban et al., 2001; Chrzanowska-Wodnicka and Burridge, 1996; Ridley and Hall, 1992). To test these hypotheses we examined how local RhoA activation affected traction forces and focal adhesions. Cells expressing mCherry-vinculin, a marker of focal adhesions, were plated on polyacrylamide gels coated with fibronectin and traction stresses were measured via Traction Force Microscopy (Fig. 2a,b) (Sabass et al., 2008; Soiné et al., 2015). During local activation of RhoA, traction stresses increased at focal adhesion sites, on a similar timescale to that of myosin localization (Fig. 21g). Despite the increased force, the total number of adhesions remained essentially constant (Fig. 22c). Individual adhesion morphology and vinculin intensity were also unaffected (Fig. 22d). Too much RhoA activation, however, results in adhesion failure and detachment from the substrate (Supplementary Fig. 15). These result are consistent with previous results that tension alone is not sufficient to drive changes in focal adhesion size (Oakes et al., 2012).

To determine the effect of local RhoA activation on the overall contractility of the cell, we used traction force microscopy to measure the total strain energy, which reflects the amount of mechanical work done by the cell on its environment (Oakes et al., 2014). Activation induced a rapid increase in both traction stresses and strain energy (Fig.22b,c) At the end of the activation period, the strain energy decreased to their original baseline values (Fig. 22c). Interestingly, traction stresses were mostly seen to increase at the cell periphery, where traction stresses were already established, and in areas immediately adjacent to the activation region. No change was

seen in the activation area itself (Fig. 22b). This suggests that locally generated forces balance within the activation region and only unbalanced forces at the edge of this region are turned into productive traction forces. Thus, a local increase of tension leads to globally distributed traction forces at pre-existing focal adhesions.

**5.5 Cells maintain a contractile set point**

That cells return to a similar baseline contractility following a period of exogenous RhoA activation is consistent with previously established ideas of tensional homeostasis (Ingber, 2003; Oakes et al., 2014; Webster et al., 2014). To explicitly probe this behavior, we performed a series of local activations of different sizes on a single cell (Fig. 22e). After measuring the strain energy at an initial steady state, a cell was exposed to three 15 min periods of local RhoA activation of increasing size with relaxation periods between each activation (Fig. 22f). The strain energy increased concomitant with the size of the activation region. During activation, both local stresses immediately surrounding the activation region, and long-range stresses at the cell periphery could be seen to increase (Fig. 22e). Following each activation, the strain energy returned to the initial baseline level (Fig. 22f).

To elucidate the underlying mechanical principles, we built a physical model that would capture this physical response. We constructed a continuum model of the cell as a contractile element in series with a viscous and an elastic element (Fig. 22g; Supplementary Data). Contractility was assumed to increase with an exponentially plateauing ramp in the activated region, consistent with the observed accumulation profiles for actin and myosin (Fig.21g), and the substrate was represented as an elastic spring coupled to the cell by a friction element. The model parameters

for the elastic modulus, viscosity, friction and contractility were found by fitting the model to the strain energy data, while the value of the substrate stiffness was fixed. This procedure resulted in a curve in good agreement with the experimental data (Fig. 22f and Supplementary Data).

We find that both the viscous and elastic elements are necessary to accurately capture the behavior of the system. The ratio of viscosity (~7*10^6 Pa*s) to elasticity (~2*10^3 Pa) defines a viscoelastic relaxation time of approximately 50 minutes; this time scale determines the transition from when the cytoskeleton behaves predominately elastic-like (< 50 min) to predominately fluid-like (> 50 min) (Supplementary Data). Our results thus indicate that stress fibers are predominantly elastic on the scale of tens of minutes, despite proteins within the stress fiber turning over on timescales of tens of seconds (Hotulainen et al., 2005). This strong elastic behavior is also consistent with the immediate increase in cell traction stresses at the cell periphery (Fig. 22b,e) upon local activation of RhoA in the center of the cell.

**5.6 Stress fibers contract independent of the background network**

To investigate the cytoskeletal architectures that give rise to this strong contractility, we tracked myosin dynamics during local RhoA activation. In the steady state, as new actomyosin is polymerized and incorporated into stress fibers, there is a retrograde flow of actomoysin from the periphery towards the cell center (Gardel et al., 2010; Hotulainen and Lappalainen, 2006). Using particle image velocimetry (PIV) (Brox and Weickert, 2006) we measured both the local direction and magnitude of myosin flow. We found that myosin flow rates along the stress fiber increased as myosin accumulated in the activation region creating a local contraction, and that this flow was directed along the orientation of the stress fibers spanning the activation region

(Fig. 23a,b; Supplementary Fig. 16). The flow direction was independent of the activation region geometry, with the direction always being determined by the stress fiber orientation.

The cytoskeleton of a strongly adherent cell is typically thought to be a 2D material comprised of stress fibers embedded in an isotropic cortex (Cai et al., 2010; Soiné et al., 2015; Xu et al., 2012). Since flows induced by local RhoA activation appear to track the orientation of the stress fibers (Figs. 23a,b and 16), we sought to address the relative contractile contributions of the stress fibers and the actin networks. We therefore built a 2D discrete model analogous to the 1D continuum model described above (Fig. 23c). The model consists of a triangular mesh with the same contractile, viscous and elastic elements connected in series, with lines of increased contractility representing the stress fibers. Using a simple rectangular cell, we first verified that, without stress fibers, this model recapitulates the results from the one-dimensional continuum model (Fig. 23d). Similar to the 1D model above, the contractile components in a region in the center of the cell were slowly increased with an exponentially plateauing ramp, (Fig. 23c; Supplementary Data). The parameters were then adjusted so that the model both qualitatively and quantitatively recapitulated the expected flow patterns of the 1D continuum model (Fig. 23d).

To explore the relative contributions of the background mesh and the stress fibers, we considered two test cases: (1) If both the mesh and the stress fibers contained contractile elements, the stress fibers pinched inward transverse to their orientation during local activation (Fig. 23e); and (2) when contractile elements were only included in the stress fibers, the cytoskeletal flow was restricted to directions along the stress fiber (Fig. 23f), consistent with our experimental results

(Fig. 23a,b; Supplementary Fig. 16). Since transverse deformations were never seen in experiments, it is clear that the stress fibers must be the predominant contractile elements observable at this resolution which respond to local RhoA-induced contractions. Furthermore, this result illustrates that it is appropriate to think of a stress fiber as a one-dimensional contractile element with viscous and elastic components embedded in a passive viscoelastic network.

**5.7 Stress fibers flow in response to local strain induced by RhoA activation**

Having identified the stress fiber as the main contractile unit responding to exogenous RhoA activation, we next sought to address whether stress fibers undergo deformation during contraction. Since stress fibers can be considered as 1D structures, we analyzed myosin flow along the fiber using kymographs. A kymograph drawn along a single stress fiber illustrates that myosin puncta flowed from both ends towards the activation regions when RhoA was activated locally (Fig. 24a,b; Supplementary Fig. 17). Similarly, a kymograph drawn by projecting the flow speed along the stress fiber from the velocity field created by our PIV analysis illustrates even more clearly how cytoskeletal flow was perturbed by local RhoA activation. Flow of myosin from both ends of the stress fiber reoriented towards the recruitment regions and increased from ~1 nm/s on average to more than 3 nm/s during activation (Fig. 24c; Supplementary Fig. 17). Strikingly, the flow was also seen to reverse direction, flowing away from the recruitment region and towards the cell periphery, during the relaxation period following the local activation (Fig. 24b,c). This flow reversal is reminiscent of the restoring force in elastic objects that restores its original shape after removal of external force (e.g. recoil of an elastic band after stretch).

We next developed a protocol to measure the magnitude of the stress fiber displacement during these periods of contraction and relaxation (Fig. 24d). The displacement in a given fiber was determined by measuring the relative position of puncta along the fiber following 15 minutes of local RhoA activation and 15 minutes after it ceased. During contraction, puncta on either side of the activation region contracted on average ~3 μm from their original position before relaxing back to ~1 μm from their original position (Fig. 24d). The relaxation response across many stress fibers from multiple cells could be further clustered into two groups, one which exhibited strong reversal (~80% of the original position) and one which exhibited little to no reversal (~25% of the original position) (Fig. 24d).

To determine whether stress fibers were stretching due to the local contraction, we used cells expressing mApple--actinin, an actin crosslinker which localizes to well defined puncta on stress fibers (Fig. 24e). We created kymographs of α-actinin flow during local activation of RhoA and tracked paths of individual puncta (Fig. 24f). The velocity of individual puncta was determined from the slope of the tracks in the kymograph and plotted as a function of distance from the activation zone (Fig. 24g). Puncta along the stress fiber moved at similar speeds, indicating that, in general, the stress fiber was translating as a rigid rod during the local contraction (Fig.24g). Where present, changes in velocity between neighboring puncta were abrupt (blue arrow Fig 24g), suggesting points of structural failure along a fiber. These results indicate that the strain induced in the stress fiber is restricted to the local contraction in the activation region and discrete sites of extension in regions outside the activation region.

By fitting the experimental kymographs to both our 1D continuum and 2D discrete models, we show that similar flow patterns emerge naturally from the mechanics of the system (Fig. 24h and Supplementary Data). The high elasticity of the stress fiber, specifically the ratio of elasticity to viscosity, is sufficient to recapitulate the flow profiles that were seen during both RhoA activation and relaxation. Furthermore, the parameters found from the kymograph fitting process were consistent with the parameter values found when fitting the strain energy (Supplementary Data).

### 5.8 Zyxin is recruited to sites of extension and compression on stress fibers

In order to probe the underlying molecular basis of this elasticity, we sought to identify stress fiber-associated proteins that could contribute to the recoil behavior. Zyxin has been previously established as a mechanosensitive protein that dynamically localizes to sites of strain along stress fibers (Colombelli et al., 2009; Yoshigi et al., 2005), in addition to focal adhesions (Zaidel-Bar et al., 2003). Using cells expressing mCherry-zyxin, we monitored zyxin activity during RhoA activation (Fig. 25a). Zyxin recruitment was consistently observed at peripheral focal adhesions (Fig. 25b). Surprisingly, we found that zyxin also accumulated along stress fibers in the region of local activation (Fig. 25c,d). Given the myosin accumulation and direction of flow, this suggests that zyxin is recruited to both sites of compression and extension.

### 5.9 Zyxin is required for stress fibers to behave elastically

To further explore the role of zyxin in stress fiber mechanical behavior we used mouse embryonic fibroblast cells derived from zyxin$^{-/-}$ mice (Hoffman et al., 2006). Despite the loss of zyxin, these cells form actin stress fibers and focal adhesions and are highly contractile (Smith et

al., 2010). When we locally activated RhoA in the zyxin$^{-/-}$ cells, myosin accumulated in the activation region (Fig. 25e). This accumulation drove a contractile flow into the local activation area that was indistinguishable from wild type cells. Upon stopping the GEF recruitment in zyxin$^{-/-}$ cells, cytoskeletal flow returned to pre-activation rates, consistent with the reduced local contraction, but did not reverse direction (Fig. 25f,i; Supplementary Fig. 17). Expression of EGFP-zyxin in this cell line restored the flow reversal (Fig. 25g,i; Supplementary Fig. 17). Together these results indicate that zyxin is required for the flow reversal occurring after local RhoA activation ends.

Using the kymographs produced in the zyin$^{-/-}$ and zyxin$^{-/-}$+EGFP-zyxin cells, we again fit the data to our mechanical model (Figs. 25j,k; Supplementary Data & Fig. 18). For the zyxin$^{-/-}$ cells, we found the viscoelastic relaxation time reduced to 1 sec, indicating that the stress fibers are predominately fluid-like at all physiological time scales. Rescue of the zyxin$^{-/-}$ cells with EGFP-zyxin resulted in parameter fits that were consistent with the NIH 3T3 fibroblast data. Zyxin is thus important for maintaining the qualitative mechanical response of stress fibers, ensuring they are predominately elastic at ~1 hr time scales.

**5.10 Discussion**

This study demonstrates that the mechanical behavior of adherent cells is strongly shaped by stress fibers and their ability rapid force transmission and cytoskeletal architecture even in the face of molecular turnover and flow. Using an optogenetic probe to locally activate RhoA via recruitment of the DH domain of LARG, a RhoA specific GEF, we find that we can stimulate a local contraction in stress fibers due to an increased accumulation of actin and myosin in the

activation area (Fig. 26, 1). This local contraction causes a tension gradient and a flow towards the activation region (Fig. 26, 2). The flow of myosin and -actinin increases the strain both on the interface coupling the stress fiber to the adhesion and in the activation region, leading to recruitment of the mechanosensitive protein zyxin (Fig. 26, 3). When local activation of RhoA is stopped, the system relaxes to the pre-activation state, mainly driven by elastic energy accumulated in the strained regions, and results in a cytoskeletal flow of material away from the local activation region (Fig. 26, 4).

This elastic behavior is dependent on zyxin. Previous reports have shown that zyxin localizes along the stress fiber at the interface of the adhesion (Guo and Wang, 2007; Kanchanawong et al., 2010). This positioning suggests that previously reported zyxin mediated stress fiber repair mechanisms (Smith et al., 2010; 2013) are also occurring at the adhesion interface as actin is assembled and is incorporated into the stress fiber while under tension. The localization of zyxin to sites of compression, however, is novel. While it is known that the LIM domain of zyxin is sufficient for localization (Uemura et al., 2011), the exact mechanism through which zyxin recognizes sites of strain remains unknown.

These data further illustrate that RhoA activity and its downstream effectors are tightly regulated by the cell. We see no evidence that RhoA activation alone leads to *de novo* stress fiber formation or adhesion maturation. Instead these processes likely result from concurrent changes in cytoskeletal architecture (Aratyn-Schaus et al., 2011; Oakes et al., 2012). More interestingly, the data suggest cells regulate total RhoA activity to maintain a constant homeostasis (Ingber, 2003; Oakes et al., 2014; Webster et al., 2014). Specifically, the relaxation kinetics of the

downstream effectors match the kinetics of the optogenetic probe (Strickland et al., 2012), thus indicating that there is no positive feedback loop whereby production of RhoA•GTP alone is sufficient to promote further activation of RhoA. To sustain a given contractile state, therefore, the cell must actively regulate and maintain a specific RhoA•GTP concentration.

By using an optogenetic approach to perturb the local mechanical balance within the cell, we were able probe the material properties of the cytoskeleton in ways previously inaccessible. Given that typical turnover rates for proteins in the cytoskeleton are on the order of tens of seconds (Hotulainen and Lappalainen, 2006), it is surprising that the cell behaves elastically on timescales of ~1 hour. The viscous behavior of cells is typically associated with irreversible changes brought on through remodeling and dynamic activity of proteins (e.g. cytoskeletal remodeling during migration) (Besser and Schwarz, 2007; Callan-Jones and Voituriez, 2013; Prost et al., 2015). Conversely, elasticity has typically been used to describe cellular material properties that ignore the dynamic activity of the components (Edwards and Schwarz, 2011; Farsad and Vernerey, 2012; Oakes et al., 2014). The finding that cells can maintain their elasticity and their dynamic activity simultaneously has exciting implications for interpreting the underlying physics of active materials. The fact that this behavior can be controlled by the activity of a single protein suggests intriguing potential mechanisms to regulate cell mechanics during morphogenesis and development.

## 5.11 Methods

### Cell culture and transfection

NIH 3T3 fibroblasts (American Type Culture Collection, Manassas, VA) were cultured in DMEM media (Mediatech, Herndon, VA) and supplemented with 10% FBS (HyClone; ThermoFisher Scientific, Hampton, NH), 2 mM L-glutamine (Invitrogen, Caarlsbad, CA) and penicillin-streptomycin (Invitrogen). Zyxin$^{-/-}$ and zyxin$^{-/-}$+EGFP-zyxin Mouse Embryonic Fibroblast cells were a gift of Mary Beckerle's lab (University of Utah, Salt Lake City, UT) and cultured similarly to the NIH 3T3 fibroblasts(Smith et al., 2010). All cells were transiently transfected via electroporation 24 hrs prior to experiment using a Neon Transfection system (ThermoFisher Scientific). Following transfection, cells were plated on glass coverslips and imaged the next day.

### Drug treatments

Cells were treated with either the 10 μM SMIFH2 a pan-formin inhibitor(Rizvi et al., 2009) or 1μM of Y-27632 which inhibits ROCK (ThermoFisher Scientific), for at least 30 minutes prior to imaging.

### Plasmids

The optogenetic membrane tether consisting of Stargazin-GFP-LOVpep and prGEF constructs used are previously described(Wagner and Glotzer, 2016). prGEF-YFP was constructed in an identical manner to prGEF with YFP replacing mCherry. This construct was used in experiments where the effects on various downstream markers were visualized. To examine effects on the actin and myosin networks, we used mApple-Actin and mApple-MLC constructs (gifts from M

Davidson, University of Florida, Gainesville FL), mCherry-Vinculin (gift from V Weaver, University of California at San Francisco, San Francisco, CA) and mCherry-zyxin (gift from M Beckerle, University of Utah, Salt Lake City, UT).

**Live cell imaging**

Glass coverslips were placed in a Chamlide magnetic chamber (Live Cell Instrument, Seoul, Korea) in culture media supplemented with 10 mM HEPES and 30μL/mL Oxyrase (Oxyrase Inc., Mansfield, OH) and maintained at 37˚C. Cells were imaged on an inverted Nikon Ti-E microscope (Nikon, Melville, NY) with a Yokogawa CSU-X confocal scanhead (Yokogawa Electric, Tokyo, Japan), and laser merge module containing 491nm, 561nm, and 642nm laser lines (Spectral Applied Research, Ontario, Canada). Images were collected on either a CoolSNAP HQ2 CCD (Roper Scientific, Trenton, NJ) or Zyla 4.2 sCMOS Camera (Andor, Belfast, United Kingdom). Local recruitment using the optogenetic probe was performed using a 405 nM laser coupled to a Mosaic digital micromirror device (Andor). Images were collected using a 60x 1.49 NA ApoTIRF oil immersion objective (Nikon). All hardware was controlled using MetaMorph Automation and Image Analysis Software (Molecular Devices, Sunnyvale, CA).

Unless otherwise stated, cells were imaged in the 561 channel every 20 s for 45 min, with the first 15 min used to determine the steady state of the system, the second 15 min to perform local recruitment, and the final 15 min to record any recovery. During recruitment a local region drawn in MetaMorph was illuminated by the 405nm laser for 960 ms at a power < 1 μJ/s immediately prior to the acquisition of each 561 image.

**Local recruitment analysis**

All data analysis was performed using MATLAB (Mathworks, Natick, MA). Regions of interest (ROIs) were drawn to calculate the average intensity in the local recruitment region, a control area within the cell but far away from the recruitment area, and a background area outside of the cell. The average background intensity was subtracted from the control region and this curve was used to determine a photobleaching correction. The photobleaching correction was then applied to the background subtracted average intensity in the local recruitment region and normalized to the average value of the first 15 min of the data.

**Focal adhesion analysis**

Images were corrected for photobleaching and then thresholded and segmented to create binary masks. The binary mask was then used to calculate the total number, average area, total area, and average intensity of adhesions in each frame.

**Kymograph and local displacement analysis**

Kymographs were created in MATLAB by drawing lines along stress fibers and averaging across a width of 9 pixels. Local displacement was determined by locating a feature 5μm from the edge of the activation zone in a kymograph immediately prior to activation. The location of this feature was then tracked and recorded following the 15 minute period of activation, and then again following 15 minutes of relaxation.

**Cytoskeletal flow analysis**

Images were first corrected for bleaching and then filtered with a 3D Gaussian filter to remove noise. Flow fields were calculated using an implementation of the Brox et al. optical flow algorithm(Brox and Weickert, 2006) that ensures spatial and temporal smoothness. Flow field kymographs were generated by projecting the flow vectors onto the line defining the kymograph. To compare the direction of flow with the organization of the cytoskeleton, the local orientation of actin fibers was extracted from the structure tensor(Weichsel et al., 2012).

**Actinin spacing analysis**

Kymographs were drawn as above. For each timepoint in the kymograph, local peaks in the linescan were determined. Peaks were then connected to create tracks across the kymograph. Local velocity was determined by isolating the section of the track during the activation period and fitting the trajectory to a straight line. The fitted slope was taken as the velocity.

**Traction force microscopy**

Traction force microscopy was performed as described previously(Oakes et al., 2014; Sabass et al., 2008; Soiné et al., 2015). Briefly, polyacrylamide gels embedded with 40-nm fluorescent microspheres (Invitrogen) were polymerized on activated glass coverslips. The shear modulus of the gels used in these experiments was 8.6 kPa. Following polymerization gels were washed with PBS and crosslinked with the extracellular matrix protein fibronectin (Millipore, Billerica, MA) using the photoactivatable crosslinker sulfo-sanpah (Thermo Fisher Scientific). Cells were plated and allowed to spread for at least 4 hours prior to imaging as described above.

Following imaging, cells were removed from the substrate using 0.5% sodium dodecyl sulfate and a reference image of the fluorescent beads in the unstrained substrate was taken. The image stack was then aligned to correct for drift and compared to the reference image using particle imaging velocimetry to create a displacement field with a grid spacing of 0.86 μm. Displacement vectors were filtered and interpolated using the Kriging interpolation method. Traction stresses were reconstructed via Fourier Transform Traction Cytometry(Butler et al., 2002; Sabass et al., 2008), with a regularization parameter chosen by minimizing the L2 curve(Soiné et al., 2015). The strain energy was calculated as one half the integral of the traction stress field dotted into the displacement field(Oakes et al., 2014).

**Modeling**

See Supplementary Data for the details of both the continuum and discrete models.

**Statistical analysis**

All experiments were repeated a minimum of 3 times. Box plots represent the $25^{th}$, $50^{th}$ and $75^{th}$ percentiles of the data. Whiskers on the boxplot extend to the most extreme data points not considered outliers. Error bars represent the standard deviation. Statistical significance was determined using independent two-sample Student's *t* tests of the mean to compare groups of data. Statistical significance is indicated by asterisks: (*) represents a $p$-value < 0.05; (**) represents a $p$-value < 0.01.

## 5.12 Appendix 5

Figure 21

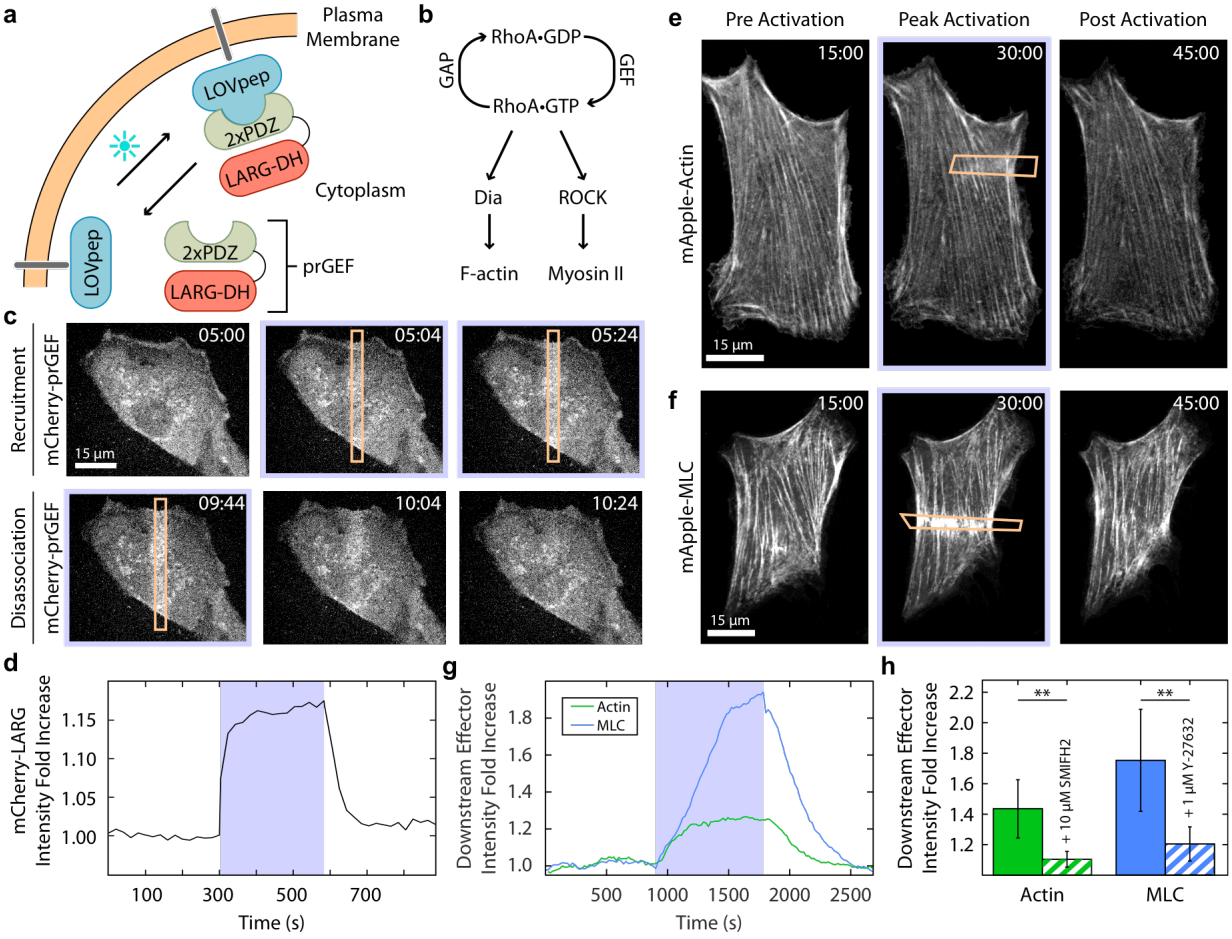

Figure 21, continued: RhoA activity can be spatiotemporally controlled via an optogenetic probe. (a) Spatiotemporal control of RhoA activity is achieved using an optogenetic probe to recruit the RhoA specific GEF LARG to the plasma membrane. A LOVpep molecule is anchored to the membrane via fusion to the transmembrane protein Stargazin, while a protein consisting of tandem PDZ domains fused to the DH domain of LARG (prGEF) is distributed throughout the cytosol. Upon stimulation with 405nm light, the LOVpep undergoes a conformational change exposing a high-affinity binding site which drives the prGEF to the membrane where it can activate RhoA. When the activating light is removed, the LOVpep undergoes a thermodynamically driven refolding halting further recruitment of prGEF. (b) The RhoA signaling pathway. RhoA*GTP activates both Dia and ROCK, which in turn promote actin polymerization and myosin II activation, respectively. (c) Representative images of a 3T3 fibroblast expressing an mCherry-tagged version of prGEF. Upon local activation (top row – orange box) mCherry-prGEF rapidly accumulates in the activation region. Removal of the activating light (bottom row) results in the accumulated mCherry-prGEF dispersing back into the cytosol. (d) Quantification of the local intensity increase of mCherry-prGEF in the activation region of the cell shown in c. The activation period is indicated by a blue background. (e-f) Representative images of cells expressing either mApple-Actin (e) or mApple-Myosin Light Chain (f) prior to activation, following 15 minutes of activation in the region indicated, and following 15 minutes of relaxation. Both actin and myosin exhibit increases in intensity in the local region of activation. (g) Quantification of the local intensity increase of actin and myosin from the cells in e-f. Both signals begin increasing immediately upon RhoA activation, and dissipate as soon as the activating light is switched off. (h) Mean maximum intensity fold-increase of actin or myosin in regions of activation in control cells, or cells treated with 10 μM SMIFH2 (Dia inhibitor) or 1μM Y-27632 (ROCK inhibitor). Inhibition of either Dia or ROCK results in reduced average increases in local intensity during RhoA activation. Time is min:sec.

Figure 22:

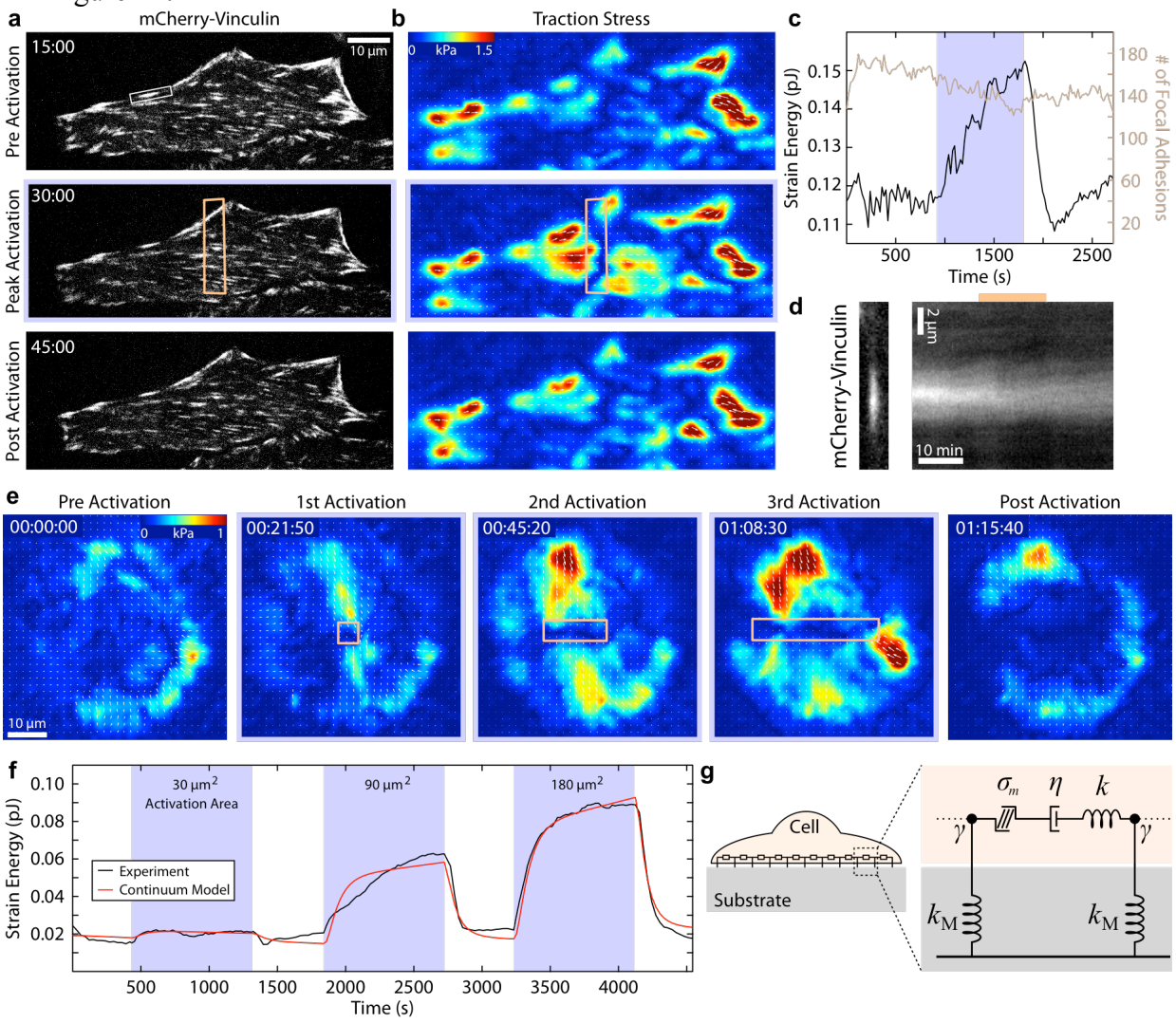
a
mCherry-Vinculin
15:00
10 μm
Pre Activation
30:00
Peak Activation
45:00
Post Activation
b
Traction Stress
0 kPa 1.5
c
Strain Energy (pJ)
0.15
0.14
0.13
0.12
0.11
500
1500
2500
Time (s)
180
140
100
60
20
# of Focal Adhesions
d
mCherry-Vinculin
2 μm
10 min
e
Pre Activation
1st Activation
2nd Activation
3rd Activation
Post Activation
00:00:00
0 kPa 1
00:21:50
00:45:20
01:08:30
01:15:40
10 μm
f
Strain Energy (pJ)
0.10
0.08
0.06
0.04
0.02
30 μm2
Activation Area
90 μm2
180 μm2
Experiment
Continuum Model
500
1000
1500
2000
2500
3000
3500
4000
Time (s)
g
Cell
Substrate
σm
η
k
γ
γ
kM
kM

Figure 22, continued: Increased RhoA activity leads to increased cell contractility. (a) A cell expressing mCherry-Vinculin is shown prior to activation, after 15 minutes of activation, and after 15 minutes of relaxation. The activation region is indicated by the orange box. (b) The corresponding traction stress maps for the time series shown in a. (c) A plot showing the strain energy versus time and the number of focal adhesions versus time, with the activation period indicated by the blue background. The strain energy begins to increase immediately upon activation, and begins to relax as soon as the activating light is removed. In contrast, the number of focal adhesions remains relatively constant and does not respond to the local increase in RhoA activity. (d) The focal adhesion shown in the white boxed region of a and a kymograph created by drawing a line along the long axis of the adhesion. The focal adhesion maintains a constant length and intensity throughout the activation period (orange bar above kymograph), indicating that focal adhesion morphology is not affected by distant RhoA activation. (e) A sequence of traction maps from a cell exposed to a series of activations in regions of different size. Time is hr:min:sec. (f) A plot of the experimental (black line) and theoretical (red line) strain energy vs time for the cell shown in e. The contractile response of the cell is proportional to the size of the activation region and retreats to a baseline value following each activation period. (g) A cartoon of the continuum model used to describe the cell in f. The model consists of a contractile element (m) in series with a viscous () and an elastic element (k), connected via a frictional elements () to an elastic substrate (kM).

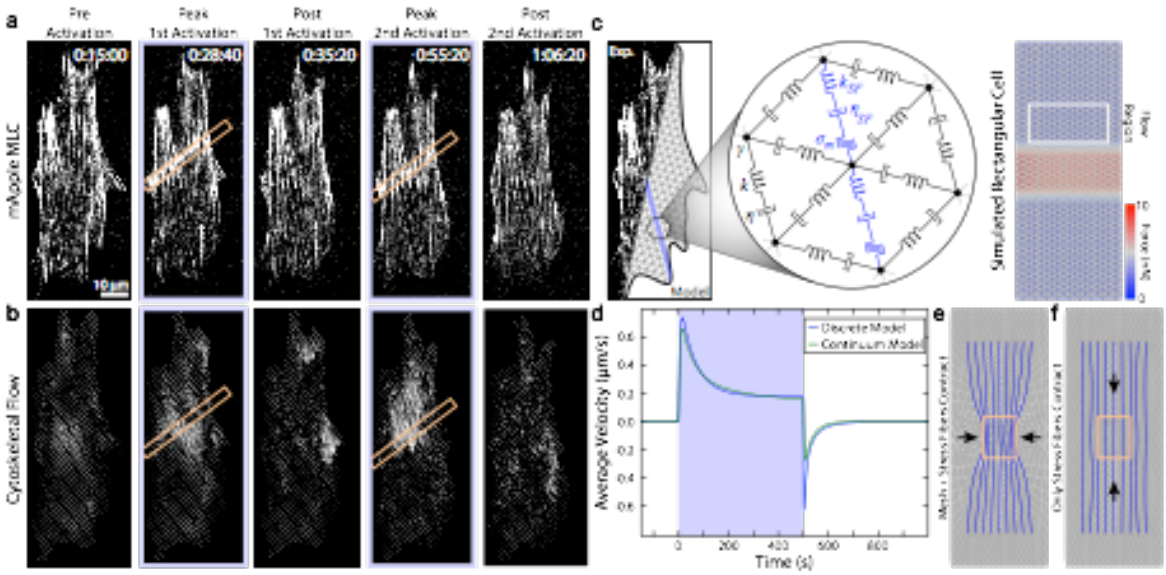


Figure 23: Stress fibers direct contractile flow. (a) Fluorescence time series of a cell expressing mApple-MLC shown prior and after two separate periods of activation (orange boxes). (b) Flow fields of myosin calculated from the images in a. Flow is always directed along the direction of the stress fibers. (c) A two dimensional model of the cell was created using a triangular mesh of viscoelastic-cables (k,) connected at vertices viscously coupled () to the environment. Stress fibers (blue line) consisting of contractile ($_m$), viscous ($_{SF}$) and elastic elements ($k_{SF}$) were embedded in the network. Using a simplified rectangular cell with this network, local RhoA activation could be simulated by activating force dipoles in network links in a region in the center of the cell. (d) To calibrate the 2D discrete model, the average flow (white box in c), was measured and compared to the 1D continuum model presented above. (e-f) The 2D discrete model was used to explore two contractile scenarios: (e) contractile stress fibers (blue) embedded in a contractile mesh (grey); and (f) contractile stress fibers embedded in a non-contractile background. If both the stress fibers and mesh are contractile, a transverse contraction pinches together the stress fibers. If only the stress fibers contract, the flow profile is restricted to the orientation of the fibers, mimicking the experimental results.

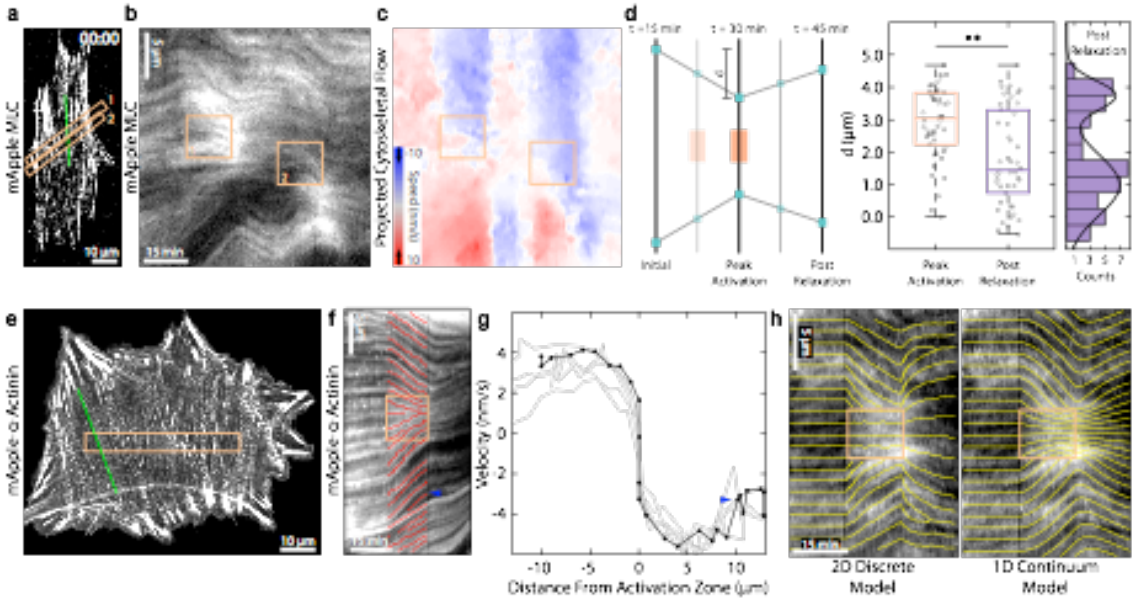


Figure 24: Stress fibers behave elastically. (a) Image showing a cell labeled with mApple-MLC. The activation regions are indicated by the orange boxes. (b) A kymograph drawn along the stress fiber (green line in a). During activation periods myosin flows towards the activation regions. (c) A kymograph created from the same region as b using the flow maps determined previously. Flow was projected onto the stress fiber and color coded to indicate speed and direction. This flow map illustrates that during relaxation periods, myosin flow reverses direction away from the activation periods. (d) A quantification of displacement of stress fibers during contraction and relaxation. Puncta ~5 µm from the activation zone were tracked and measured following 15 minutes of activation, and again following 15 min of relaxation. Puncta translated about 3 µm from their original position, and relaxed to ~1 µm from their original position elastically. The relaxation response could be further broken into two groups, one with a strong reversal (~80% of their original position) and one with a weak reversal (~25% of their original position). (e) A cell transfected with mApple--actinin. The activation area is indicated by the orange box. (f) A kymograph drawn along the direction indicated in e, overlain with tracks of the individual -actinin puncta during activation. (g) The velocity of individual puncta along the stress fiber is measured from the slope of the tracks and plotted against the distance from the activation region. Adjacent puncta all move at approximately the same speed. Sudden changes in velocity (blue arrowhead) correlate with what appear to be site of mechanical failure along the stress fiber and the appearance of new puncta. The black line represents the stress fiber from f, while the grey lines are other stress fibers from the same cell. (h) A representative kymograph is fit to both the 1D continuum and 2D discrete models. Both models are able to recapitulate the flow patterns seen experimentally.

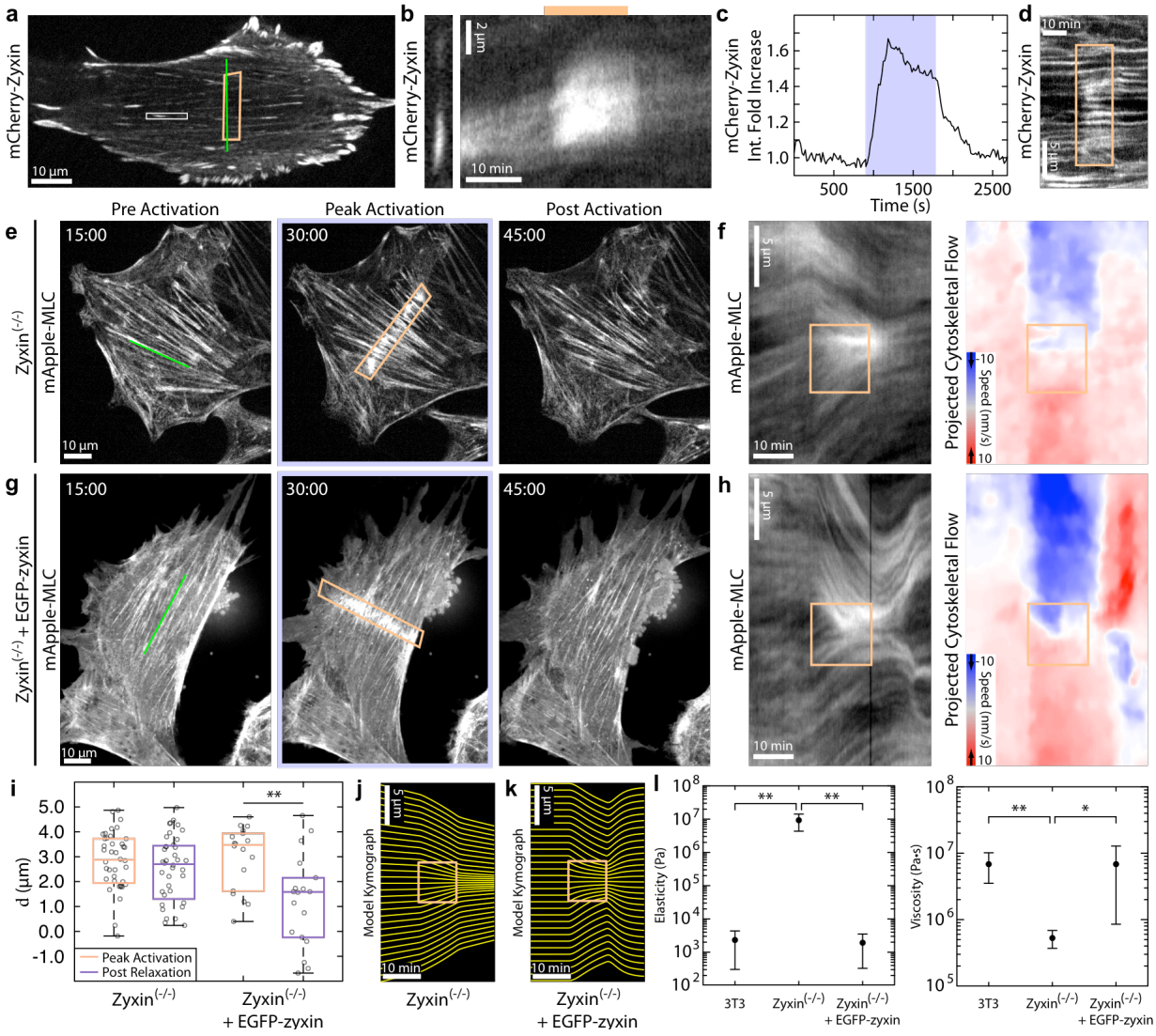
a
mCherry-Zyxin
10 µm
b
mCherry-Zyxin
2 µm
10 min
c
mCherry-Zyxin
Int. Fold Increase
1.6
1.4
1.2
1.0
500
1500
2500
Time (s)
d
10 min
mCherry-Zyxin
5 µm
Pre Activation
Peak Activation
Post Activation
e
Zyxin(-/-)
mApple-MLC
15:00
30:00
45:00
10 µm
f
mApple-MLC
5 µm
10 min
Projected Cytoskeletal Flow
10
Speed (nm/s)
10
g
Zyxin(-/-) + EGFP-zyxin
mApple-MLC
15:00
30:00
45:00
10 µm
h
mApple-MLC
5 µm
10 min
Projected Cytoskeletal Flow
10
Speed (nm/s)
10
i
d (µm)
5.0
4.0
3.0
2.0
1.0
0.0
-1.0
**
Peak Activation
Post Relaxation
Zyxin(-/-)
Zyxin(-/-)
+ EGFP-zyxin
j
Model Kymograph
5 µm
10 min
Zyxin(-/-)
k
Model Kymograph
5 µm
10 min
Zyxin(-/-)
+ EGFP-zyxin
l
Elasticity (Pa)
10^8
10^7
10^6
10^5
10^4
10^3
10^2
**
**
3T3
Zyxin(-/-)
Zyxin(-/-)
+ EGFP-zyxin
Viscosity (Pa•s)
10^8
10^7
10^6
10^5
**
*
3T3
Zyxin(-/-)
Zyxin(-/-)
+ EGFP-zyxin

Figure 25: Zyxin is required for stress fibers to behave elastically. (a) A NIH 3T3 expressing mCherry-zyxin. The activation region is indicated by the orange box. (b) The focal adhesion indicated by the white box in a, and a kymograph created by drawing a line along its long axis. During activation (orange bar) zyxin is rapidly recruited to the focal adhesion and elongates. (c) Zyxin accumulation during activation (blue background). (d) A kymograph drawn along the green line in a illustrates that zyxin is also recruited to the region of activation. (e) A zyxin(-/-) MEF expressing mApple-MLC before activation, at peak activation, and following relaxation. Myosin accumulates as in 3T3s. (f) A kymograph of myosin intensity and flow speed drawn along the green line indicated in e. Zyxin(-/-) MEFS exhibit little to no elastic flow reversal. (g) A zyxin(-/-) MEF rescued with EGFP-zyxin and expressing mApple-MLC, during an activation sequence. (h) A kymograph of myosin and flow illustrating a strong elastic flow reversal along the line drawn in g. (i) Displacement analysis of the zyxin(-/-) and zyxin(-/-)+EGFP-zyxin MEFs. Without zyxin, cells do not exhibit an elastic response. (j) A kymograph representing the average fit of the continuum model to the zyxin(-/-) data. (k) A kymograph representing the average fit of the continuum model to the zyxin(-/-)+EGFP-zyxin data. (l) The elastic (E) and viscous () parameters found from fitting the experimental kymographs to the continuum model. Without zyxin, the elasticity increases and the viscosity decreases.

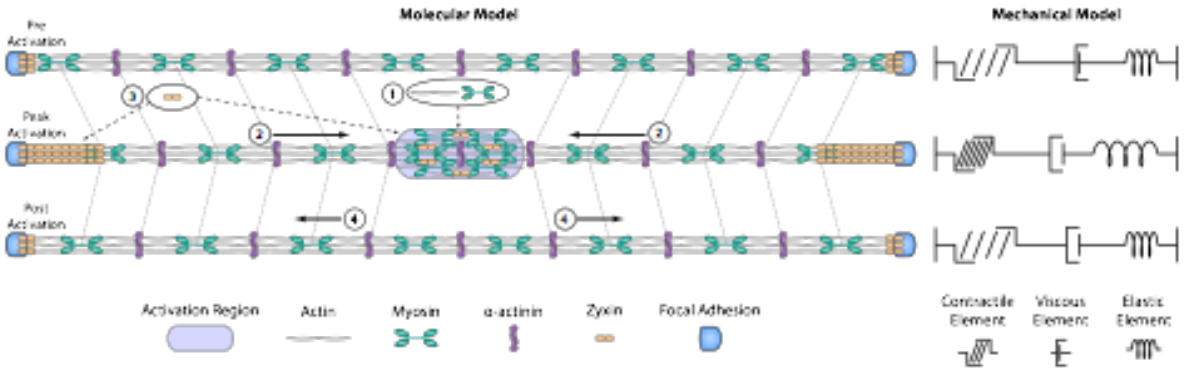


Figure 26: Molecular and mechanical models of local RhoA activation in stress fibers. Molecular model: (1) Local recruitment of prGEF leads to activation of RhoA and accumulation of actin and myosin. The local increase in actin and myosin in turn stimulates a local contraction in the stress fiber. (2) The increased local contractility induces a flow of myosin and -actinin along the stress fiber towards the activation region. (3) Increased flow induces higher strain at both the interface coupling the stress fiber to the focal adhesion and the activation region, resulting in recruitment of the mechanosensitive protein zyxin. (4) When local activation of RhoA stops, the flow reverses direction as the stress fiber relaxes elastically. Mechanical model: The stress fiber is represented as a contractile, viscous and elastic element connected in series. Upon local activation of RhoA, the contractile element is compressed, leading to extension of both the viscous and elastic elements. As local activation stops, the energy stored in the elastic element allows it to relax back to its original state, while the energy in the viscous element is lost.

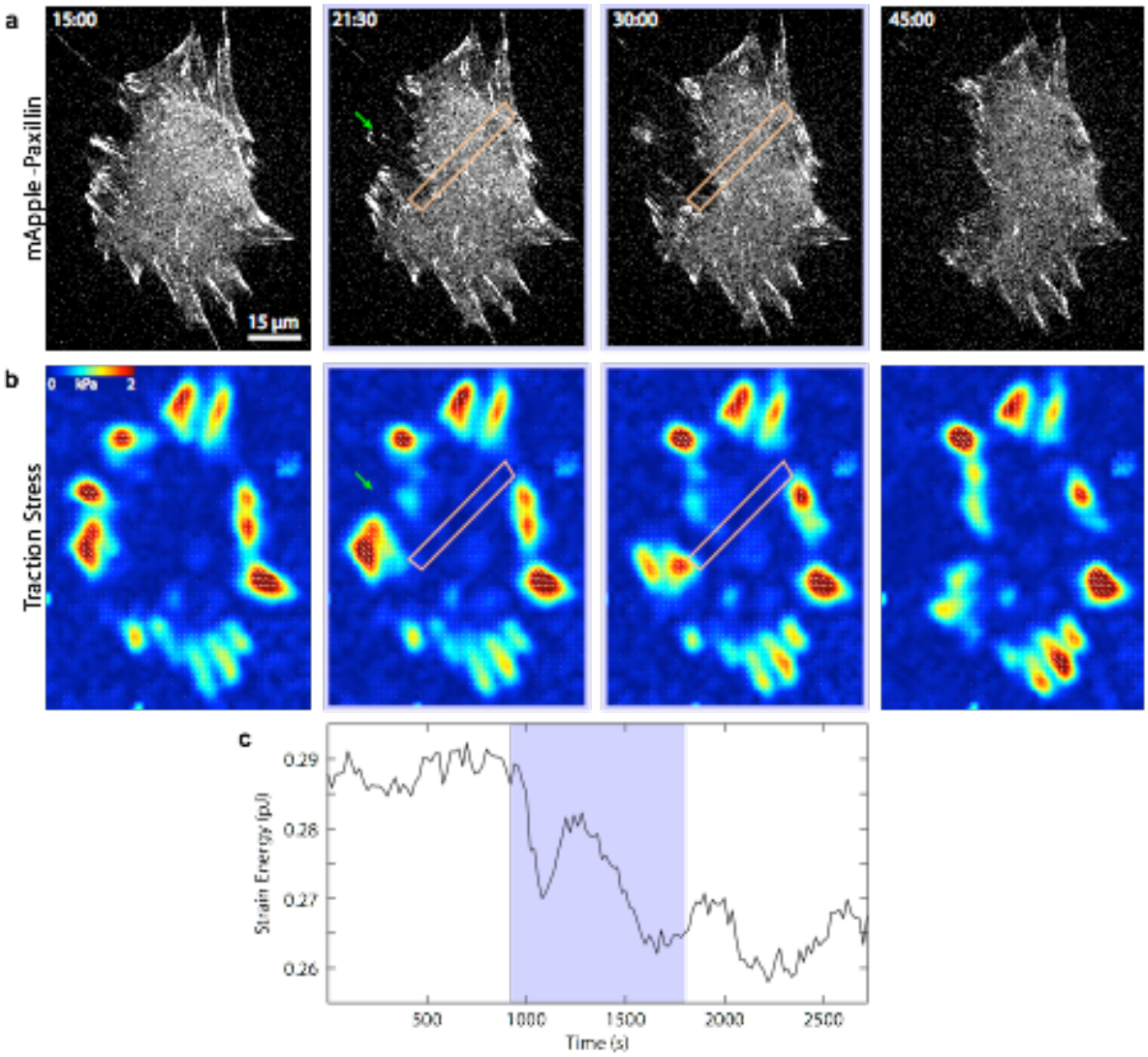


Sup Figure 15: Too much local activation can result in adhesion failure. (a) A time series showing a cell expressing mApple-paxillin during local activation of RhoA (orange box). The green arrow illustrates the focal adhesion that ruptures upon local activation. Time is min:sec. (b) The corresponding traction maps for the cell shown in a. (c) The strain energy as a function of time during local RhoA activation (blue background). Upon local activation a focal adhesion rips off the substrate leading to a sudden loss in stain energy.

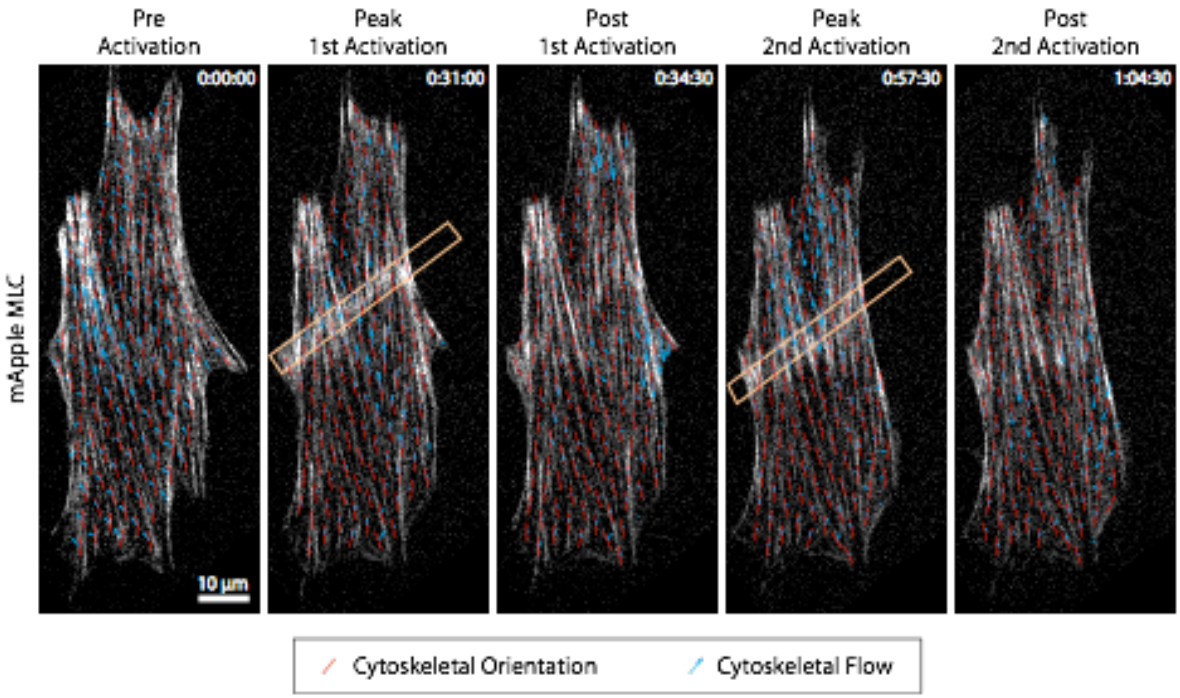


Supp Figure 16: Cytoskeletal flow is primarily directed along the orientation of stress fibers. A time series of local RhoA activation (orange box) in a cell expressing mApple-MLC. The local cytoskeletal orientation is overlaid as red bars, while the local cytoskeletal flow vectors are shown in blue arrows. Time is hr:min:sec.

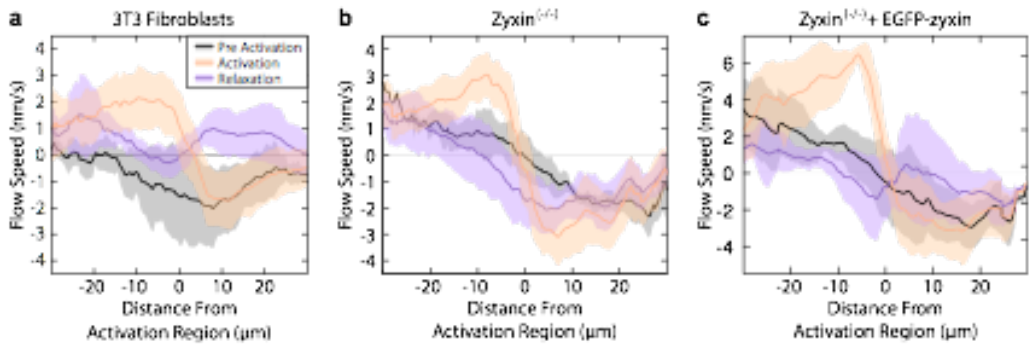


Supp Figure 17: Average flow rates during local activation of RhoA. (a) The average flow rates along stress fibers before, during, and after local RhoA activation in NIH 3T3 fibroblasts. During activation flow increases from both ends of the fiber toward the activation region. During relaxation, flow speeds reverse direction around the activation region. (b) Average flow rates in zyxin$^{(-/-)}$ MEFs. During activation, flow still increases from both ends of the fiber toward the activation region. During relaxation, however, flow speeds return to pre-activation rates but do not exhibit any reversal of direction. (c) Average flow rates in zyxin$^{(-/-)}$+EGFP-zyxin MEFs. Rescue of zyxin in the knockout cells recovers the elastic flow reversal behavior seen in the 3T3s.

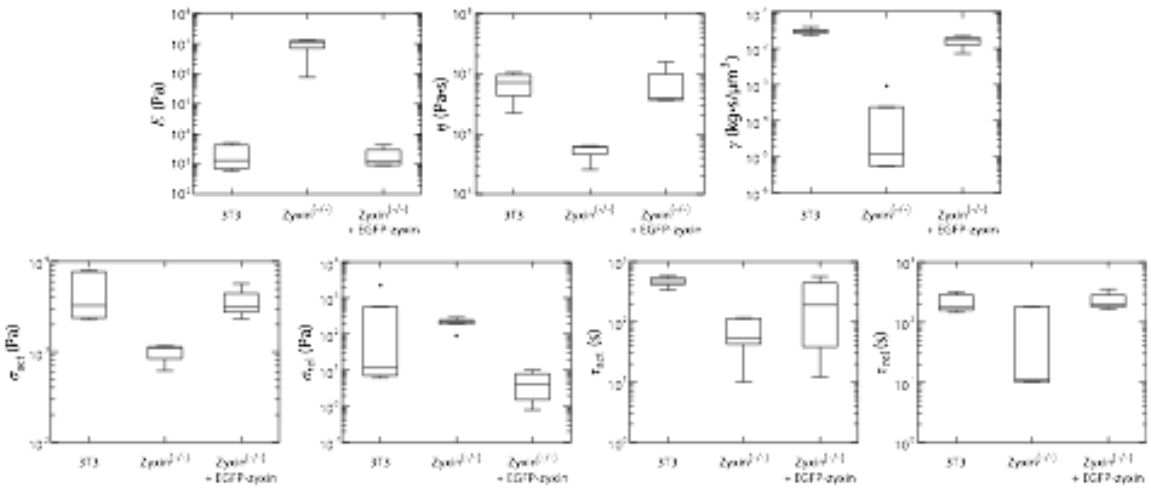

Supp Figure 18: Boxplots representing the fitting parameters for the continuum model for 3T3s, zyxin$^{(-/-)}$ MEFs and zyxin$^{(-/-)}$+EGFP-zyxin MEFs. The parameters represent the elastic modulus (E), the viscosity (), the frictional coefficient (), the activation stress ($_{act}$), the relaxation stress ($_{rel}$), the activation stress time constant ($_{act}$) and the relaxation time constant ($_{rel}$).

# Chapter 6: Discussion

## 6.1 Optogenetics

The spatial and dynamic control of cell signaling has a fundamental role in controlling cell biology. To better understand how these biological processes are being regulated, we need to be able to manipulate signaling in space and time at the subcellular level. The recent development of optogenetic tools which use light to reversible control signaling with subcellular precision, have provided unprecedented potential to probe underlying molecular mechanisms which orchestrate complex cellular behavior. Due to the powerful promise of these tools, over the past decade or so there has been a large focus on developing and optimizing numerous optogenetic modules which can manipulate signaling with varying levels of spatial and temporal control. However, the field has been a bit slower moving beyond proof of concept and implementing these tools to address critical questions about how cell signaling is regulated in space and time. Some of the most successful examples include demonstrating light-directed local activation of Rac1 was sufficient to induce local protrusions and direct light-mediated cell migration(Levskaya et al., 2009; Wu et al., 2009). Moving upstream of Rac1 activation, light-directed spatial gradients of GPCR signaling was sufficient to direct migration of chemotaxing macrophages(O'Neill and Gautam, 2014). In budding yeast, light-directed activation of Cdc42 was sufficient to direct bud site selection(Strickland et al., 2012).

Despite these and other studies utilizing optogenetic tools to address biological questions, the question remains what has prevented more wide-spread use of optogenetic tools? As discussed in detail in Chapter 1.4, there are several critical limitations associated with the available

optogenetic systems, such as the requirement for exogenous co-factors, special microscopic equipment, or rigorous engineering to gain light-mediated control of protein activity. The TULIPs light-induced dimerization module overcomes most of these limitations and has the added benefit of being easily tunable making this an attractive tool to study wide variety of signaling pathways which may be more or less responsive to light-mediated activation. Nonetheless, even with an optimal optogenetic system utilizing these tools is not trivial and I will discuss below some of the specific technical challenges I and probably others have encountered when constructing optogenetic control of cell signaling.

### 6.1.1 Designing and implementing an optogenetic strategy to control protein activity

One the most significant hurdles is to design a strategy to obtain optogenetic control of a protein's activity or signaling pathway. In many instances, by controlling protein localization, one can control a protein's activity. For example, to induce GTPase activation, light-regulated membrane recruitment of RhoGEFs has worked well for us(Wagner and Glotzer, 2016) and others (Strickland et al., 2008), although there is still a significant amount engineering required to design a light-regulated GEF. Specifically this required the GEF to remain inactive in the cytosol, yet be able to activate GTPase signaling upon light-induced membrane localization. Removal the N-terminus which is often involved in endogenous regulation of GEF activity (discussed in Chapter 1.1) was sufficient to gain light-mediated control of the RhoGEF's Tiam1 and Intersectin (Levskaya et al., 2009). However in our work, removal of the C-terminal portion of the RhoA GEF's Ect2 and LARG, created constitutively active GEF's due to their inherent ability to associate with the membrane in the absence of light-mediated recruitment. To dampen background activity, we had to further truncate each GEF to the minimal catalytic DH domain.

This reduced the background activity of Ect2, however light-induced membrane recruitment of the Ect2 DH only weakly activated RhoA. On the other hand, membrane recruitment of the LARG DH induced robust activation of RhoA, but also induces higher levels of background RhoA activation. The balance between low background levels and high light-mediated activation is an important factor critical for successful optogenetic control of cell signaling and as observed in our work can require a great deal of engineering. As described in section 6.1.5, expression levels of the optogenetic probes is another critical factor which can effect these levels.

In addition to controlling localization, other strategies have included light-induced oligomerization to induce signaling by clustering and light-induced sequestration to inactivate signaling by preventing endogenous localization. However, these strategies are difficult to spatially control and may only work for a small subset of proteins. As the use of optogenetic tools expands to more diverse protein activities, the strategies to engineer light-regulated control will also have to expand.

### 6.1.2 Quantification of light-induced signaling

To demonstrate functionality one requires the availability of a sensitive readout/s. For example, FRET biosensors have been widely used to detect Rho GTPase activity with relatively high sensitivity(Pertz, 2010). However, we were unable to use FRET biosensors, since the LOV domain is activated between 400-500 nm light precluding the ability to simultaneously image the biosensor while locally photoactivating the cell. Instead, we used a previously validated RhoA biosensor consisting of the mCherry-tagged RhoA binding domain of anilin (AHDPH) (Piekny

and Glotzer, 2008). Although, this works well to detect local increases in RhoA activation during cytokinesis, in interphase cells the biosensor appears aggregated and cortical prior to photoactivation. It was unclear if this is due to endogenous levels of RhoA activity or a non-specific artifact of the probe which could dampen its ability to detect RhoA activation. This question of sensitivity was an issue when trying to confirm whether light-mediated recruitment of the Ect2 DH domain could activate RhoA. In response to local illumination, we observed little to no accumulation of the biosensor, however when we examined light-mediated recruitment of LARG DH we were able to detect robust recruitment of the RhoA biosensor. Demonstrating the RhoA biosensor was functional and could detect local increases in RhoA activation and the minimal accumulation observed using the Ect2 DH was most likely due to low levels of RhoA activation. Without a sensitive readout that is compatible to use with the optogenetic system, designing a light-regulated control cell signaling is nearly impossible and will require the development and validation of novel readouts.

### 6.1.4 Inactivation or Suppression of the endogenous signaling pathway

To unequivocally determine that light-directed activation of a protein is sufficient to direct a specific cellular process, one must inactivate or suppress the endogenous signaling pathway. For example, to demonstrate light-mediated activation of RhoA was sufficient to initiate furrow formation, we needed to inactivate the endogenous RhoA activation pathway during cytokinesis. There are several ways to prevent RhoA activation during cytokinesis using either chemical or genetic techniques, however, it was important to consider if there were additional effects which could disrupt potential parallel pathways contributing to furrow formation. Ultimately we tested several different conditions to inhibit the endogenous RhoA activation pathway including; PLK1

inhibition, Cyk4 KD, and endogenous Cdk1 inhibition, to be confident the results observed upon light-mediated activation of RhoA were robust.

### 6.1.5 Expression levels

Another important factor which we found could greatly influence our experiments, was the level of expression of the optogenetic components. At higher the levels of expression, the levels of local recruitment of PR_GEF and RhoA activation were higher. However, higher expression of PR_GEF also increased the background levels of RhoA activation. Lower PR_GEF expression decreased background levels of RhoA activation, but also the levels of light-induced PM recruitment. The background levels of RhoA was a critical factor in my mitotic experiments where we have shown higher levels of global RhoA activation and cortical tension can directly modulate the response to local RhoA activation. In addition to concerns of background RhoA activity, variability in expression generates variability in the response to local PR_GEF recruitment. Ideally, we could limit this variability in expression levels by generating stable lines expressing our optogenetic components. However, we were unsuccessful in generating stable lines that stably expressed at sufficiently high levels and therefore, for all our experiments cells were transiently transfected and selected based on (arbitrarily-determined) optimal levels of expression. Although this was not ideal and increased variability, we were still observed relatively robust effects upon light-mediated activation of RhoA. One possible way we could improve our signal to noise, is to swap the peptide/PDZ interaction tags with the small high-affinity SSpB/SSra interaction tags. Fellow lab members have demonstrated in *Drosophila* embryos and tissue culture, the LOVssRA and SSpB fusion system is functional to induce light-mediated membrane recruitment even at lower levels of SSpB tagged protein expression.

Therefore, it would be useful to see if switching to this system could allow for even lower levels SSpb-GEF expression, lowering undesired background RhoA activity, while maintaining the ability to strongly activate RhoA upon light-induced membrane recruitment.

### 6.1.6 Identifying tractable questions and interpreting results

Nearly all biological processes depend on precise spatial and temporal coordination of molecular events. Although optogenetic tools provide a powerful means to start investigating spatiotemporal regulation of these molecular mechanisms, their use has been relatively limited. In addition to the specific technical challenges we have highlighted above, there are additional broader considerations which limit the use of optogenetic systems. The most successful studies utilizing optogenetic tools have been those investigating cellular processes which are associated with the polarized function of a specific molecular component/s. For example the local activation of Rac1 at the leading edge of migrating cells, Cdc42 activation during bud selection in budding yeast, and RhoA activation prior to and during furrow ingression. In each case, the GTPase activity is spatially and temporally correlated and required for their respective cellular process. However, whether or not their local activation was sufficient was unclear and presented an attractive question which could be easily addressed by optogenetic tools. However, there are numerous examples of cellular processes for which the underlying molecular details are relatively unknown and therefore it's unclear how to design optogenetic approaches to determine their regulation. For example, there are multiple lines of evidence demonstrating astral microtubules negatively regulate contractility and my results demonstrate this must be occurring upstream of RhoA activation. Until we have identified potential molecular candidates for astral inhibition by using conventional genetic techniques, we can not utilize optogenetic tools.

Another important consideration, is how to interpret the results upon optogenetic activation of a signaling pathway. In the previous examples, it was found that indeed the respective GTPase activity was sufficient to induce their corresponding cellular response. Positive results are easy to interpret and lend themselves to even further investigation if and how this response is spatially and temporally regulated. The absence of cellular response, although may still be biologically relevant, is much more difficult to interpret. Is the level of optogenetic activation insufficient or are there unknown additional requirements? As is usually the case, it is difficult to be confident in a negative result.

The successful use of opotogenetic tools require specific question and hypothesis, assays for optimization, patience and tenacity. As we have experienced, designing optogenetic control of cell signaling can require a lot of effort to answer a yes/no question, but once control is obtained there are second level questions that are often more informative and interesting. Our work is excellent example of how utilizing these systems can illuminate the underlying molecular mechanisms of fundamental cellular processes, like cytokinesis, which are spatially and temporally regulated. As the discovery of fluorescent tags revolutionized cell biology by allowing direct observation of proteins in vivo, the ability to directly manipulate protein activities with spatial and temporal precision using optogenetics will be transformative to molecular and cellular biology fields.

## 6.2 RhoA Signaling

The main motivation for obtaining optogenetic control of RhoA was to investigate spatiotemporal regulation of RhoA-mediated cleavage furrow formation. While engineering and validating TULIPs-mediated regulation of RhoA activation, we also observed several interesting results related to more general regulation of Rho GTPases signaling.

### 6.2.1 Difference in Cell line response

Expression of PR_GEF in different cell lines had different effects on the actomyosin cytoskeleton network in adherent interphase cells. In endothelial HeLa cells, which are normally relatively devoid of stress fibers, PR_GEF expression induces pronounced stress fiber formation, indicating PR_GEF is activating RhoA independent of TULIPs-mediated membrane recruitment. However, in fibroblast NIH3T3 cells, which normally contain stress fibers, PR_GEF expression did not appear to greatly alter or induce changes in the actomyosin cytoskeleton. The cell-line specific differences observed upon PR_GEF expression may be due to different levels of background RhoA activation, RhoGAP activity, or regulation/turnover of the actomyosin cytoskeleton network.

### 6.2.2 Different response to RhoA activation depending on cell adherence

In both HeLa and NIH3T3 cells, local recruitment of PR_GEF induces local activation of RhoA as indicated by accumulation of the RhoA biosensor. In adherent Hela cells, in which PR_GEF expression induces de novo assembly of abundant stress fibers, recruitment results in subtle changes. The reason is not known, but I speculate that the assembly of these structures limits the availability of downstream effectors to induce further actin and myosin accumulation upon light-

meditated recruitment of PR_GEF, indeed competition for available actin monomer effects the assembly of actomyosin structures in fission yeast(Burke et al., 2014) and mammalian cells(Lomakin et al., 2015). NIH3T3 cells in contrast, normally contain more elaborate actomyosin cytoskeletal networks in the absence of PR_GEF expression and may have more downstream effectors available, robustly respond to RhoA activation. Surprisingly, in adherent HeLa and NIH3T3 interphase cells we rarely observed drastic and permanent morphology changes in response to local RhoA activation.

However, in non-adherent interphase or mitotic HeLa and NIH3T3 cells, local activation of RhoA induces strong cortical actin and myosin accumulation and is able to generate robust local changes in cell morphology. We suspect this differential response to RhoA activation is dependent on disassembly of stress-fibers and focal adhesions which occurs when cells enter mitosis and during cell detachment. Disassembly of these structures could provide a pool of downstream effectors, actin, and myosin which can now be more readily assembled at cortex in response to RhoA activation and in the absence restrictive forces focal adhesions and stress fibers provide this cortical actomyosin network can easily induce cell deformations. Alternatively cell rounding and decreased adhesion could influence this response irrespective of the presence of stress fibers and focal adhesions. To test if cell adhesion in the absence of stress fibers and focal adhesions alters the ability of local RhoA activation to induce cell morphology changes, we plated NIH3T3 onto poly-L-lysine coated coverslips which promoted cell spreading and attachment through non-specific electrostatic interactions. Upon local activation of RhoA, dramatic changes in cell morphology were observed further supporting our hypothesis that stress fibers and focal adhesions influences RhoA-mediated cell morphology changes.

### 6.2.3 RhoA activation in adherent cells is insufficient to induce polarization or cell retraction

As mentioned in Chapter 1.1, the activities of Rac1, Cdc42, and RhoA are all reported to play important roles in coordinating cell migration. In fibroblasts, activation of Rac1 and Cdc42 are commonly localized to the leading edge and are associated with membrane protrusion. While in the cell body and rear, RhoA-induced contractility is suspected to drive focal adhesion disassembly to promote tail retraction(Ridley et al., 2003). Using photoactivatable RhoA, Wu was able to demonstrate local activation of Rac1 was sufficient to direct cell protrusion and induce migration of fibroblasts(Wu et al., 2009). In a similar fashion using optogenetic control of RhoA, we were interested in testing whether local activation of RhoA sufficient to induce contractility driven cell contraction or retraction. As mentioned above local activation of RhoA in fibroblast NIH3T3's induces robust increases in actomyosin accumulation, and contractile forces (measured by traction force microscopy), yet we rarely observed any local changes in cell morphology. Only in small population of cells, did local activation of RhoA induce cell ripping, however, we suspect these cells were either initially weakly adherent as they often were moving or retracting prior to photoactivation or possibly the levels of RhoA activation were substantially higher in these particular cells. These results indicated that although local activation of RhoA may correlate with tail retraction during migration (Ridley et al., 2003), it's activity may not be sufficient to induce changes in cell retraction in adherent cells. As supported by studies suggesting in addition to RhoA-induced contractility(Even-Ram et al., 2007; Smith et al., 2003; Vicente-Manzanares et al., 2011; 2007), FAK activity(Ezratty et al., 2005), microtubule

disassembly(Efimov and Kaverina, 2009; Ezratty et al., 2005), and endocytosis(Pierini et al., 2000) may all play a role in focal adhesion disassembly in the trailing edge of migrating cells.

### 6.2.4 Can local activation of RhoA induce cell polarity?

Although local activation of Rac1 is sufficient to direct cell migration, there is evidence in fibroblasts and keratocytes that in the absence of any guidance cue, activation of RhoA in the cell rear can trigger the breaking of cell symmetry, and the initiation of migration(Mseka et al., 2007). Although we were not specifically investigating this question, upon local activation of RhoA we did not observe any obvious changes in front/rear symmetry of NIH3T3 cells, however these cells had already established polarity and this mechanism may not apply to already polarized cells (Fig 27). A better experiment may be to examine if we can establish polarity using local RhoA activation in cells which have just adhered and not yet established polarity.

### 6.2.5 Does RhoA induce/suppress other signaling pathways?

As mentioned in Chapter 1.1, there is also a significant amount of crosstalk between Rho GTPases. Both Rac1 and RhoA are reported to directly antagonize one another and indeed, light-mediated activation of Rac1 was sufficient to locally inactivate RhoA. Utilizing TULIP's-mediated activation of RhoA we could in principle determine if RhoA activation is sufficient to inhibit Rac1 activity. Currently, we are unable to test this due to our inability to use the available Rac1 FRET-based biosensors and we placed this question at a lower priority. One possibility could be to generate a Rac1 biosensor based using the PAK1 CRIB domain, which has been used in mitotic HeLa cells to detect Rac1 activity(Bastos et al., 2012). RhoA activity has been associated with other functions including, activation of the ERK signaling pathway and

regulation(Li et al., 2009) of gene transcription(Hill et al., 1995). If light-mediated activation of RhoA is altering these additional signaling pathways, does this effect the cellular responses we have observed?

### 6.3 Cytokinesis

By directly manipulating the mitotic spindle, Rappaport was able to demonstrate that the mitotic spindle was directly responsible for controlling position of furrow formation by controlling the zone of RhoA activation. Building off this work, by directly manipulating RhoA activation we demonstrated this is sufficient initiate furrow formation independent of spindle position or cell cycle stage. These results strongly demonstrate that mitotic spindle is not directing furrow formation by regulating active GTP-bound RhoA or its downstream effectors, but rather through either regulation of upstream activation pathway of RhoA or additional signaling pathways.

#### 6.3.1 Anaphase cortex is equally responsive

As mentioned in Chapter 1, the mitotic spindle is responsible for directing the local zone of RhoA activation and cleavage furrow formation through both positive and negative regulation. Specifically, the central spindle plays an important role in promoting contractility by localizing upstream activation components of RhoA. While this is an essential function, it may not be sufficient. The spindle may also provide additional positive cues, such as directed membrane trafficking (Drechsel et al., 1997) and local accumulation of mitotic kinases, such as Aurora B(Douglas et al., 2010). Conversely, dynamic aster MT's negatively regulate cortical contractility in the cell poles(Murthy and Wadsworth, 2008; Werner et al., 2007). However, the specific molecular mechanism of this inhibition is unknown. Since we are able to induce RhoA

activation anywhere on the cortex, we wanted to determine if these mitotic spindle-directed parallel pathways play a role in directly regulating active GTP-bound RhoA or its downstream effectors. PLK1 inhibition was used to specifically block the endogenous upstream activation pathway of RhoA, while presumably these parallel pathways would remain intact. In these experiments, local activation of RhoA was able to initiate furrow formation equally well in midzone or poles, when either individually or simultaneously activated. These results demonstrated that the anaphase cortex is equally responsive to RhoA activation indicating that there are no other spindle-directed activities that promote furrow formation in equatorial region. Secondly, astral inhibition is not acting at the level of regulating active RhoA or its downstream effectors, but is most likely acting on the upstream regulators of RhoA activation. Although recent evidence suggest polar relaxation may be mediated through kinetochore associated phosphatase which locally inactivates of the ERM protein, moesin. ERM proteins play a critical role in regulating the structural integrity of the actomyosin cortex by acting as link between the membrane and actomyosin cytoskeleton network (Rodrigues et al., 2015). As the chromosome separate and the kinetochores become closer to the poles local dephosphorylation and inactivation of moesin is thought to decrease cortical tension. However, we observe no differential effect on furrow formation upon ectopic activation of RhoA in the poles. Either RhoA activation can overcome decreased cortical association of the actomyosin network or this is not the main molecular mechanism of astral-inhibition of cortical contractility.

### 6.3.2 RhoA-mediated furrow formation is not cell-cycle regulated

RhoA-mediated furrow formation is not regulated in cell cycle-dependent manner, as we were able to induce furrow formation throughout the cell cycle. Local activation of RhoA induces

furrow formation during metaphase, and these behaved very similar to furrows induced during anaphase, indicating there is no metaphase-specific regulation of active RhoA or downstream effectors. These results were not unexpected, as cells progressing through metaphase undergo isotropic increases in actomyosin cortical accumulation and cortical tension levels (Ramanathan et al., 2015; Stewart et al., 2011) indicating these pathways are active.

### 6.3.3 Decreased cell adhesion and cell rounding may be an important for RhoA-mediated furrow formation

As discussed in section 6.2.3, although we observe robust increases in actin and myosin accumulation when RhoA is locally activated in adherent interphase cells, no furrow-like behavior was observed. One common phenomena of mitotic cells, even within tissues, is they will decrease their adherence to the substrate or cell-cell contacts and round up as they enter mitosis. We hypothesized, that maybe cell rounding and decreased adhesion could alter the response to local RhoA activation in interphase cells. Surprisingly, upon local activation of RhoA in rounded non-adherent interphase cells rapidly induces furrow formation and these furrows can ingress nearly to completion. We suspect this differential response between adherent versus non-adherent interphase cells is due to dramatic reorganization of actomyosin cytoskeleton network cells undergo during detachment as their stress fiber and focal adhesion structures are disassembled resulting in cell rounding. Interestingly, by using polarization microscopy to examine the organization of the actin cytoskeleton, Fishkind observed that cells entering mitosis undergo a similar remodeling of their actin cytoskeleton(Fishkind and Wang, 1993). During interphase the actin filaments were highly ordered into stress fiber structures and as cells entered in mitosis the actin filaments underwent pronounced reorganization as stress

fibers were disassembled. As the cells entered anaphase, actin filaments become locally ordered along the equator in the region of furrow formation (Fishkind and Wang, 1993). Stress fibers, although dynamic, are load-bearing, tension-generating structures that generate cellular rigidity. In response to increased tension, similar to what is occurring upon light-mediated activation of RhoA, these mechanosentive structures are also responsible for reinforcing and increasing cell tension levels, primarily through mechanosenstive GEFs which can further activate RhoA(Chen et al., 2004; Lessey et al., 2012). Therefore we suspect the ability of local RhoA activation to induce furrow formation, is dependent on the balance between the locally induced and global resistive forces. In adherent cells the presence of stress fibers provides higher resistive forces that limit or prevent local furrow formation upon local activation of RhoA. However, by detaching and disassembling stress fibers in interphase cells, we have lowered these resistive forces now permitting furrow formation upon local activation of RhoA. Further indicating that RhoA-mediated furrow formation is not cell-cycle regulated and no mitotic-specific factors are required for contractile ring assembly and furrow ingression. Importantly, these results suggest that cell detachment and rounding which occurs in nearly all mitotic cells, may be a critical factor for the ability of active RhoA to induce cleavage formation during cytokinesis. There are examples of cells which do remain relatively flat (Fishkind and Wang, 1993; Lancaster et al., 2013) and are still capable of undergoing cytokinesis, however, there is still pronounced remodeling of actin cytoskeleton which may be important for cleavage furrow formation.

### 6.3.4 Cortical tension levels modulate the extent of furrow formation.

As mentioned in the previous section, the ability of cells to generate cleavage furrow requires the local actomyosin-based forces at the furrow can overcome global resistive forces. There is

evidence that as cells enter the mitotic cycle there is a substantial increase cortical tension and hydrostatic pressure, which was measured to be about 3x times higher then rounded interphase cells(Stewart et al., 2011). Therefore, we suspected that the enhanced furrow ingression observed in interphase cells may be because these cells are more compliant.

Consistent with compliance impacting furrow ingression, I have found that increasing global cortical tension in non-adherent interphase cells decreases the extent and rate of furrow ingression upon local activation. Conversely, if I decreased the global hydrostatic pressure in mitotic cells with EIPA treatment, the extent of furrow ingression was enhanced. By modulating the global cortical tension levels in either rounded non-adherent NIH3T3 cells or mitotic HeLa cells, we could directly modulate the extent of RhoA-mediated furrow ingression. These results also support why exogenous activation of RhoA in the poles may slow or completely block endogenous furrow formation by increasing cortical tension levels and providing mechanical forces that impede proper furrow formation.

### 6.3.5 Why does ectopic activation of RhoA only induce partial furrow ingression?

#### 6.3.5.1 Does PLK1 activity promote furrow formation?

Although local activation of RhoA is sufficient to initiate furrow formation, these furrows only partially ingressed in mitotic cells where the upstream activation pathway has been inactivated by either PLK1 inhibition or through endogenous Cdk1 activity. This raises the question of what is required for RhoA-mediated furrows to fully ingress? One possibility, is Plk1 may have additional roles in promoting furrow formation downstream of RhoA activation during anaphase (Liu et al., 2004; Lowery et al., 2007; Neef et al., 2003). However if the endogenous pathway is inhibited in a different manner by knocking-down Cyk4, similar results are observed upon light-

mediated RhoA activation at the midzone. A caveat to this interpretation is that another consequence of Cyk4 depletion is improper formation of the central spindle. Therefore, if the unknown function of Plk1 requires it's central spindle localization this would be disrupted when Cyk4 is knocked down. A better experiment would to be knockdown Ect2 which prevents endogenous activation of RhoA and furrow formation, but does not disrupt central spindle assembly or Plk1 localization. However, in our hands, the knockdown of Ect2 was weaker, and a significant portion of control cells would partially furrow or even complete furrow ingression, rendering this approach inconclusive.

#### 6.3.5.2 Insufficient levels of RhoA activation?

Incomplete ingression could also be a result of insufficient levels of RhoA activation or downstream effectors in comparison to cells dividing normally. However we observed that the localization and levels of active RhoA seem comparable to those in normally dividing cells. We also observed the downstream effects on actin and myosin and found these to be also roughly comparable to those in normally dividing cells. Due to variable expression levels, we observed variability in the membrane accumulation of each marker, even in the normally dividing cells. However, ectopic activation of RhoA was sufficient to compete with the endogenous furrow suggesting we are capable of activating biological relevant levels of RhoA. Therefore, incomplete ingression seems not be due to significantly reduced activation of RhoA or its key effectors.

Another possibility is the precise location and timing of RhoA activation may effect furrow ingression. In cells dividing normally, the zones of RhoA activation, actin and myosin

accumulation initially appear in a relatively broad zone which then becomes sharpened as the furrow forms and ingresses. The maximum levels of RhoA activation, actin, and myosin accumulation also occur at later stages of furrow ingression in normally dividing cells. In comparison during light-mediated furrow formation, the localization of RhoA activation and downstream effects was tightly defined by the zone of illumination (typically 2μm zone) and the kinetics of RhoA activation, actin polymerization, and myosin II accumulation typically occurred more quickly (within a few minutes). However, there may be subtle differences in the precise localization, timing, and levels of RhoA activation and its downstream effects on the ingressing furrow which I was unable to accurately detect and could be important for driving furrow formation. Indeed, ectopic activation of RhoA in wider zone at the equatorial region slows furrow ingression in normally dividing cells.

#### 6.3.5.3 Increased cortical tension due to background levels of RhoA activation

Another concern was the expression of PR_GEF may induce background levels of RhoA activation which would globally increase cortical tension and we have demonstrated cortical tension levels can modulate the extent of furrow ingression. In the absence of a way to measure cortical tension levels in mitotic cells, we examined the global cortical levels of RhoA activation, actin, and myosin and they did not appear to be higher in mitotic cells expressing PR_GEF compared to control cells. Expression of PR_GEF also did not affect the ability of cells to divide normally (ingress with a similar rate to control cells). Therefore, although we know PR_GEF can induce pronounced stress fiber formation in adherent interphase cells, the background levels of RhoA activation and effects on cortical tension do not appear to be the main factor limiting light-induced furrow formation.

#### 6.3.5.4 Centralspindlin localized GEF support furrow formation

An attractive model we favor is that as furrows ingress in normally dividing cells they encounter the centralspindlin:Ect2 complex localized on the central spindle. This highly concentrated pool of GEF may help to enhance the levels of RhoA activation at ingressing tip promoting full furrow ingression.

To test if central spindle localized GEF, can enhance furrow formation we fused the LARG DH domain to microtubule bundling protein PRC1. The PRC1-mCherry-LARG DH construct localized well to the central spindle, however upon light-mediated recruitment of PR_GEF the presence of central spindle localized GEF did not appear to enhance furrow formation in the majority of cells. However, we have noticed that the central spindle is not as broad when cells are treated with the PLK inhibitor and as a consequence the light-mediated furrows in these experiments frequently do not ingress far enough to interact with central spindle localized pool of GEF. To slightly increase the extent of furrow we included an EIPA treatment in addition to PLK1 inhibition. In these experiments 4 out of 6 cells ingressed nearly 75% which is much further then EIPA +PLK1 inhibitor (45%) or PLK inhibitor alone (35%) suggesting that central spindle localized GEF may enhance furrow formation. Although promising, these results have been difficult to reproduce. We are unable to use the Cyk4 KD instead of PLK1 inhibition, as the loss of Cyk4 disrupts central spindle assembly.

#### 6.3.5.5 Positive feedback

Another non-mutually exclusive possibility we strongly favor, is there is positive feedback dependent on the centralspindlin:Ect2 complex, increases and sharpens the zone of RhoA activation promoting furrow ingression. Autocatalytic, ECT-2 dependent waves of RhoA activity on the cortex of anaphase vertebrate and invertebrate oocytes and embryos, indicate that this machinery is capable of exhibiting positive feedback behavior(Bement et al., 2015). However the mechanism of this positive feedback is not clear. Additionally, independent studies our lab provided genetic evidence that positive feedback may exist through RhoA and centralspindlin:Ect2 complex(Zhang and Glotzer, 2015). In particular, the ability of Cyk4 GAP domain to bind RhoA-GTP was required to promote RhoA activation in *C. elegans* embryos. We suspect in addition with the membrane binding of Ect2 and the C1 domain of Cyk4, the interaction between Cyk4's GAP domain and active RhoA may help to localize centralspindlin:Ect2 complex to equatorial cortex, promoting positive feedback of RhoA activation. In addition, a second binding interaction between Cyk4 GAP domain and the DHPH domain of Ect2 may play a role in enhancing Ect2's GEF activity further promoting RhoA activation.

In all of my experiments where we induced RhoA-mediated furrow formation, the upstream activation pathway was suppressed by either by PLK1 inhibition, Cyk4 KD, or by Cdk1 activity thereby blocking potential for positive feedback. To directly test if positive feedback exists, we need a way to keep the endogenous activation pathway intact, yet still be able to control furrow induction with TULIP's mediated activation of RhoA. One way we have envisioned doing this experiment is to use monopolar arrested HeLa cells. Monopolar arrested cells, generated by

treatment with the kinesin-5 inhibitor, can be synchronously forced to enter cytokinesis upon treatment with the Cdk1 inhibitor purvalanol A. Upon exit, the spindle, upstream activators including Cyk4, Ect2, and RhoA activity are initially organized in radially symmetric manner. Gradually, the cells undergo symmetry breaking that simultaneously polarizes microtubules, upstream activators, and RhoA activation on the cell cortex. Over time, the polarized RhoA activity generates a "furrow-like cortex" that protrudes from the cell body and starts to ingress and form a distinctive furrow between the cell body and the protrusion. The mechanisms of furrow ingression during monopolar cytokinesis appear to closely parallel those that occur during normal bipolar cytokinesis. Using this background, I can determine if TULIP's mediated local activation of RhoA can direct the location of symmetry breaking and "furrow" formation. If positive feedback is occurring and required for the ability of local RhoA activation to direct polarization and furrow formation, this result would be dependent on the upstream activation pathway remaining intact. We could then systematically determine the specific requirements for feedback, for example by examining the effects of PLK1 inhibition or Cyk4 KD. Unfortunately, I have not been able to consistently observe mitotic exit and polarization of monopolar arrested HeLa cells upon the addition of purvalonal A and therefore have not been able to test if local activation of RhoA can direct polarization or furrow formation.

### 6.3.6 Is formin mediated actin polymerization and myosin II activation sufficient to induce furrow formation?

Local activation of RhoA in mitotic cells is sufficient to initiate furrow formation mediated by local increases in formin-directed actin polymerization and ROCK induced myosin activation. Indeed using either the ROCK kinase inhibitor, Y27632, or formin inhibitor, SMIFH2, would

impair light-directed furrow formation. However in addition to activation of the formin, mDia, and ROCK, there are other downstream effectors of RhoA during cytokinesis, including the putative scaffold protein, anilin, and citron kinase which also activates myosin and is suggested to play a role in later stages of cytokinesis including abscission. Do these effectors contribute to RhoA-mediated furrow initiation? If we could optogenetically control mDia and ROCK activation, would light-directed co-activation induce similar effect as local RhoA activation?

### 6.3.5 How is the upstream RhoA activation pathway regulated during cytokinesis?

In addition to determining the requirements for full ingression, my work highlights the need to further investigate how the mitotic spindle directly regulates the localization of the upstream activation pathway. Work from another lab member, Angika Basant, has identified the role of Aurora B kinase in promoting cytokinesis by inducing oligomerization and cortical localization of centralspindlin in *C.elegans* embryos. To directly demonstrate localized Aurora B activity is sufficient to direct local activation of RhoA by promoting membrane localization of centralspindlin:Ect2 complex, Angika is now utilizing the TULIPs system to control Aurora B activation. In a similar fashion to my work, she will then determine if exogenous activation of Aurora B is sufficient to induce RhoA-mediated furrow formation in mammalian cells. In addition to Aurora B regulation of membrane localization of centralspindlin, additional genetic evidence suggest there are additional negative regulatory signals mediated by astral microtubules regulating cortical localization of the centralspindlin complex, however, the nature of this signal is currently unknown.

## 6.4 Appendix 6

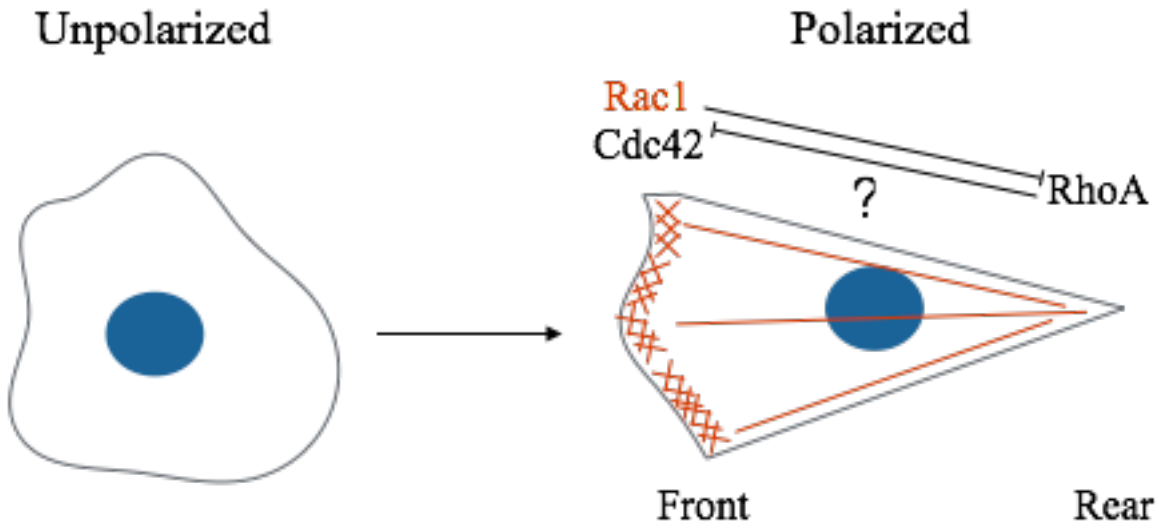


Figure27: Cell polarization and Migration. Local activation of Rac1 is sufficient to induce protrusion, cell migration. and antagonize RhoA activity. Is the local activation of RhoA sufficient to induce front/rear symmetry, migration, and antagonize Rac1 activity?

References

Abo, A., Pick, E., Hall, A., Totty, N., Teahan, C.G., and Segal, A.W. (1991). Activation of the NADPH oxidase involves the small GTP-binding protein p21rac1. Nature *353*, 668–670.

Aghajanian, A., Wittchen, E.S., Campbell, S.L., and Burridge, K. (2009). Direct activation of RhoA by reactive oxygen species requires a redox-sensitive motif. PLoS ONE *4*, e8045.

Aittaleb, M., Gao, G., Evelyn, C.R., Neubig, R.R., and Tesmer, J.J.G. (2009). A conserved hydrophobic surface of the LARG pleckstrin homology domain is critical for RhoA activation in cells. Cell. Signal. *21*, 1569–1578.

Alexandre, M.T.A., Arents, J.C., van Grondelle, R., Hellingwerf, K.J., and Kennis, J.T.M. (2007). A base-catalyzed mechanism for dark state recovery in the Avena sativa phototropin-1 LOV2 domain. Biochemistry *46*, 3129–3137.

Amano, M., Ito, M., Kimura, K., Fukata, Y., Chihara, K., Nakano, T., Matsuura, Y., and Kaibuchi, K. (1996). Phosphorylation and activation of myosin by Rho-associated kinase (Rho-kinase). J. Biol. Chem. *271*, 20246–20249.

Aratyn-Schaus, Y., Oakes, P.W., and Gardel, M.L. (2011). Dynamic and structural signatures of lamellar actomyosin force generation. Mol. Biol. Cell *22*, 1330–1339.

Balaban, N.Q., Schwarz, U.S., Riveline, D., Goichberg, P., Tzur, G., Sabanay, I., Mahalu, D., Safran, S., Bershadsky, A., Addadi, L., et al. (2001). Force and focal adhesion assembly: a close relationship studied using elastic micropatterned substrates. Nat. Cell Biol. *3*, 466–472.

Barr, F.A., and Gruneberg, U. (2007). Cytokinesis: placing and making the final cut. *131*, 847–860.

Barr, F.A., Silljé, H.H.W., and Nigg, E.A. (2004). Polo-like kinases and the orchestration of cell division. Nat. Rev. Mol. Cell Biol. *5*, 429–440.

Baruni, J.K., Munro, E.M., and Dassow, von, G. (2008). Cytokinetic furrowing in toroidal, binucleate and anucleate cells in C. elegans embryos. J. Cell. Sci. *121*, 306–316.

Basant, A., Lekomtsev, S., Tse, Y.C., Zhang, D., Longhini, K.M., Petronczki, M., and Glotzer, M. (2015). Aurora B kinase promotes cytokinesis by inducing centralspindlin oligomers that associate with the plasma membrane. Dev. Cell *33*, 204–215.

Bastos, R.N., Penate, X., Bates, M., Hammond, D., and Barr, F.A. (2012). CYK4 inhibits Rac1-dependent PAK1 and ARHGEF7 effector pathways during cytokinesis. J. Cell Biol. *198*, 865–880.

Bement, W.M., Benink, H.A., and Dassow, von, G. (2005). A microtubule-dependent zone of active RhoA during cleavage plane specification. Journal of Cell Biology *170*, 91–101.

Bement, W.M., Leda, M., Moe, A.M., Kita, A.M., Larson, M.E., Golding, A.E., Pfeuti, C., Su, K.-C., Miller, A.L., Goryachev, A.B., et al. (2015). Activator-inhibitor coupling between Rho signalling and actin assembly makes the cell cortex an excitable medium. Nat. Cell Biol. *17*, 1471–1483.

Besser, A., and Schwarz, U.S. (2007). Coupling biochemistry and mechanics in cell adhesion: a model for inhomogeneous stress fiber contraction. New J. Phys. *9*, 425–425.

Bhattacharyya, R., and Wedegaertner, P.B. (2000). Galpha 13 requires palmitoylation for plasma membrane localization, Rho-dependent signaling, and promotion of p115-RhoGEF membrane binding. J. Biol. Chem. *275*, 14992–14999.

Blanchoin, L., Boujemaa-Paterski, R., Sykes, C., and Plastino, J. (2014). Actin dynamics, architecture, and mechanics in cell motility. Physiol. Rev. *94*, 235–263.

Bodvard, K., Wrangborg, D., Tapani, S., Logg, K., Sliwa, P., Blomberg, A., Kvarnström, M., and Käll, M. (2011). Continuous light exposure causes cumulative stress that affects the localization oscillation dynamics of the transcription factor Msn2p. Biochim. Biophys. Acta *1813*, 358–366.

Broedersz, C.P., and MacKintosh, F.C. (2014). Modeling semiflexible polymer networks. Rev. Mod. Phys. *86*, 995–1036.

Brox, T., and Weickert, J. (2006). Level set segmentation with multiple regions. IEEE Trans Image Process *15*, 3213–3218.

Buckley, C.E., Moore, R.E., Reade, A., Goldberg, A.R., Weiner, O.D., and Clarke, J.D.W. (2016). Reversible Optogenetic Control of Subcellular Protein Localization in a Live Vertebrate Embryo. Dev. Cell *36*, 117–126.

Burke, T.A., Christensen, J.R., Barone, E., Suarez, C., Sirotkin, V., and Kovar, D.R. (2014). Homeostatic actin cytoskeleton networks are regulated by assembly factor competition for monomers. Curr. Biol. *24*, 579–585.

Bustelo, X.R. (2000). Regulatory and signaling properties of the Vav family. Mol. Cell. Biol. *20*, 1461–1477.

Butler, J.P., Tolić-Nørrelykke, I.M., Fabry, B., and Fredberg, J.J. (2002). Traction fields, moments, and strain energy that cells exert on their surroundings. Am. J. Physiol., Cell Physiol. *282*, C595–C605.

Cai, Y., Rossier, O., Gauthier, N.C., Biais, N., Fardin, M.-A., Zhang, X., Miller, L.W., Ladoux, B., Cornish, V.W., and Sheetz, M.P. (2010). Cytoskeletal coherence requires myosin-IIA contractility. J. Cell. Sci. *123*, 413–423.

Callan-Jones, A.C., and Voituriez, R. (2013). Active gel model of amoeboid cell motility. New J. Phys. *15*, 025022.

Cao, L.G., and Wang, Y.L. (1996). Signals from the spindle midzone are required for the stimulation of cytokinesis in cultured epithelial cells. Mol. Biol. Cell *7*, 225–232.

Chan, A.M., Takai, S., Yamada, K., and Miki, T. (1996). Isolation of a novel oncogene, NET1, from neuroepithelioma cells by expression cDNA cloning. Oncogene *12*, 1259–1266.

Chen, C.S., Tan, J., and Tien, J. (2004). Mechanotransduction at cell-matrix and cell-cell contacts. Annu Rev Biomed Eng *6*, 275–302.

Chen, W., Foss, M., Tseng, K.-F., and Zhang, D. (2008). Redundant mechanisms recruit actin into the contractile ring in silkworm spermatocytes. PLoS Biol. *6*, e209.

Christie, J.M., Reymond, P., Powell, G.K., Bernasconi, P., Raibekas, A.A., Liscum, E., and Briggs, W.R. (1998). Arabidopsis NPH1: a flavoprotein with the properties of a photoreceptor for phototropism. Science *282*, 1698–1701.

Christie, J.M., Corchnoy, S.B., Swartz, T.E., Hokenson, M., Han, I.-S., Briggs, W.R., and Bogomolni, R.A. (2007). Steric interactions stabilize the signaling state of the LOV2 domain of phototropin 1. Biochemistry *46*, 9310–9319.

Chrzanowska-Wodnicka, M., and Burridge, K. (1996). Rho-stimulated contractility drives the formation of stress fibers and focal adhesions. J. Cell Biol. *133*, 1403–1415.

Colombelli, J., Besser, A., Kress, H., Reynaud, E.G., Girard, P., Caussinus, E., Haselmann, U., Small, J.V., Schwarz, U.S., and Stelzer, E.H.K. (2009). Mechanosensing in actin stress fibers revealed by a close correlation between force and protein localization. J. Cell. Sci. *122*, 1665–1679.

Coso, O.A., Chiariello, M., Yu, J.C., Teramoto, H., Crespo, P., Xu, N., Miki, T., and Gutkind, J.S. (1995). The small GTP-binding proteins Rac1 and Cdc42 regulate the activity of the JNK/SAPK signaling pathway. *81*, 1137–1146.

Coyle, S.M., and Lim, W.A. (2016). Mapping the functional versatility and fragility of Ras GTPase signaling circuits through in vitro network reconstitution. Elife *5*, 779.

Crosson, S., and Moffat, K. (2001). Structure of a flavin-binding plant photoreceptor domain: insights into light-mediated signal transduction. Proc. Natl. Acad. Sci. U.S.a. *98*, 2995–3000.

Dechant, R., and Glotzer, M. (2003). Centrosome separation and central spindle assembly act in redundant pathways that regulate microtubule density and trigger cleavage furrow formation. Dev. Cell *4*, 333–344.

Devreotes, P., and Horwitz, A.R. (2015). Signaling networks that regulate cell migration. Cold Spring Harb Perspect Biol *7*, a005959.

Douglas, M.E., Davies, T., Joseph, N., and Mishima, M. (2010). Aurora B and 14-3-3 coordinately regulate clustering of centralspindlin during cytokinesis. Curr. Biol. *20*, 927–933.

Drechsel, D.N., Hyman, A.A., Hall, A., and Glotzer, M. (1997). A requirement for Rho and Cdc42 during cytokinesis in Xenopus embryos. Curr. Biol. *7*, 12–23.

Dueber, J.E., Yeh, B.J., Chak, K., and Lim, W.A. (2003). Reprogramming control of an allosteric signaling switch through modular recombination. Science *301*, 1904–1908.

Eden, S., Rohatgi, R., Podtelejnikov, A.V., Mann, M., and Kirschner, M.W. (2002). Mechanism of regulation of WAVE1-induced actin nucleation by Rac1 and Nck. Nature *418*, 790–793.

Edwards, C.M., and Schwarz, U.S. (2011). Force localization in contracting cell layers. Phys. Rev. Lett. *107*, 128101.

Efimov, A., and Kaverina, I. (2009). Significance of microtubule catastrophes at focal adhesion sites. Cell Adh Migr *3*, 285–287.

Even-Ram, S., Doyle, A.D., Conti, M.A., Matsumoto, K., Adelstein, R.S., and Yamada, K.M. (2007). Myosin IIA regulates cell motility and actomyosin-microtubule crosstalk. Nat. Cell Biol. *9*, 299–309.

Ezratty, E.J., Partridge, M.A., and Gundersen, G.G. (2005). Microtubule-induced focal adhesion disassembly is mediated by dynamin and focal adhesion kinase. Nat. Cell Biol. *7*, 581–590.

Farsad, M., and Vernerey, F.J. (2012). An XFEM‐based numerical strategy to model mechanical interactions between biological cells and a deformable substrate. International Journal for Numerical ….

Fenno, L., Yizhar, O., and Deisseroth, K. (2011). The Development and Application of Optogenetics. Http://Dx.Doi.org/10.1146/Annurev-Neuro-061010-113817.

Fishkind, D.J., and Wang, Y.L. (1993). Orientation and three-dimensional organization of actin filaments in dividing cultured cells. J. Cell Biol. *123*, 837–848.

Fletcher, D.A., and Mullins, R.D. (2010). Cell mechanics and the cytoskeleton. Nature *463*, 485–492.

Frenette, P., Haines, E., Loloyan, M., Kinal, M., Pakarian, P., and Piekny, A. (2012). An anillin-Ect2 complex stabilizes central spindle microtubules at the cortex during cytokinesis. PLoS ONE *7*, e34888.

Gardel, M.L., Schneider, I.C., Aratyn-Schaus, Y., and Waterman, C.M. (2010). Mechanical integration of actin and adhesion dynamics in cell migration. Annu. Rev. Cell Dev. Biol. *26*, 315–333.

Gibson, D.G., Young, L., Chuang, R.-Y., Venter, J.C., Hutchison, C.A., and Smith, H.O. (2009). Enzymatic assembly of DNA molecules up to several hundred kilobases. Nat. Methods *6*, 343–345.

Gietz, R.D., and Sugino, A. (1988). New yeast-Escherichia coli shuttle vectors constructed with in vitro mutagenized yeast genes lacking six-base pair restriction sites. Gene *74*, 527–534.

Gietz, R.D., and Woods, R.A. (2002). Transformation of yeast by lithium acetate/single-stranded carrier DNA/polyethylene glycol method. Meth. Enzymol. *350*, 87–96.

Guilluy, C., Swaminathan, V., Garcia-Mata, R., O'Brien, E.T., Superfine, R., and Burridge, K. (2011). The Rho GEFs LARG and GEF-H1 regulate the mechanical response to force on integrins. Nat. Cell Biol. *13*, 722–727.

Guo, W.-H., and Wang, Y.-L. (2007). Retrograde fluxes of focal adhesion proteins in response to cell migration and mechanical signals. Mol. Biol. Cell *18*, 4519–4527.

Halavaty, A.S., and Moffat, K. (2007). N- and C-terminal flanking regions modulate light-induced signal transduction in the LOV2 domain of the blue light sensor phototropin 1 from Avena sativa. Biochemistry *46*, 14001–14009.

Hall, A. (1998). Rho GTPases and the actin cytoskeleton. Science *279*, 509–514.

Harper, S.M., Christie, J.M., and Gardner, K.H. (2004). Disruption of the LOV-Jalpha helix interaction activates phototropin kinase activity. Biochemistry *43*, 16184–16192.

Harper, S.M., Neil, L.C., and Gardner, K.H. (2003). Structural basis of a phototropin light switch. Science *301*, 1541–1544.

Hart, M.J., Eva, A., Zangrilli, D., Aaronson, S.A., Evans, T., Cerione, R.A., and Zheng, Y. (1994). Cellular transformation and guanine nucleotide exchange activity are catalyzed by a common domain on the dbl oncogene product. J. Biol. Chem. *269*, 62–65.

Hartman, N.C., and Groves, J.T. (2011). Signaling clusters in the cell membrane. Current Opinion in Cell Biology *23*, 370–376.

Hill, C.S., Wynne, J., and Treisman, R. (1995). The Rho family GTPases RhoA, Rac1, and CDC42Hs regulate transcriptional activation by SRF. *81*, 1159–1170.

Hiramoto, Y. (1956). Cell division without mitotic apparatus in sea urchin eggs. Exp. Cell Res. *11*, 630–636.

Hoffman, B.D., and Crocker, J.C. (2009). Cell mechanics: dissecting the physical responses of cells to force. Annu Rev Biomed Eng *11*, 259–288.

Hoffman, L.M., Jensen, C.C., Kloeker, S., Wang, C.-L.A., Yoshigi, M., and Beckerle, M.C. (2006). Genetic ablation of zyxin causes Mena/VASP mislocalization, increased motility, and deficits in actin remodeling. J. Cell Biol. *172*, 771–782.

Hotulainen, P., and Lappalainen, P. (2006). Stress fibers are generated by two distinct actin assembly mechanisms in motile cells. J. Cell Biol. *173*, 383–394.

Hotulainen, P., Paunola, E., Vartiainen, M.K., and Lappalainen, P. (2005). Actin-depolymerizing factor and cofilin-1 play overlapping roles in promoting rapid F-actin depolymerization in mammalian nonmuscle cells. Mol. Biol. Cell *16*, 649–664.

Huang, J., Koide, A., Makabe, K., and Koide, S. (2008). Design of protein function leaps by directed domain interface evolution. Proc. Natl. Acad. Sci. U.S.a. *105*, 6578–6583.

Huang, J., Makabe, K., Biancalana, M., Koide, A., and Koide, S. (2009). Structural basis for exquisite specificity of affinity clamps, synthetic binding proteins generated through directed domain-interface evolution. J. Mol. Biol. *392*, 1221–1231.

Hughes, R.M., Bolger, S., Tapadia, H., and Tucker, C.L. (2012). Light-mediated control of DNA transcription in yeast. Methods *58*, 385–391.

Huh, W.-K., Falvo, J.V., Gerke, L.C., Carroll, A.S., Howson, R.W., Weissman, J.S., and O'Shea, E.K. (2003). Global analysis of protein localization in budding yeast. Nature *425*, 686–691.

Hussain, N.K., Jenna, S., Glogauer, M., Quinn, C.C., Wasiak, S., Guipponi, M., Antonarakis, S.E., Kay, B.K., Stossel, T.P., Lamarche-Vane, N., et al. (2001). Endocytic protein intersectin-l regulates actin assembly via Cdc42 and N-WASP. Nat. Cell Biol. *3*, 927–932.

Hutterer, A., Glotzer, M., and Mishima, M. (2009). Clustering of centralspindlin is essential for its accumulation to the central spindle and the midbody. Curr. Biol. *19*, 2043–2049.

Idevall-Hagren, O., Dickson, E.J., Hille, B., Toomre, D.K., and De Camilli, P. (2012). Optogenetic control of phosphoinositide metabolism. Proc. Natl. Acad. Sci. U.S.a. *109*, E2316–E2323.

Ingber, D.E. (2003). Tensegrity I. Cell structure and hierarchical systems biology. J. Cell. Sci. *116*, 1157–1173.

Inoue, T., Heo, W.D., Grimley, J.S., Wandless, T.J., and Meyer, T. (2005). An inducible translocation strategy to rapidly activate and inhibit small GTPase signaling pathways. Nat. Methods *2*, 415–418.

Iskratsch, T., Wolfenson, H., and Sheetz, M.P. (2014). Appreciating force and shape—the rise of mechanotransduction in cell biology. Nat. Rev. Mol. Cell Biol. *15*, 825–833.

Jaiswal, M., Gremer, L., Dvorsky, R., Haeusler, L.C., Cirstea, I.C., Uhlenbrock, K., and Ahmadian, M.R. (2011). Mechanistic insights into specificity, activity, and regulatory elements of the regulator of G-protein signaling (RGS)-containing Rho-specific guanine nucleotide exchange factors (GEFs) p115, PDZ-RhoGEF (PRG), and leukemia-associated RhoGEF (LARG). J. Biol. Chem. *286*, 18202–18212.

Janke, C., Magiera, M.M., Rathfelder, N., Taxis, C., Reber, S., Maekawa, H., Moreno-Borchart, A., Doenges, G., Schwob, E., Schiebel, E., et al. (2004). A versatile toolbox for PCR-based tagging of yeast genes: new fluorescent proteins, more markers and promoter substitution

cassettes. Yeast *21*, 947–962.

Jansen, G., Wu, C., Schade, B., Thomas, D.Y., and Whiteway, M. (2005). Drag&Drop cloning in yeast. Gene *344*, 43–51.

Jiang, W., Jimenez, G., Wells, N.J., Hope, T.J., Wahl, G.M., Hunter, T., and Fukunaga, R. (1998). PRC1: a human mitotic spindle-associated CDK substrate protein required for cytokinesis. Mol. Cell *2*, 877–885.

Kanchanawong, P., Shtengel, G., Pasapera, A.M., Ramko, E.B., Davidson, M.W., Hess, H.F., and Waterman, C.M. (2010). Nanoscale architecture of integrin-based cell adhesions. Nature *468*, 580–584.

Katzav, S., Cleveland, J.L., Heslop, H.E., and Pulido, D. (1991). Loss of the amino-terminal helix-loop-helix domain of the vav proto-oncogene activates its transforming potential. Mol. Cell. Biol. *11*, 1912–1920.

Kennedy, M.J., Hughes, R.M., Peteya, L.A., Schwartz, J.W., Ehlers, M.D., and Tucker, C.L. (2010). Rapid blue-light-mediated induction of protein interactions in living cells. Nat. Methods *7*, 973–975.

Kim, J.-E., Billadeau, D.D., and Chen, J. (2005). The tandem BRCT domains of Ect2 are required for both negative and positive regulation of Ect2 in cytokinesis. J. Biol. Chem. *280*, 5733–5739.

Kimura, K., Ito, M., Amano, M., Chihara, K., Fukata, Y., Nakafuku, M., Yamamori, B., Feng, J., Nakano, T., Okawa, K., et al. (1996). Regulation of myosin phosphatase by Rho and Rho-associated kinase (Rho-kinase). Science *273*, 245–248.

Kishi, K., Sasaki, T., Kuroda, S., Itoh, T., and Takai, Y. (1993). Regulation of cytoplasmic division of Xenopus embryo by rho p21 and its inhibitory GDP/GTP exchange protein (rho GDI). J. Cell Biol. *120*, 1187–1195.

Kristelly, R., Gao, G., and Tesmer, J.J.G. (2004). Structural determinants of RhoA binding and nucleotide exchange in leukemia-associated Rho guanine-nucleotide exchange factor. J. Biol. Chem. *279*, 47352–47362.

Kuo, J.-C., Han, X., Hsiao, C.-T., Yates, J.R., and Waterman, C.M. (2011). Analysis of the myosin-II-responsive focal adhesion proteome reveals a role for β-Pix in negative regulation of focal adhesion maturation. Nat. Cell Biol. *13*, 383–393.

Lancaster, O.M., Le Berre, M., Dimitracopoulos, A., Bonazzi, D., Zlotek-Zlotkiewicz, E., Picone, R., Duke, T., Piel, M., and Baum, B. (2013). Mitotic rounding alters cell geometry to ensure efficient bipolar spindle formation. Dev. Cell *25*, 270–283.

Lecuit, T., Lenne, P.-F., and Munro, E. (2011). Force generation, transmission, and integration during cell and tissue morphogenesis. Annu. Rev. Cell Dev. Biol. *27*, 157–184.

Lekomtsev, S., Su, K.-C., Pye, V.E., Blight, K., Sundaramoorthy, S., Takaki, T., Collinson, L.M., Cherepanov, P., Divecha, N., and Petronczki, M. (2012). Centralspindlin links the mitotic spindle to the plasma membrane during cytokinesis. Nature *492*, 276–279.

Lemmon, M.A., and Ferguson, K.M. (2000). Signal-dependent membrane targeting by pleckstrin homology (PH) domains. Biochem. J. *350 Pt 1*, 1–18.

Lessey, E.C., Guilluy, C., and Burridge, K. (2012). From mechanical force to RhoA activation. Biochemistry *51*, 7420–7432.

Leung, D.W., Otomo, C., Chory, J., and Rosen, M.K. (2008). Genetically encoded photoswitching of actin assembly through the Cdc42-WASP-Arp2/3 complex pathway. Proc. Natl. Acad. Sci. U.S.a. *105*, 12797–12802.

Levskaya, A., Weiner, O.D., Lim, W.A., and Voigt, C.A. (2009). Spatiotemporal control of cell signalling using a light-switchable protein interaction. Nature *461*, 997–1001.

Lénárt, P., Petronczki, M., Steegmaier, M., Di Fiore, B., Lipp, J.J., Hoffmann, M., Rettig, W.J., Kraut, N., and Peters, J.-M. (2007). The small-molecule inhibitor BI 2536 reveals novel insights into mitotic roles of polo-like kinase 1. Curr. Biol. *17*, 304–315.

Li, H., Ung, C.Y., Ma, X.H., Li, B.W., Low, B.C., Cao, Z.W., and Chen, Y.Z. (2009). Simulation of crosstalk between small GTPase RhoA and EGFR-ERK signaling pathway via MEKK1. Bioinformatics *25*, 358–364.

Li, Z., Hannigan, M., Mo, Z., Liu, B., Lu, W., Wu, Y., Smrcka, A.V., Wu, G., Li, L., Liu, M., et al. (2003). Directional sensing requires G beta gamma-mediated PAK1 and PIX alpha-dependent activation of Cdc42. *114*, 215–227.

Liu, H., Gomez, G., Lin, S., Lin, S., and Lin, C. (2012). Optogenetic control of transcription in zebrafish. PLoS ONE *7*, e50738.

Liu, X., Zhou, T., Kuriyama, R., and Erikson, R.L. (2004). Molecular interactions of Polo-like-kinase 1 with the mitotic kinesin-like protein CHO1/MKLP-1. J. Cell. Sci. *117*, 3233–3246.

Lomakin, A.J., Lee, K.-C., Han, S.J., Bui, D.A., Davidson, M., Mogilner, A., and Danuser, G. (2015). Competition for actin between two distinct F-actin networks defines a bistable switch for cell polarization. Nat. Cell Biol. *17*, 1435–1445.

Longtine, M.S., McKenzie, A., Demarini, D.J., Shah, N.G., Wach, A., Brachat, A., Philippsen, P., and Pringle, J.R. (1998). Additional modules for versatile and economical PCR-based gene deletion and modification in Saccharomyces cerevisiae. Yeast *14*, 953–961.

Lowery, D.M., Clauser, K.R., Hjerrild, M., Lim, D., Alexander, J., Kishi, K., Ong, S.E., Gammeltoft, S., Carr, S.A., and Yaffe, M.B. (2007). Proteomic screen defines the Polo‐box domain interactome and identifies Rock2 as a Plk1 substrate. The EMBO Journal *26*, 2262–2273.

Mabuchi, I., Hamaguchi, Y., Fujimoto, H., Morii, N., Mishima, M., and Narumiya, S. (1993). A rho-like protein is involved in the organisation of the contractile ring in dividing sand dollar eggs. Zygote *1*, 325–331.

Machacek, M., Hodgson, L., Welch, C., Elliott, H., Pertz, O., Nalbant, P., Abell, A., Johnson, G.L., Hahn, K.M., and Danuser, G. (2009). Coordination of Rho GTPase activities during cell protrusion. Nature *461*, 99–103.

Martin, A.C., Gelbart, M., Fernandez-Gonzalez, R., Kaschube, M., and Wieschaus, E.F. (2010). Integration of contractile forces during tissue invagination. J. Cell Biol. *188*, 735–749.

McBeath, R., Pirone, D.M., Nelson, C.M., Bhadriraju, K., and Chen, C.S. (2004). Cell shape, cytoskeletal tension, and RhoA regulate stem cell lineage commitment. Dev. Cell *6*, 483–495.

McInnes, C., Mazumdar, A., Mezna, M., Meades, C., Midgley, C., Scaerou, F., Carpenter, L., Mackenzie, M., Taylor, P., Walkinshaw, M., et al. (2006). Inhibitors of Polo-like kinase reveal roles in spindle-pole maintenance. Nat. Chem. Biol. *2*, 608–617.

Melvin, A.T., Welf, E.S., Wang, Y., Irvine, D.J., and Haugh, J.M. (2011). In chemotaxing fibroblasts, both high-fidelity and weakly biased cell movements track the localization of PI3K signaling. Biophys. J. *100*, 1893–1901.

Miki, T., Smith, C.L., Long, J.E., Eva, A., and Fleming, T.P. (1993). Oncogene ect2 is related to regulators of small GTP-binding proteins. Nature *362*, 462–465.

Minden, A., Lin, A., Claret, F.X., Abo, A., and Karin, M. (1995). Selective activation of the JNK signaling cascade and c-Jun transcriptional activity by the small GTPases Rac and Cdc42Hs. *81*, 1147–1157.

Miralles, F., Posern, G., Zaromytidou, A.-I., and Treisman, R. (2003). Actin dynamics control SRF activity by regulation of its coactivator MAL. *113*, 329–342.

Mishima, M., Kaitna, S., and Glotzer, M. (2002). Central spindle assembly and cytokinesis require a kinesin-like protein/RhoGAP complex with microtubule bundling activity. Dev. Cell *2*, 41–54.

Mishima, M., Pavicic, V., Gruneberg, U., Nigg, E.A., and Glotzer, M. (2004). Cell cycle regulation of central spindle assembly. Nature *430*, 908–913.

Mollinari, C., Kleman, J.-P., Jiang, W., Schoehn, G., Hunter, T., and Margolis, R.L. (2002). PRC1 is a microtubule binding and bundling protein essential to maintain the mitotic spindle midzone. J. Cell Biol. *157*, 1175–1186.

Möglich, A., and Moffat, K. (2010). Engineered photoreceptors as novel optogenetic tools. Photochem. Photobiol. Sci. *9*, 1286–1300.

Mseka, T., Bamburg, J.R., and Cramer, L.P. (2007). ADF/cofilin family proteins control

formation of oriented actin-filament bundles in the cell body to trigger fibroblast polarization. J. Cell. Sci. *120*, 4332–4344.

Murrell, M., Oakes, P.W., Lenz, M., and Gardel, M.L. (2015). Forcing cells into shape: the mechanics of actomyosin contractility. Nat. Rev. Mol. Cell Biol. *16*, 486–498.

Murthy, K., and Wadsworth, P. (2008). Dual role for microtubules in regulating cortical contractility during cytokinesis. J. Cell. Sci. *121*, 2350–2359.

Müller, T., Rumpel, E., Hradetzky, S., Bollig, F., Wegner, H., Blumenthal, A., Greinacher, A., Endlich, K., and Endlich, N. (2011). Non-muscle myosin IIA is required for the development of the zebrafish glomerulus. Kidney Int. *80*, 1055–1063.

Neef, R., Preisinger, C., Sutcliffe, J., Kopajtich, R., Nigg, E.A., Mayer, T.U., and Barr, F.A. (2003). Phosphorylation of mitotic kinesin-like protein 2 by polo-like kinase 1 is required for cytokinesis. J. Cell Biol. *162*, 863–875.

Nigg, E.A. (2001). Mitotic kinases as regulators of cell division and its checkpoints. Nat. Rev. Mol. Cell Biol. *2*, 21–32.

Niiya, F., Tatsumoto, T., Lee, K.S., and Miki, T. (2006). Phosphorylation of the cytokinesis regulator ECT2 at G2/M phase stimulates association of the mitotic kinase Plk1 and accumulation of GTP-bound RhoA. Oncogene *25*, 827–837.

Nimnual, A.S., Taylor, L.J., and Bar-Sagi, D. (2003). Redox-dependent downregulation of Rho by Rac. Nat. Cell Biol. *5*, 236–241.

O'Neill, P.R., and Gautam, N. (2014). Subcellular optogenetic inhibition of G proteins generates signaling gradients and cell migration. Mol. Biol. Cell *25*, 2305–2314.

Oakes, P.W., Banerjee, S., Marchetti, M.C., and Gardel, M.L. (2014). Geometry regulates traction stresses in adherent cells. Biophys. J. *107*, 825–833.

Oakes, P.W., Beckham, Y., Stricker, J., and Gardel, M.L. (2012). Tension is required but not sufficient for focal adhesion maturation without a stress fiber template. J. Cell Biol. *196*, 363–374.

Ohta, Y., Hartwig, J.H., and Stossel, T.P. (2006). FilGAP, a Rho- and ROCK-regulated GAP for Rac binds filamin A to control actin remodelling. Nat. Cell Biol. *8*, 803–814.

Otomo, T., Otomo, C., Tomchick, D.R., Machius, M., and Rosen, M.K. (2005). Structural basis of Rho GTPase-mediated activation of the formin mDia1. Mol. Cell *18*, 273–281.

Paluch, E., and Heisenberg, C.-P. (2009). Biology and physics of cell shape changes in development. Curr. Biol. *19*, R790–R799.

Park, H.-O., and Bi, E. (2007). Central roles of small GTPases in the development of cell

polarity in yeast and beyond. Microbiol. Mol. Biol. Rev. *71*, 48–96.

Pertz, O. (2010). Spatio-temporal Rho GTPase signaling - where are we now? J. Cell. Sci. *123*, 1841–1850.

Pertz, O., Hodgson, L., Klemke, R.L., and Hahn, K.M. (2006). Spatiotemporal dynamics of RhoA activity in migrating cells. Nature *440*, 1069–1072.

Peters, U., Cherian, J., Kim, J.H., Kwok, B.H., and Kapoor, T.M. (2006). Probing cell-division phenotype space and Polo-like kinase function using small molecules. Nat. Chem. Biol. *2*, 618–626.

Petronczki, M., Glotzer, M., Kraut, N., and Peters, J.-M. (2007). Polo-like kinase 1 triggers the initiation of cytokinesis in human cells by promoting recruitment of the RhoGEF Ect2 to the central spindle. Dev. Cell *12*, 713–725.

Picard, D. (2000). Posttranslational regulation of proteins by fusions to steroid-binding domains. Meth. Enzymol. *327*, 385–401.

Piekny, A.J., and Glotzer, M. (2008). Anillin is a scaffold protein that links RhoA, actin, and myosin during cytokinesis. Curr. Biol. *18*, 30–36.

Pierini, L.M., Lawson, M.A., Eddy, R.J., Hendey, B., and Maxfield, F.R. (2000). Oriented endocytic recycling of alpha5beta1 in motile neutrophils. Blood *95*, 2471–2480.

Pintard, L., Willis, J.H., Willems, A., Johnson, J.-L.F., Srayko, M., Kurz, T., Glaser, S., Mains, P.E., Tyers, M., Bowerman, B., et al. (2003). The BTB protein MEL-26 is a substrate-specific adaptor of the CUL-3 ubiquitin-ligase. Nature *425*, 311–316.

Plotnikov, S.V., and Waterman, C.M. (2013). Guiding cell migration by tugging. Current Opinion in Cell Biology *25*, 619–626.

Prokopenko, S.N., Brumby, A., O'Keefe, L., Prior, L., He, Y., Saint, R., and Bellen, H.J. (1999). A putative exchange factor for Rho1 GTPase is required for initiation of cytokinesis in Drosophila. Genes Dev. *13*, 2301–2314.

Prost, J., JULICHER, F., and Joanny, J.F. (2015). Active gel physics. Nat Phys *11*, 111–117.

Pryciak, P.M., and Huntress, F.A. (1998). Membrane recruitment of the kinase cascade scaffold protein Ste5 by the Gbetagamma complex underlies activation of the yeast pheromone response pathway. Genes Dev. *12*, 2684–2697.

Pryciak, P.M. (2009). Designing new cellular signaling pathways. Chem. Biol. *16*, 249–254.

Ramanathan, S.P., Helenius, J., Stewart, M.P., Cattin, C.J., Hyman, A.A., and Muller, D.J. (2015). Cdk1-dependent mitotic enrichment of cortical myosin II promotes cell rounding against confinement. Nat. Cell Biol. *17*, 148–159.

Rappaport, R. (1961). Experiments concerning the cleavage stimulus in sand dollar eggs. Journal of Experimental Zoology *148*, 81–89.

Rappaport, R. (1985). Repeated furrow formation from a single mitotic apparatus in cylindrical sand dollar eggs. J. Exp. Zool. *234*, 167–171.

Rebecchi, M.J., and Scarlata, S. (1998). Pleckstrin homology domains: a common fold with diverse functions. Annu Rev Biophys Biomol Struct *27*, 503–528.

Ridley, A.J., and Hall, A. (1992). The small GTP-binding protein rho regulates the assembly of focal adhesions and actin stress fibers in response to growth factors. Cell *70*, 389–399.

Ridley, A.J., Schwartz, M.A., Burridge, K., Firtel, R.A., Ginsberg, M.H., Borisy, G., Parsons, J.T., and Horwitz, A.R. (2003). Cell migration: integrating signals from front to back. Science *302*, 1704–1709.

Rieder, C.L., Khodjakov, A., Paliulis, L.V., Fortier, T.M., Cole, R.W., and Sluder, G. (1997). Mitosis in vertebrate somatic cells with two spindles: implications for the metaphase/anaphase transition checkpoint and cleavage. Proc. Natl. Acad. Sci. U.S.a. *94*, 5107–5112.

Rizvi, S.A., Neidt, E.M., Cui, J., Feiger, Z., Skau, C.T., Gardel, M.L., Kozmin, S.A., and Kovar, D.R. (2009). Identification and Characterization of a Small Molecule Inhibitor of Formin-Mediated Actin Assembly. Chem. Biol. *16*, 1158–1168.

Roberts, P.J., Mitin, N., Keller, P.J., Chenette, E.J., Madigan, J.P., Currin, R.O., Cox, A.D., Wilson, O., Kirschmeier, P., and Der, C.J. (2008). Rho Family GTPase modification and dependence on CAAX motif-signaled posttranslational modification. J. Biol. Chem. *283*, 25150–25163.

Rodrigues, N.T.L., Lekomtsev, S., Jananji, S., Kriston-Vizi, J., Hickson, G.R.X., and Baum, B. (2015). Kinetochore-localized PP1-Sds22 couples chromosome segregation to polar relaxation. Nature *524*, 489–492.

Rohatgi, R., Ma, L., Miki, H., Lopez, M., Kirchhausen, T., Takenawa, T., and Kirschner, M.W. (1999). The interaction between N-WASP and the Arp2/3 complex links Cdc42-dependent signals to actin assembly. *97*, 221–231.

Rojas, A.M., Fuentes, G., Rausell, A., and Valencia, A. (2012). The ras protein superfamily: Evolutionary tree and role of conserved amino acids. Journal of Cell Biology *196*, 545–4648.

Rosenfeldt, H., Castellone, M.D., Randazzo, P.A., and Gutkind, J.S. (2006). Rac inhibits thrombin-induced Rho activation: evidence of a Pak-dependent GTPase crosstalk. J Mol Signal *1*, 8.

Rossman, K.L., Der, C.J., and Sondek, J. (2005). GEF means go: turning on RHO GTPases with guanine nucleotide-exchange factors. Nat. Rev. Mol. Cell Biol. *6*, 167–180.

Rossman, K.L., Worthylake, D.K., Snyder, J.T., Cheng, L., Whitehead, I.P., and Sondek, J. (2002). Functional analysis of cdc42 residues required for Guanine nucleotide exchange. J. Biol. Chem. *277*, 50893–50898.

Sabass, B., Gardel, M.L., Waterman, C.M., and Schwarz, U.S. (2008). High resolution traction force microscopy based on experimental and computational advances. Biophys. J. *94*, 207–220.

Sanders, L.C., Matsumura, F., Bokoch, G.M., and de Lanerolle, P. (1999). Inhibition of myosin light chain kinase by p21-activated kinase. Science *283*, 2083–2085.

Schmidt, A., and Hall, A. (2002a). Guanine nucleotide exchange factors for Rho GTPases: turning on the switch. Genes Dev. *16*, 1587–1609.

Schmidt, A., and Hall, A. (2002b). The Rho exchange factor Net1 is regulated by nuclear sequestration. J. Biol. Chem. *277*, 14581–14588.

Schwarz, U.S., and Gardel, M.L. (2012). United we stand: integrating the actin cytoskeleton and cell-matrix adhesions in cellular mechanotransduction. J. Cell. Sci. *125*, 3051–3060.

Schwarz, U.S., and Safran, S.A. (2013). Physics of adherent cells. Rev. Mod. Phys. *85*, 1327–1381.

Shimada, Y., Wiget, P., Gulli, M.-P., Bi, E., and Peter, M. (2004). The nucleotide exchange factor Cdc24p may be regulated by auto-inhibition. The EMBO Journal *23*, 1051–1062.

Shimizu-Sato, S., Huq, E., Tepperman, J.M., and Quail, P.H. (2002). A light-switchable gene promoter system. Nat. Biotechnol. *20*, 1041–1044.

Smith, A., Bracke, M., Leitinger, B., Porter, J.C., and Hogg, N. (2003). LFA-1-induced T cell migration on ICAM-1 involves regulation of MLCK-mediated attachment and ROCK-dependent detachment. J. Cell. Sci. *116*, 3123–3133.

Smith, M.A., Blankman, E., Deakin, N.O., Hoffman, L.M., Jensen, C.C., Turner, C.E., and Beckerle, M.C. (2013). LIM domains target actin regulators paxillin and zyxin to sites of stress fiber strain. PLoS ONE *8*, e69378.

Smith, M.A., Blankman, E., Gardel, M.L., Luettjohann, L., Waterman, C.M., and Beckerle, M.C. (2010). A zyxin-mediated mechanism for actin stress fiber maintenance and repair. Dev. Cell *19*, 365–376.

Soiné, J.R.D., Brand, C.A., Stricker, J., Oakes, P.W., Gardel, M.L., and Schwarz, U.S. (2015). Model-based traction force microscopy reveals differential tension in cellular actin bundles. PLoS Comput. Biol. *11*, e1004076.

Stewart, M.P., Helenius, J., Toyoda, Y., Ramanathan, S.P., Muller, D.J., and Hyman, A.A. (2011). Hydrostatic pressure and the actomyosin cortex drive mitotic cell rounding. Nature *469*, 226–230.

Storici, F., and Resnick, M.A. (2006). The delitto perfetto approach to in vivo site-directed mutagenesis and chromosome rearrangements with synthetic oligonucleotides in yeast. Meth. Enzymol. *409*, 329–345.

Strack, R.L., Strongin, D.E., Bhattacharyya, D., Tao, W., Berman, A., Broxmeyer, H.E., Keenan, R.J., and Glick, B.S. (2008). A noncytotoxic DsRed variant for whole-cell labeling. Nat. Methods *5*, 955–957.

Stricker, J., Falzone, T., and Gardel, M.L. (2010). Mechanics of the F-actin cytoskeleton. Journal of Biomechanics *43*, 9–14.

Strickland, D., Lin, Y., Wagner, E., Hope, C.M., Zayner, J., Antoniou, C., Sosnick, T.R., Weiss, E.L., and Glotzer, M. (2012). TULIPs: tunable, light-controlled interacting protein tags for cell biology. Nat. Methods *9*, 379–384.

Strickland, D., Moffat, K., and Sosnick, T.R. (2008). Light-activated DNA binding in a designed allosteric protein. Proc. Natl. Acad. Sci. U.S.a. *105*, 10709–10714.

Strickland, D., Yao, X., Gawlak, G., Rosen, M.K., Gardner, K.H., and Sosnick, T.R. (2010). Rationally improving LOV domain-based photoswitches. Nat. Methods *7*, 623–626.

Su, K.-C., Takaki, T., and Petronczki, M. (2011). Targeting of the RhoGEF Ect2 to the equatorial membrane controls cleavage furrow formation during cytokinesis. Dev. Cell *21*, 1104–1115.

Tatsumoto, T., Xie, X., Blumenthal, R., Okamoto, I., and Miki, T. (1999). Human Ect2 Is an Exchange Factor for Rho Gtpases, Phosphorylated in G2/M Phases, and Involved in Cytokinesis. J. Cell Biol. *147*, 921–928.

Thévenaz, P., Ruttimann, U.E., and Unser, M. (1998). A pyramid approach to subpixel registration based on intensity. IEEE Trans Image Process *7*, 27–41.

Thorn, K. (2010). Spinning-disk confocal microscopy of yeast. Meth. Enzymol. *470*, 581–602.

Toettcher, J.E., Voigt, C.A., Weiner, O.D., and Lim, W.A. (2011). The promise of optogenetics in cell biology: interrogating molecular circuits in space and time. Nat. Methods *8*, 35–38.

Toettcher, J.E., Weiner, O.D., and Lim, W.A. (2013). Using optogenetics to interrogate the dynamic control of signal transmission by the Ras/Erk module. *155*, 1422–1434.

Tsuji, T., Ishizaki, T., Okamoto, M., Higashida, C., Kimura, K., Furuyashiki, T., Arakawa, Y., Birge, R.B., Nakamoto, T., Hirai, H., et al. (2002). ROCK and mDia1 antagonize in Rho-dependent Rac activation in Swiss 3T3 fibroblasts. J. Cell Biol. *157*, 819–830.

Uemura, A., Nguyen, T.-N., Steele, A.N., and Yamada, S. (2011). The LIM domain of zyxin is sufficient for force-induced accumulation of zyxin during cell migration. Biophys. J. *101*, 1069–1075.

van de Weerdt, B.C.M., and Medema, R.H. (2006). Polo-Like Kinases: A Team in Control of the Division. Cell Cycle.

van Leeuwen, F.N., van der Kammen, R.A., Habets, G.G., and Collard, J.G. (1995). Oncogenic activity of Tiam1 and Rac1 in NIH3T3 cells. Oncogene *11*, 2215–2221.

van Oostende Triplet, C., Jaramillo Garcia, M., Haji Bik, H., Beaudet, D., and Piekny, A. (2014). Anillin interacts with microtubules and is part of the astral pathway that defines cortical domains. J. Cell. Sci. *127*, 3699–3710.

Vetter, I.R., and Wittinghofer, A. (2001). The guanine nucleotide-binding switch in three dimensions. Science *294*, 1299–1304.

Vicente-Manzanares, M., Newell-Litwa, K., Bachir, A.I., Whitmore, L.A., and Horwitz, A.R. (2011). Myosin IIA/IIB restrict adhesive and protrusive signaling to generate front-back polarity in migrating cells. J. Cell Biol. *193*, 381–396.

Vicente-Manzanares, M., Zareno, J., Whitmore, L., Choi, C.K., and Horwitz, A.F. (2007). Regulation of protrusion, adhesion dynamics, and polarity by myosins IIA and IIB in migrating cells. J. Cell Biol. *176*, 573–580.

Wagner, E., and Glotzer, M. (2016). Local RhoA activation induces cytokinetic furrows independent of spindle position and cell cycle stage. J. Cell Biol. *213*, 641–649.

Wang, A., Ma, X., Conti, M.A., Liu, C., Kawamoto, S., and Adelstein, R.S. (2010a). Nonmuscle myosin II isoform and domain specificity during early mouse development. Proc. Natl. Acad. Sci. U.S.a. *107*, 14645–14650.

Wang, X., He, L., Wu, Y.I., Hahn, K.M., and Montell, D.J. (2010b). Light-mediated activation reveals a key role for Rac in collective guidance of cell movement in vivo. Nat. Cell Biol. *12*, 591–597.

Watanabe, N., Kato, T., Fujita, A., Ishizaki, T., and Narumiya, S. (1999). Cooperation between mDia1 and ROCK in Rho-induced actin reorganization. Nat. Cell Biol. *1*, 136–143.

Watanabe, S., Ando, Y., Yasuda, S., Hosoya, H., Watanabe, N., Ishizaki, T., and Narumiya, S. (2008). mDia2 induces the actin scaffold for the contractile ring and stabilizes its position during cytokinesis in NIH 3T3 cells. Mol. Biol. Cell *19*, 2328–2338.

Watts, J.L., Etemad-Moghadam, B., Guo, S., Boyd, L., Draper, B.W., Mello, C.C., Priess, J.R., and Kemphues, K.J. (1996). par-6, a gene involved in the establishment of asymmetry in early C. elegans embryos, mediates the asymmetric localization of PAR-3. Development *122*, 3133–3140.

Webster, K.D., Ng, W.P., and Fletcher, D.A. (2014). Tensional homeostasis in single fibroblasts. Biophys. J. *107*, 146–155.

Weichsel, J., Urban, E., Small, J.V., and Schwarz, U.S. (2012). Reconstructing the orientation distribution of actin filaments in the lamellipodium of migrating keratocytes from electron microscopy tomography data. Cytometry A *81*, 496–507.

Welchman, D.P., Mathies, L.D., and Ahringer, J. (2007). Similar requirements for CDC-42 and the PAR-3/PAR-6/PKC-3 complex in diverse cell types. Dev. Biol. *305*, 347–357.

Werner, M., Munro, E., and Glotzer, M. (2007). Astral signals spatially bias cortical myosin recruitment to break symmetry and promote cytokinesis. Curr. Biol. *17*, 1286–1297.

Wheatley, S.P., and Wang, Y. (1996). Midzone microtubule bundles are continuously required for cytokinesis in cultured epithelial cells. J. Cell Biol. *135*, 981–989.

Winters, M.J., Lamson, R.E., Nakanishi, H., Neiman, A.M., and Pryciak, P.M. (2005). A membrane binding domain in the ste5 scaffold synergizes with gbetagamma binding to control localization and signaling in pheromone response. Mol. Cell *20*, 21–32.

Wolfe, B.A., Takaki, T., Petronczki, M., and Glotzer, M. (2009). Polo-like kinase 1 directs assembly of the HsCyk-4 RhoGAP/Ect2 RhoGEF complex to initiate cleavage furrow formation. PLoS Biol. *7*, e1000110.

Wu, Y.I., Frey, D., Lungu, O.I., Jaehrig, A., Schlichting, I., Kuhlman, B., and Hahn, K.M. (2009). A genetically encoded photoactivatable Rac controls the motility of living cells. Nature *461*, 104–108.

Xu, K., Babcock, H.P., and Zhuang, X. (2012). Dual-objective STORM reveals three-dimensional filament organization in the actin cytoskeleton. Nat. Methods *9*, 185–188.

Yao, X., Rosen, M.K., and Gardner, K.H. (2008). Estimation of the available free energy in a LOV2-J alpha photoswitch. Nat. Chem. Biol. *4*, 491–497.

Yazawa, M., Sadaghiani, A.M., Hsueh, B., and Dolmetsch, R.E. (2009). Induction of protein-protein interactions in live cells using light. Nat. Biotechnol. *27*, 941–945.

Yoo, S.K., Deng, Q., Cavnar, P.J., Wu, Y.I., Hahn, K.M., and Huttenlocher, A. (2010). Differential regulation of protrusion and polarity by PI3K during neutrophil motility in live zebrafish. Dev. Cell *18*, 226–236.

Yoshigi, M., Hoffman, L.M., Jensen, C.C., Yost, H.J., and Beckerle, M.C. (2005). Mechanical force mobilizes zyxin from focal adhesions to actin filaments and regulates cytoskeletal reinforcement. J. Cell Biol. *171*, 209–215.

Yüce, O., Piekny, A., and Glotzer, M. (2005). An ECT2-centralspindlin complex regulates the localization and function of RhoA. J. Cell Biol. *170*, 571–582.

Zaidel-Bar, R., Ballestrem, C., Kam, Z., and Geiger, B. (2003). Early molecular events in the assembly of matrix adhesions at the leading edge of migrating cells. J. Cell. Sci. *116*, 4605–

4613.

Zhang, D., and Glotzer, M. (2015). The RhoGAP activity of CYK-4/MgcRacGAP functions non-canonically by promoting RhoA activation during cytokinesis. Elife *4*, 204.

Zhang, K., Duan, L., Ong, Q., Lin, Z., Varman, P.M., Sung, K., and Cui, B. (2014). Light-mediated kinetic control reveals the temporal effect of the Raf/MEK/ERK pathway in PC12 cell neurite outgrowth. PLoS ONE *9*, e92917.

Zhao, W.-M., and Fang, G. (2005). Anillin Is a Substrate of Anaphase-promoting Complex/Cyclosome (APC/C) That Controls Spatial Contractility of Myosin during Late Cytokinesis. J. Biol. Chem. *280*, 33516–33524.

Zhu, C., Bao, G., and Wang, N. (2000). Cell mechanics: mechanical response, cell adhesion, and molecular deformation. Annu Rev Biomed Eng *2*, 189–226.

Zoltowski, B.D., Vaccaro, B., and Crane, B.R. (2009). Mechanism-based tuning of a LOV domain photoreceptor. Nat. Chem. Biol. *5*, 827–834.